

---

# Radiative corrections to the decay of the top quark

---

Luisa Oggero



PHYSIKALISCHES INSTITUT  
FAKULTÄT FÜR MATHEMATIK UND PHYSIK  
ALBERT-LUDWIGS-UNIVERSITÄT FREIBURG

Dezember 2014



---

# Radiative corrections to the decay of the top quark

---

Luisa Oggero

DISSERTATION

zur Erlangung des Doktorgrades  
der Fakultät für Mathematik und Physik der

ALBERT-LUDWIGS-UNIVERSITÄT  
Freiburg im Breisgau

vorgelegt von

**Luisa Oggero**

Dezember 2014

Dekan: Prof. Dr. Michael Růžička

Referent: Prof. Dr. Stefan Dittmaier

Koreferent: Prof. Dr. Thomas Filk

Tag der mündlichen Prüfung: 23. Februar 2015

# Contents

<b>1</b>	<b>Introduction</b>	<b>5</b>
<b>2</b>	<b>Overview of the Standard Model</b>	<b>9</b>
2.1	The SM Lagrangian . . . . .	10
2.1.1	Kinetic terms . . . . .	10
2.1.2	The Higgs mechanism . . . . .	11
2.1.3	Masses of the particles . . . . .	13
2.1.4	Gauge fixing and ghost terms . . . . .	14
2.2	Renormalization of the theory . . . . .	14
2.3	Unstable particles and the complex-mass scheme . . . . .	17
<b>3</b>	<b>Calculation of the amplitudes</b>	<b>21</b>
3.1	The Weyl–van-der-Waerden formalism . . . . .	22
3.2	Born Amplitudes . . . . .	25
3.3	Real corrections . . . . .	25
3.4	Virtual corrections and counterterms . . . . .	30
<b>4</b>	<b>The one-cutoff phase-space slicing method</b>	<b>35</b>
4.1	Overview of the method . . . . .	36
4.2	Singular region . . . . .	37
4.2.1	Final-state spectator and final-state emitter . . . . .	40
4.2.2	Final-state emitter and initial-state spectator, and vice versa . . . . .	47
4.2.3	Summary of the singular contributions . . . . .	50
4.3	Quasi-soft region . . . . .	52
<b>5</b>	<b>Phase-space integration</b>	<b>55</b>
5.1	VEGAS . . . . .	55
5.2	Phase-space parameterizations . . . . .	56
5.3	$1 \rightarrow 3$ particle phase space . . . . .	59
5.4	$1 \rightarrow 4$ particle phase space . . . . .	60
<b>6</b>	<b>Numerical results</b>	<b>65</b>
6.1	Second independent calculation . . . . .	65
6.2	Input parameters . . . . .	66
6.3	Event selection . . . . .	67
6.4	Numerical results for the top-quark decay width . . . . .	68

6.4.1	Numerical results for the semileptonic decay . . . . .	70
6.4.2	Numerical results for the hadronic decay . . . . .	76
6.5	Total top-quark decay width . . . . .	81
<b>7</b>	<b>Conclusions</b>	<b>83</b>
<b>A</b>	<b>Narrow-Width Approximation</b>	<b>85</b>
<b>B</b>	<b>Soft-photon approximation</b>	<b>89</b>
<b>C</b>	<b>Feynman rules</b>	<b>91</b>
	<b>Bibliography</b>	<b>97</b>
	<b>Acknowledgements</b>	<b>105</b>

# Chapter 1

## Introduction

The top quark is the heaviest elementary particle in the Standard Model (SM) of particle physics. It was discovered in 1995 at the Tevatron particle accelerator by the experiments CDF [1] and D0 [2]. Due to its large mass, it is the only quark that decays before hadronization can occur (see, e.g., Ref. [3]), providing an important testing ground for QCD, i.e. it allows a more direct access to the heavy-quark dynamics. The top quark decays almost exclusively into a bottom quark and a  $W$  boson, reflecting the special role of the 3rd generation, where  $V_{tb} \sim 1$  and  $|V_{td}|, |V_{ts}| \ll 1$ . The quantities  $V_{ij}$  are elements of the Cabibbo–Kobayashi–Maskawa matrix. Because of this property, the top quark plays a key role in any model to explain the flavor structure. In addition, it has a Yukawa coupling to the Higgs boson of order one. For these reasons the top quark is a unique window to test the SM on one side, and to have access to indications of new physics beyond the SM on the other side. A detailed knowledge of its properties (mass, decay width, couplings, etc.) is crucial for a better understanding of the mechanism of electroweak symmetry breaking (EWSB). Hence, processes comprising top quarks are being carefully scrutinized at the Tevatron and at the Large Hadron Collider (LHC). For example, besides fully inclusive top-quark production, more exclusive final states can be accessed at hadron colliders, whose cross sections are typically much smaller, yet they can provide important information on the properties of the top quark. Typical such processes are  $tV + \text{jets}$  and  $t\bar{t} + V(V)$  ( $V = \gamma, Z, W^\pm$ ),  $t\bar{t} + \text{jets}$ ,  $t\bar{t}H$ ,  $t\bar{t}b\bar{b}$ , and  $t\bar{t}t\bar{t}$ . All of these can be considered as signals to test the SM, and subsequently as backgrounds to BSM searches.

Another consequence of the large top-quark mass is its large width  $\Gamma_t$ . The top-quark width is an important ingredient in the theoretical evaluation of processes which have the top-quark as an intermediate state. As an example we can consider top-quark pairs ( $t\bar{t}$ ), which are abundantly produced both at the LHC and the Tevatron, and are used to study the properties of the top quark. Therefore, very precise theoretical calculations have been performed on the  $t\bar{t}$  production [4] and on its generalization obtained considering the top quarks off-shell ( $W^+W^-b\bar{b}$  production). As described in Refs. [5–8], off-shell effects and non-resonant backgrounds have to be taken into account in the calculation of the NLO QCD corrections, e.g. using the complex-mass scheme [9–11]. For consistency, it is thus important to retain the same NLO accuracy for the input parameter  $\Gamma_t$ . The same argument is valid for other calculations, such as the NLO QCD corrections to single top production processes described in Ref. [12]. Moreover, to compare the current experimental measurements of  $\Gamma_t$  with the SM

predictions, the theoretical calculations must have an adequate accuracy. A precise knowledge of the top-quark decay width is therefore fundamental and it is the main goal of this thesis.

In the last 30 years much effort has been invested on the theoretical side to calculate the top-quark decay width with increasing precision within the SM. The first LO predictions for the semileptonic decay rate were calculated in Refs. [13,14], long before the first direct measurement of the top-quark mass. In 1988, knowing that the top quark was much heavier than all other quarks, Jezabek and Kühn presented the first analytic formula for the QCD corrections to the semileptonic decay rate of a heavy quark in Refs. [15,16], taking into account the off-shell effects of the  $W$  boson and the  $b$ -quark mass. Later, many predictions for the QCD [17,18] and EW [19–25] corrections have been worked out for the dominant decay channel of the top quark,  $t \rightarrow bW$ , in the approximation of stable  $W$  bosons. After the top-quark discovery in 1995, having precise theoretical predictions for its width became even more important. Therefore, various  $\mathcal{O}(\alpha_s^2)$  corrections to  $\Gamma(t \rightarrow Wb)$  were performed using different levels of approximations [26–28]. More recently, the first results on the fully differential decay rates for semileptonic top-quark decay at NNLO in QCD have been presented in Ref. [29], including NLO EW corrections. So far, however, the off-shellness of the  $W$  boson has been taken into account only in Refs. [15,16] for the case of NLO QCD corrections to the semileptonic decay. No other corrections to the three-body decay of the top quark, accounting for the  $W$  off-shellness in the complex-mass scheme and keeping the  $b$  quark as massive, has been yet calculated in the literature.

On the experimental side, the first direct bound on the total decay width of the top quark has been presented by the experiment CDF II (Tevatron) in 2008 [30]. Direct measurements, instead, have been presented by CDF II in Refs. [31,32] and give us only the information of a non-vanishing width. The other experiment at Tevatron, D0, determined the total top-quark width from indirect measurements [33,34], obtaining a value compatible with the SM predictions with a relative uncertainty of approximately 20%. A more precise indirect determination of the top-quark width, also in agreement with the SM predictions, has been provided by the CMS experiment (LHC) at  $\sqrt{s} = 8$  TeV [35]. The LHC will start again in 2015 to produce  $pp$  collisions at the centre-of-mass energy of 13 TeV in its Run 2. The larger amount of data that is expected to be analyzed will allow for a more precise measurement of  $\Gamma_t$ . Moreover, a higher precision may be achieved at future lepton colliders, such as the International Linear Collider (ILC) or the Future Circular Collider (FCC-ee), formerly known as Triple-Large Electron-Positron Collider (TLEP) [36].

In this thesis we calculate the fully differential QCD and EW NLO corrections to the partial widths of the top-quark decay,  $t \rightarrow b f \bar{f}'$ , taking into account also the  $W$ -boson off-shell effects and the  $b$ -quark mass. We consider the semileptonic and hadronic decay channels separately and we use these results to deliver a prediction of the total top-quark decay width at NLO, which can be compared with the experimental measurements.

To deal with the IR singularities appearing during the calculation, we use the basic idea of the one-cutoff phase-space slicing method (OCSM) [37–41]. The OCSM has the advantage that, in contrast to other techniques such as the dipole-subtraction formalism [42–45], it can be used for the generation of Monte Carlo events with weight one. For the specific case of a decay process with more than two (massive or massless) particles in the final state, however, no

valid prescription exists for the one-cutoff slicing approach in the literature yet<sup>1</sup>. Therefore, we have developed in this work a generalization of the OCSM, using some analytical results of the dipole subtraction formalism. The main idea of the method is to isolate the singularities from the real corrections, identifying two different phase-space regions: a hard region, where no soft or collinear singularities appear, and a singular region, where a further subdivision of the phase space is needed. Part of the singular region is integrated analytically over the gluon/photon phase space and, at a later stage, it has to be integrated over the remaining  $1 \rightarrow 3$  particle phase space. The mentioned analytic integrals are calculated for a general case and can be used for any other process. The remaining part of the phase space, called the quasi-soft region, has to be treated using the soft-photon/gluon approximation.

The thesis is structured as follows:

- In Chapter 2 we introduce the fundamentals of the Standard Model (SM). We start from the construction of the SM Lagrangian in Sect. 2.1, then in Sect. 2.2 we discuss the renormalization of the theory. Section 2.3 is devoted to the issue of unstable particles and to the description of the complex-mass scheme.
- In the first section of Chapter 3 we summarize the Weyl–van-der-Waerden formalism, used to calculate the various matrix elements. The explicit expressions for the Born and for the real emission amplitudes are presented in Sects. 3.2 and 3.3, respectively. Section 3.4 briefly describes the technique used to evaluate the virtual contributions and the counterterms.
- Chapter 4 explains in detail the method developed in this work to deal with the IR divergences. Section 4.1 gives an overview of the technique, while Sect. 4.2 describes how to analytically integrate the soft and collinear limits of the singular region for different pairs of fermions. The contributions of the quasi-soft region are summarized in Sect. 4.3.
- At the beginning of Chapter 5 a brief overview of an adaptive multi-dimensional Monte Carlo integration is presented. A general description of the phase-space integration techniques is given in Sect. 5.2, while Sects. 5.3 and 5.4 describe the specific cases of the  $1 \rightarrow 3$  and the  $1 \rightarrow 4$  particle phase-space integrations, respectively.
- Chapter 6 is dedicated to the numerical results for the NLO corrections to the top-quark partial decay widths. We start describing the settings of the independent calculation to which we compare our results. Then, in Sect. 6.2, the input parameters of the calculation are listed. Section 6.3 contains the details of the event selections used in this work. Section 6.4 shows the existence of a region where the results are independent from the choice of the technical cut parameter for the one-cutoff phase-space slicing method. The values of the QCD and EW corrections to the semileptonic (hadronic) top-quark decay width and various differential distributions are shown in Sect. 6.4.1 (6.4.2). The chapter ends with a comparison of the theoretical total top-quark decay width with the experimental measurements.

---

<sup>1</sup>An extension of the dipole-subtraction formalism to treat decay kinematics has been recently developed [46]. The details will be presented, together with a description of our method and the results of this thesis, in Ref. [47].

- In Chapter 7 we conclude summarizing the results presented in this thesis.
- In Apps. A and B we discuss the narrow-width and the soft-photon approximations, respectively. In App. C the Feynman rules used in this work are collected.

# Chapter 2

## Overview of the Standard Model

The Standard Model (SM) is the quantum field theory of the *strong* and the *electroweak* (EW) *interactions* of elementary particles. It is a gauge theory based on the

$$SU(3)_c \times SU(2)_W \times U(1)_Y \quad (2.1)$$

gauge group, where  $SU(3)_c$  is the colour group of the strong interactions,  $SU(2)_W$  is the weak isospin symmetry group, and  $U(1)_Y$  is the hypercharge symmetry group.

The SM includes spin- $\frac{1}{2}$  fermions: They consist in six quarks (up, down, charm, strange, top, bottom) and six leptons (electron, muon, tau, and the corresponding neutrinos). These fermions are grouped into three generations reflecting their mass hierarchy and interact with each other through the four fundamental forces (strong, weak, electromagnetic and gravitational<sup>1</sup>). They are all affected by the weak interactions, mediated by the massive  $W^\pm$  and  $Z$  bosons, and by the electromagnetic (EM) interaction, mediated by the photon. The weak and the electromagnetic interactions are unified in the electroweak *Glashow–Weinberg–Salam* (GWS) *model* [48–50], where the gauge group  $SU(2)_W \times U(1)_Y$  is spontaneously broken, through the Higgs mechanism, down to the electromagnetic gauge group  $U(1)_{EM}$ . As a consequence of the breaking mechanism, a new neutral scalar particle is predicted: the Higgs boson. Moreover, the quarks are also subject to the strong interactions, mediated by the gluons.

The SM is formulated as local quantum field theory, i.e. in the *Lagrangian formalism*, which incorporates all the ingredients of the theory in the Lagrangian density  $\mathcal{L}$ , which yields the action of the theory after being integrated over the space-time.

In this chapter we give a brief overview of the Standard Model of particle physics: Section 2.1 is dedicated to the construction of the SM Lagrangian and the renormalization of the theory is discussed in Sect. 2.2. In Sect. 2.3 we deal with the issue of unstable particles and we describe the complex-mass scheme. More details regarding the SM can be found in Refs. [51–55].

---

<sup>1</sup>The gravitational force is much weaker than the electrical force and is not included in the SM. The theory of gravity is described by Einstein’s general relativity.

## 2.1 The SM Lagrangian

The SM Lagrangian  $\mathcal{L} = \mathcal{L}(\Phi, \partial_\mu \Phi)$  of a generic field multiplet  $\Phi$  is invariant under the global symmetry transformation

$$U(\theta_c, \theta_W, \theta_Y) = \exp \left\{ ig_s t^a \theta_c^a + ig I^i \theta_W^i - ig' \frac{Y}{2} \theta_Y \right\}, \quad (2.2)$$

where  $g_s$ ,  $g$ , and  $g'$  are coupling constants, and  $\theta_c^a$ ,  $\theta_W^i$  and  $\theta_Y$  are arbitrary real group parameters. In Eq. (2.2),  $t^a$  ( $a = 1, \dots, 8$ ),  $I^i$  ( $i = 1, 2, 3$ ), and  $Y$  are the generators of the groups  $SU(3)_c$ ,  $SU(2)_W$ , and  $U(1)_Y$ , respectively. In the fundamental representation they can be written as  $t^a = \lambda^a/2$  and  $I^i = \sigma^i/2$ , where  $\lambda^a$  are the Gell-Mann matrices and  $\sigma^i$  the Pauli matrices. The value of the hypercharge  $Y$  is determined by the *Gell-Mann–Nishijima relation*

$$Q = I_W^3 + \frac{Y}{2}, \quad (2.3)$$

with  $Q$  the electric charge of the particle.

A gauge theory is a field theory which is invariant under a local gauge transformation. In order to make the transition from a global to a local symmetry,  $\theta \rightarrow \theta(x)$ , with  $x$  the space-time coordinate, it is necessary to substitute the partial space-time derivative  $\partial^\mu$  appearing in the Lagrangian with the covariant derivative

$$D_\mu = \partial_\mu - ig_s G_\mu^a t^a - ig W_\mu^i I^i + ig' B_\mu \frac{Y}{2}. \quad (2.4)$$

Here,  $G_\mu^a$ ,  $W_\mu^i$ , and  $B_\mu$  are the gauge fields associated to the groups  $SU(3)_c$ ,  $SU(2)_W$ , and  $U(1)_Y$ , respectively. They transform under the local gauge transformation as

$$\begin{aligned} G_\mu^a t^a &\rightarrow G_\mu'^a t^a = U(\theta_c) G_\mu^a t^a U(\theta_c)^{-1} + \frac{i}{g_s} (\partial_\mu U(\theta_c)) U(\theta_c)^{-1}, \\ W_\mu^i I^i &\rightarrow W_\mu'^i I^i = U(\theta_W) W_\mu^i I^i U(\theta_W)^{-1} + \frac{i}{g} (\partial_\mu U(\theta_W)) U(\theta_W)^{-1}, \\ B_\mu &\rightarrow B_\mu' = B_\mu - \partial_\mu \theta_Y. \end{aligned} \quad (2.5)$$

In the following sections we describe the different contributions to the SM Lagrangian.

### 2.1.1 Kinetic terms

We start by defining the Yang Mills Lagrangian  $\mathcal{L}_{\text{YM}}$ , which contains the gauge-invariant kinetic terms of the gauge fields,

$$\mathcal{L}_{\text{YM}} = -\frac{1}{4} G_{\mu\nu}^a G^{a,\mu\nu} - \frac{1}{4} W_{\mu\nu}^i W^{i,\mu\nu} - \frac{1}{4} B_{\mu\nu} B^{\mu\nu}. \quad (2.6)$$

The field-strength tensors are defined as

$$\begin{aligned} G_{\mu\nu}^a &= \partial_\mu G_\nu^a - \partial_\nu G_\mu^a - g_s f^{abc} G_\mu^b G_\nu^c, \\ W_{\mu\nu}^i &= \partial_\mu W_\nu^i - \partial_\nu W_\mu^i - g \epsilon^{ijk} W_\mu^j W_\nu^k, \\ B_{\mu\nu} &= \partial_\mu B_\nu - \partial_\nu B_\mu, \end{aligned} \quad (2.7)$$

where  $f^{abc}$  and  $\epsilon^{ijk}$  are the structure constants of the Lie algebra of  $SU(3)_c$  and  $SU(2)_W$ , respectively. It is worth to mention that adding explicitly a mass term in the Lagrangian would violate the gauge invariance of the theory, even though we know from the experiments that the  $W$  and  $Z$  bosons are massive particles.

Concerning the fermions, we can distinguish between three generations of leptons ( $\ell$  and  $\nu$ ) and quarks ( $u$  and  $d$ ). Depending on their chirality, they can be left-handed and transform as  $SU(2)_W$  doublets

$$L'_{i,L} = \begin{pmatrix} \nu'_i \\ \ell'_i \end{pmatrix}_L, \quad Q'_{i,L} = \begin{pmatrix} u'_i \\ d'_i \end{pmatrix}_L, \quad (2.8)$$

where  $i = 1, 2, 3$  is the generation index, or right-handed,

$$\ell'_{i,R}, \quad u'_{i,R}, \quad d'_{i,R}, \quad (2.9)$$

and transform instead as  $SU(2)_W$  singlets. The prime on the fermionic fields indicates that they are eigenstates of the EW interaction. The quarks have three colour degrees of freedom (red, green, and blue), with respect to the  $SU(3)_c$  gauge group, whose index is suppressed in the notation above.

Using the definition of the covariant derivative in Eq. (2.4), it is possible to write the kinetic terms for the fermions in a gauge invariant way,

$$\mathcal{L}_{\text{ferm}} = \sum_{i=1}^3 (\bar{L}'_{i,L} i \not{D} L'_{i,L} + \bar{Q}'_{i,L} i \not{D} Q'_{i,L} + \bar{\ell}'_{i,R} i \not{D} \ell'_{i,R} + \bar{u}'_{i,R} i \not{D} u'_{i,R} + \bar{d}'_{i,R} i \not{D} d'_{i,R}). \quad (2.10)$$

Also for the fermions, it is not possible to directly add mass terms in the Lagrangian: The addition would mix the two chiralities spoiling gauge invariance.

An elegant possibility to generate the masses in a gauge invariant way is to use the mechanism of *spontaneous symmetry breaking* (SSB). This mechanism was proposed in the early sixties by Brout, Englert, and Higgs [56–60]. For this theory contribution, Higgs and Englert were awarded the 2013 Nobel Prize in Physics, after the discovery of the Higgs particle in the CERN laboratory in July 2012 [61, 62].

### 2.1.2 The Higgs mechanism

The Higgs mechanism introduces a complex scalar field, also known as the *Higgs field*, with a weak hypercharge  $Y_\Phi = 1$ , that transforms as an  $SU(2)_W$  doublet,

$$\Phi(x) = \begin{pmatrix} \phi^+(x) \\ \phi^0(x) \end{pmatrix}. \quad (2.11)$$

The contribution of the Higgs field to the Lagrangian density is given by

$$\mathcal{L}_{\text{Higgs}} = (D_\mu \Phi)^\dagger (D^\mu \Phi) - V(\Phi), \quad (2.12)$$

with a gauge-invariant potential

$$V(\Phi) = \frac{\lambda}{4} (\Phi^\dagger \Phi)^2 - \mu^2 (\Phi^\dagger \Phi), \quad \text{with} \quad \lambda, \mu^2 > 0, \quad (2.13)$$

defined in such a way that the Higgs field develops a non-vanishing vacuum-expectation value (vev),  $\Phi_0$  with

$$|\Phi_0|^2 = \frac{2\mu^2}{\lambda} \equiv \frac{v^2}{2}. \quad (2.14)$$

This vev breaks the  $SU(2)_W \times U(1)_Y$  symmetry spontaneously down to the electromagnetic gauge group  $U(1)_{EM}$ . The EM symmetry remains unbroken, i.e. one gauge boson stays massless and can be identified with the photon. The generator of the  $U(1)_{EM}$  symmetry is the electric charge  $Q$ , which is related to the unbroken generator of  $SU(2)_W \times U(1)_Y$  by the relation presented in Eq. (2.3).

In perturbation theory, we expand the Higgs doublet around the chosen vev,

$$\Phi(x) = \begin{pmatrix} \phi^+(x) \\ \frac{1}{\sqrt{2}}(v + H(x) + i\chi(x)) \end{pmatrix}. \quad (2.15)$$

The fields  $\phi^+(x)$ ,  $\phi^-(x) = (\phi^+(x))^\dagger$ , and  $\chi(x)$ , also known as *would-be Goldstone bosons* [63,64], are scalar fields with vanishing vev. They are non-physical degrees of freedom and can be eliminated by a gauge transformation (*unitary gauge*). After inserting Eq. (2.15) in the Higgs Lagrangian (Eq. (2.12)), the mass terms

$$\mathcal{L}_M = -\mu^2 H^2 + v^2 \left[ \frac{g^2}{4} W_\mu^- W^{\mu,+} + \frac{1}{8} (g' B_\mu + g W_\mu^3)^2 \right] \quad (2.16)$$

arise, with the charge eigenstates

$$W_\mu^\pm = \frac{W_\mu^1 \mp iW_\mu^2}{\sqrt{2}}. \quad (2.17)$$

From the first term we notice that the real field  $H(x)$  corresponds to a physical particle, the Higgs boson, with a mass of

$$M_H = \sqrt{2}\mu. \quad (2.18)$$

In order to identify the remaining terms of Eq. (2.16) with the  $W$ - and  $Z$ -boson masses, we need to deeper analyze the GWS model of electroweak interactions (Sect. 2.1.3).

Additionally, the Higgs field can be coupled in a gauge-invariant way with the fermion fields through *Yukawa couplings*, yielding mass terms for the fermions. The Yukawa Lagrangian is

$$\mathcal{L}_{\text{Yuk}} = \sum_{i,j=1}^3 (G_{ij}^\ell \bar{L}'_{i,L} \Phi \ell'_{j,R} + G_{ij}^u \bar{Q}'_{i,L} \Phi^c u'_{j,R} + G_{ij}^d \bar{Q}'_{i,L} \Phi d'_{j,R} + h.c.), \quad (2.19)$$

where *h.c.* denotes the hermitian conjugate,  $G_{ij}^f$  are the complex  $3 \times 3$  Yukawa coupling matrices, and the charge conjugate of the Higgs field is defined as

$$\Phi^c \equiv i\sigma_2 \Phi^\dagger. \quad (2.20)$$

It is important to notice that the quantum chromodynamics sector (QCD), belonging to the  $SU(3)_c$  symmetry, is not affected by the SSB. Thus, its mediators, the gluons, are massless.

### 2.1.3 Masses of the particles

We diagonalize the mass matrix of the fields  $B_\mu$  and  $W_\mu^3$ , as read from Eq. (2.16), by a rotation

$$\begin{pmatrix} Z_\mu \\ A_\mu \end{pmatrix} = \begin{pmatrix} \cos \theta_w & \sin \theta_w \\ -\sin \theta_w & \cos \theta_w \end{pmatrix} \begin{pmatrix} W_\mu^3 \\ B_\mu \end{pmatrix}, \quad (2.21)$$

where  $\theta_w$  is the weak-mixing angle and is defined as

$$c_w = \cos \theta_w = \frac{g}{\sqrt{g^2 + g'^2}}, \quad s_w = \sin \theta_w = \frac{g'}{\sqrt{g^2 + g'^2}}. \quad (2.22)$$

In Eq. (2.21) the massive field  $Z_\mu$  can be identified with the electrically neutral  $Z$  boson and  $A_\mu$  corresponds to the massless boson associated to the unbroken  $U(1)_{EM}$  symmetry, the photon. In  $\mathcal{L}_M$  (Eq. (2.16)) the mass terms of the gauge fields  $W_\mu^\pm$  and  $Z_\mu$  read

$$M_W = \frac{gv}{2} \quad \text{and} \quad M_Z = \frac{v}{2} \sqrt{g^2 + g'^2}. \quad (2.23)$$

Concerning the fermions, the Yukawa Lagrangian (Eq. (2.19)) contains the mass matrices

$$M_{ij}^f = \frac{v}{\sqrt{2}} G_{ij}^f, \quad (2.24)$$

which can be diagonalized,

$$m_{f,i} = \frac{v}{\sqrt{2}} \sum_{j,k} U_{ij,L}^f G_{jk}^f U_{ki,R}^{f\dagger}, \quad (2.25)$$

by a unitary transformation of the fields

$$f_{i,L} = \sum_j U_{ij,L}^f f'_{j,L} \quad \text{and} \quad f_{i,R} = \sum_j U_{ij,R}^f f'_{j,R}. \quad (2.26)$$

For the quark sector the diagonalization introduces in the Yukawa Lagrangian the combination

$$V_{ij} = \sum_k U_{ik}^u U_{kj}^{d\dagger}, \quad (2.27)$$

also known as the unitary quark-mixing *Cabibbo–Kobayashi–Maskawa matrix* (CKM) [65, 66]. The factors  $V_{ij}$  survive, however, only in the quark- $W$ -boson couplings. At tree level there are consequently no flavor-changing neutral currents.

In the leptonic sector, instead, a CKM-like matrix is not necessary, since in the SM the neutrino is originally assumed to be massless<sup>2</sup>. Its mass eigenstate is therefore conventionally chosen as

$$\nu_{i,L} = \sum_j U_{ij,L}^\ell \nu'_{j,L}, \quad (2.28)$$

so that the CKM matrix equals the unity matrix, i.e. the EW eigenstates and the mass eigenstates coincide (the diagonalization matrices are absorbed in the fields).

---

<sup>2</sup>Actually, neutrino oscillation experiments have shown that the neutrinos do have a mass [67]. However, due to its small value, the neutrino mass will be neglected in this thesis.

### 2.1.4 Gauge fixing and ghost terms

Summing all contributions collected in the previous sections, we can write the classical Lagrangian density

$$\mathcal{L}_{\text{cl}} = \mathcal{L}_{\text{YM}} + \mathcal{L}_{\text{ferm}} + \mathcal{L}_{\text{Higgs}} + \mathcal{L}_{\text{Yuk}}. \quad (2.29)$$

However, further terms need to be added in order to quantize the theory:

$$\mathcal{L}_{\text{SM}} = \mathcal{L}_{\text{cl}} + \mathcal{L}_{\text{fix}} + \mathcal{L}_{\text{FP}}. \quad (2.30)$$

A gauge-fixing Lagrangian  $\mathcal{L}_{\text{fix}}$  is introduced to avoid the integration over equivalent field configurations during the quantization process through the path-integral formalism:

$$\mathcal{L}_{\text{fix}} = -\frac{1}{2\xi_A}(F^A)^2 - \frac{1}{2\xi_Z}(F^Z)^2 - \frac{1}{\xi_W}F^+F^- - \frac{1}{2\xi_G}(F^{G,a})^2, \quad (2.31)$$

where the gauge-fixing functionals, in the *'t Hooft gauge*, are

$$\begin{aligned} F^A &= \partial^\mu A_\mu, \\ F^Z &= \partial^\mu Z_\mu - iM_Z \xi_Z \chi, \\ F^\pm &= \partial^\mu W_\mu^\pm \mp iM_W \xi_W \phi^\pm, \\ F^{G,a} &= \partial^\mu G_\mu^a. \end{aligned} \quad (2.32)$$

In this thesis we choose the *'t Hooft-Feynman gauge*, which is defined by taking  $\xi_V = 1$ , with  $V = A, Z, W, G$ . With this choice, the masses of the would-be Goldstone bosons  $\chi$  and  $\phi^\pm$  coincide with the masses of the  $Z$  and  $W$  bosons, respectively. Moreover, the mixing terms  $V^\mu \partial_\mu \chi$  and  $V^\mu \partial_\mu \phi^\pm$ , introduced by the SSB, are canceled by the gauge fixing term, simplifying the propagators.

The *Faddeev-Popov* term,

$$\mathcal{L}_{\text{FP}} = \bar{u}^\alpha(x) \frac{\delta F^\alpha}{\delta \theta^\beta(x)} u^\beta(x), \quad (2.33)$$

is introduced to cancel the over-counted degrees of freedom of the gauge fields that originate in the addition of  $\mathcal{L}_{\text{fix}}$ . The anticommuting fields  $u^\alpha(x)$  and  $\bar{u}^\alpha(x)$  are known as the *Faddeev-Popov ghosts* [68], with  $\alpha = \pm, A, Z, G$ , and occur only as virtual particles inside loops, since they are unphysical degrees of freedom.

## 2.2 Renormalization of the theory

The SM has been widely experimentally investigated, through the measurements of quantities, such as the masses of the particles<sup>3</sup>, the unit charge and the quark mixing matrix,

$$M_Z, M_W, M_H, m_f, e, V_{ij}, \quad (2.34)$$

---

<sup>3</sup>A direct measurement of the quark masses is, due to quark confinement into the hadrons, not possible. The only exception is the top quark, whose mass has been measured for the first time by the CDF experiment in 1994 [1].

which are used to parametrize the theory. In particular, the experimental values in Eq. (2.34) can be identified with the input parameters of the SM at tree level. However, higher-order calculations imply loop integrals that give rise to *ultraviolet (UV) divergences*, for large internal momenta, avoiding a physical interpretation of the parameters of the Lagrangian. A *renormalization procedure* is thus necessary to parametrize the theory in terms of physically measurable quantities. Indeed, in Refs. [69, 70] 't Hooft proved that all the non-abelian gauge theories with SSB, including the SM, are renormalizable, i.e. all UV divergences can be absorbed into input parameters by a redefinition of a finite number of parameters and fields of the Lagrangian, at each perturbative order. In this thesis the UV divergences are regularized using *dimensional regularization* [71, 72].

In the following, we briefly discuss one of the possible ways to renormalize the SM. We choose the *on-shell renormalization scheme* [73] and use the *counterterms approach* [22], which separates the *bare quantities*  $f_0$  into finite renormalized ones  $f$  plus the remaining contributions  $\delta f$ , containing also the UV divergences, which are fixed by the renormalization conditions and are known as *counterterms*. More details can be found in Ref. [22].

- **Mass parameters:**

For the SM mass parameters the renormalization transformation reads as follows:

$$\begin{aligned} M_{W,0}^2 &= M_W^2 + \delta M_W^2, \\ M_{Z,0}^2 &= M_Z^2 + \delta M_Z^2, \\ M_{H,0}^2 &= M_H^2 + \delta M_H^2, \\ m_{f,i,0} &= m_{f,i} + \delta m_{f,i}. \end{aligned} \quad (2.35)$$

We require, as a renormalization condition, that the renormalized mass parameters are equal to the physical masses, which are the real parts of the location of the pole of the particle propagators. This yields [22]

$$\begin{aligned} \delta M_W^2 &= \text{Re } \Sigma_T^W(M_W^2), \\ \delta M_Z^2 &= \text{Re } \Sigma_T^{ZZ}(M_Z^2), \\ \delta M_H^2 &= \text{Re } \Sigma_T^H(M_H^2), \end{aligned} \quad (2.36)$$

$$\delta m_{f,i} = \frac{m_{f,i}}{2} \text{Re} \left( \Sigma_{ii}^{f,L}(m_{f,i}^2) + \Sigma_{ii}^{f,R}(m_{f,i}^2) + 2\Sigma_{ii}^{f,S}(m_{f,i}^2) \right), \quad (2.37)$$

where  $\Sigma_T$  are the unrenormalized transverse self-energies of the bosons. In Eq. (2.37),  $L$ ,  $R$  and  $S$  are the left-handed, right-handed, and scalar parts of the fermions self-energies  $\Sigma^f$ , respectively.

- **Weak mixing angle:**

In the on-shell scheme the weak mixing angle of Eq. (2.22) is not a free parameter and is fixed by the relation

$$c_w^2 = 1 - s_w^2 = \frac{M_W^2}{M_Z^2}. \quad (2.38)$$

It is, however, convenient to introduce renormalization constants as follows

$$c_{w,0} = c_w + \delta c_w, \quad s_{w,0} = s_w + \delta s_w, \quad (2.39)$$

where

$$\frac{\delta c_w}{c_w} = -\frac{s_w^2}{c_w^2} \frac{\delta s_w}{s_w} = \frac{1}{2} \left( \frac{\delta M_W^2}{M_W^2} - \frac{\delta M_Z^2}{M_Z^2} \right). \quad (2.40)$$

- **Fields:**

The renormalization of the parameters appearing in Eq. (2.34) is sufficient to make the S-matrix finite<sup>4</sup>. However, the Green functions remain divergent unless a renormalization of the fields is carried out:

$$\begin{aligned} W_0^\pm &= (1 + \frac{1}{2}\delta Z_W)W^\pm, \\ \begin{pmatrix} Z_0 \\ A_0 \end{pmatrix} &= \begin{pmatrix} 1 + \frac{1}{2}\delta Z_{ZZ} & \frac{1}{2}\delta Z_{ZA} \\ \frac{1}{2}\delta Z_{AZ} & 1 + \frac{1}{2}\delta Z_{AA} \end{pmatrix} \begin{pmatrix} Z \\ A \end{pmatrix}, \\ f_{i,0}^L &= (1 + \frac{1}{2}\delta Z_{ii}^{f,L})f_i^L, \\ f_{i,0}^R &= (1 + \frac{1}{2}\delta Z_{ii}^{f,R})f_i^R. \end{aligned} \quad (2.41)$$

On-shell renormalization conditions for the fields demand that, for on-shell momenta, the residues of the particle propagators are equal to one. Consequently, no external legs corrections have to be considered in the calculation of the S-matrix elements, and the fields' renormalization constants are [22]

$$\begin{aligned} \delta Z_W &= -\text{Re} \left. \frac{\partial \Sigma_T^W(k^2)}{\partial k^2} \right|_{k^2=M_W^2}, \quad \delta Z_{AZ} = -2 \text{Re} \frac{\Sigma_T^{AZ}(M_Z^2)}{M_Z^2}, \\ \delta Z_{ZZ} &= -\text{Re} \left. \frac{\partial \Sigma_T^{ZZ}(k^2)}{\partial k^2} \right|_{k^2=M_Z^2}, \quad \delta Z_{ZA} = -2 \text{Re} \frac{\Sigma_T^{AZ}(0)}{M_Z^2}, \quad \delta Z_{AA} = -\left. \frac{\partial \Sigma_T^{AA}(k^2)}{\partial k^2} \right|_{k^2=0}, \\ \delta Z_{ii}^{f,L} &= -\text{Re} \Sigma_{ii}^{f,L}(m_{f,i}^2) - m_{f,i}^2 \frac{\partial}{\partial k^2} \text{Re} \left[ \Sigma_{ii}^{f,L}(k^2) + \Sigma_{ii}^{f,R}(k^2) + 2\Sigma_{ii}^{f,S}(k^2) \right] \Big|_{k^2=m_{f,i}^2}, \\ \delta Z_{ii}^{f,R} &= -\text{Re} \Sigma_{ii}^{f,R}(m_{f,i}^2) - m_{f,i}^2 \frac{\partial}{\partial k^2} \text{Re} \left[ \Sigma_{ii}^{f,L}(k^2) + \Sigma_{ii}^{f,R}(k^2) + 2\Sigma_{ii}^{f,S}(k^2) \right] \Big|_{k^2=m_{f,i}^2}. \end{aligned} \quad (2.42)$$

- **Electric charge renormalization:**

To renormalize the electric coupling constant we define the renormalized electric charge  $e$  to coincide with the  $ee\gamma$ -coupling of on-shell electrons [22], in the Thomson limit (zero-momentum transfer of the photon):

$$e_0 = (1 + \delta Z_e)e, \quad \text{with} \quad \delta Z_e = -\frac{1}{2}\delta Z_{AA} - \frac{s_w}{c_w} \frac{1}{2}\delta Z_{ZA}. \quad (2.43)$$

The result does not depend on the fermion species.

---

<sup>4</sup>In this work we consider a unit CKM matrix, therefore there is no need to renormalize  $V_{ij}$  (more details can be found in Ref. [22]).

The procedure of the renormalization has to be applied to all the quantities appearing in the Lagrangian density. It is therefore possible to rewrite

$$\mathcal{L}_0 = \mathcal{L} + \delta\mathcal{L}, \quad (2.44)$$

where  $\mathcal{L}$  and  $\mathcal{L}_0$  depend (in the same form) on the renormalized, and on the bare fields and parameters, respectively. The appearance of counterterms introduces new Feynman rules for vertices and propagators. The ones relevant for this work are listed in App. C.

In this thesis we use the  $G_\mu$ -input parameter scheme: The fine-structure constant  $\alpha$  is derived from the Fermi constant

$$G_\mu = \frac{\pi\alpha}{\sqrt{2}s_w^2 M_W^2} (1 + \Delta r), \quad (2.45)$$

where

$$\begin{aligned} \Delta r = & \left. \frac{\partial \Sigma_T^{AA}}{\partial q^2} \right|_{q^2=0} - \frac{c_w^2}{s_w^2} \left( \frac{\Sigma_T^{ZZ}(M_Z^2)}{M_Z^2} - \frac{\Sigma_T^{WW}(M_W^2)}{M_W^2} \right) \frac{\Sigma_T^{WW}(0) - \Sigma_T^{WW}(M_W^2)}{M_W^2} + \\ & + 2 \frac{c_w}{s_w} \frac{\Sigma_T^{AZ}(0)}{M_Z^2} + \frac{\alpha}{4\pi s_w^2} \left( 6 + \frac{7 - 4s_w^2}{2s_w^2} \ln c_w^2 \right) \end{aligned} \quad (2.46)$$

is the *radiative correction to muon decay* [74–76]. The quantity  $G_\mu$  can be indeed easily obtained from the *muon lifetime*  $\tau_\mu$ , which is very precisely measured by experiments [77, 78]. Technically, the  $G_\mu$ -scheme implies a shift of the electric charge counterterm

$$\delta Z_e \rightarrow \delta Z_e - \frac{\Delta r}{2}. \quad (2.47)$$

## 2.3 Unstable particles and the complex-mass scheme

In the SM there are unstable particles, such as  $W$ ,  $Z$ ,  $H$  bosons and the top quark, which have a very short lifetime and can be therefore experimentally detected only via their decay products. Their reconstructed invariant-mass distribution has a resonant peak around the mass value  $M$ , described by a Breit-Wigner shape with a finite width  $\Gamma$ .

In perturbation theory, the width  $\Gamma$  enters the calculation via a Dyson summation of self-energy insertions in the resonant propagators. However, the procedure of the summation generally violates gauge invariance: It leads to a mixing of perturbative orders, which can spoil the cancellation of gauge-dependent terms, and destroys Slavnov-Taylor and Ward identities [79, 80].

There are many way to perform a calculation which involves unstable particles (see Ref. [81]). For simplicity, one often works with approximations. One example is the *narrow-width approximation* (NWA), which considers the unstable particles on-shell and assumes  $\Gamma \ll M$ . This allows to factorize a process into the production of the unstable particle and its subsequent decay. The NWA gives a description of the theory correct up to order  $\mathcal{O}(\Gamma/M)$  [81, 82], even though it has several limitations, as described in Ref. [83]. More details on the NWA are presented in App. A.

In this thesis we use the *complex-mass scheme* (CMS) [9–11], a method that takes into account the effects of the instability and the off-shellness of the unstable particle in a gauge

invariant way, providing a consistent procedure at the one-loop level.

The main idea of the CMS is to consider the squared boson masses as complex quantities, defined as follows

$$\mu_V^2 = M_V^2 - iM_V\Gamma_V, \quad \text{with } V = W, Z, \quad (2.48)$$

and to introduce them directly in the Lagrangian density. To preserve gauge invariance, the complex masses have to be introduced everywhere. This implies new counterterms and a redefinition of the weak mixing angle,

$$c_w^2 = 1 - s_w^2 = \frac{\mu_W^2}{\mu_Z^2}. \quad (2.49)$$

Moreover the whole renormalization procedure has to be generalized for the case of unstable particles. In the following we will briefly describe the new counterterms. More details can be found in Refs. [10, 11].

The renormalization of the theory follows the same idea introduced in Sect. 2.2. First the bare parameters (with the subscript 0) and fields split into complex renormalized quantities and the corresponding complex counterterms,

$$\begin{aligned} M_{V,0}^2 &= \mu_V^2 + \delta\mu_V^2, \\ W_0^\pm &= (1 + \frac{1}{2}\delta\mathcal{Z}_W)W^\pm, \\ \begin{pmatrix} Z_0 \\ A_0 \end{pmatrix} &= \begin{pmatrix} 1 + \frac{1}{2}\delta\mathcal{Z}_{ZZ} & \frac{1}{2}\delta\mathcal{Z}_{ZA} \\ \frac{1}{2}\delta\mathcal{Z}_{AZ} & 1 + \frac{1}{2}\delta\mathcal{Z}_{AA} \end{pmatrix} \begin{pmatrix} Z \\ A \end{pmatrix}, \\ f_0^\sigma &= (1 + \frac{1}{2}\delta\mathcal{Z}^{f,\sigma})f^\sigma, \quad \text{with } \sigma = L, R, \\ c_{w,0} &= c_w + \delta c_w, \quad s_{w,0} = s_w + \delta s_w, \\ e_0 &= (1 + \delta\mathcal{Z}_e)e. \end{aligned} \quad (2.50)$$

In the previous equation we have used the same notation as in Sect. 2.2 and the quantities  $\delta\mathcal{Z}$  denote the complex counterterms. Then the renormalization conditions are applied to fix the new counterterms, which read [10]

$$\begin{aligned} \delta\mu_W^2 &= \Sigma_T^W(\mu_W^2), \quad \delta\mu_Z^2 = \Sigma_T^{ZZ}(\mu_Z^2), \quad \delta\mathcal{Z}_W = - \frac{\partial\Sigma_T^W(k^2)}{\partial k^2} \Big|_{k^2=\mu_W^2}, \\ \delta\mathcal{Z}_{ZZ} &= - \frac{\partial\Sigma_T^{ZZ}(k^2)}{\partial k^2} \Big|_{k^2=\mu_Z^2}, \quad \delta\mathcal{Z}_{AZ} = - \frac{2}{\mu_Z^2} \Sigma_T^{AZ}(\mu_Z^2), \\ \delta\mathcal{Z}_{ZA} &= \frac{2}{\mu_Z^2} \Sigma_T^{AZ}(0), \quad \delta\mathcal{Z}_{AA} = - \frac{\partial\Sigma_T^{AA}(k^2)}{\partial k^2} \Big|_{k^2=0}, \\ \delta\mathcal{Z}^{f,\sigma} &= - \Sigma^{f,\sigma}(m_f^2) - m_f^2 \frac{\partial}{\partial k^2} [\Sigma^{f,L}(k^2) + \Sigma^{f,R}(k^2) + 2\Sigma^{f,S}(k^2)] \Big|_{k^2=m_f^2}, \\ \frac{\delta c_w}{c_w} &= - \frac{s_w^2}{c_w^2} \frac{\delta s_w}{s_w} = \frac{1}{2} \left( \frac{\delta\mu_W^2}{\mu_W^2} - \frac{\delta\mu_Z^2}{\mu_Z^2} \right), \quad \delta\mathcal{Z}_e = - \frac{1}{2} \delta\mathcal{Z}_{AA} - \frac{s_w}{c_w} \frac{1}{2} \delta\mathcal{Z}_{ZA}. \end{aligned} \quad (2.51)$$

In Eq. (2.51) the self-energies in the first two rows appear with complex momenta. To avoid the analytic continuation of the 2-point functions to the unphysical Riemann sheet, the expressions can be expanded around the real masses  $M_V$ ,

$$\begin{aligned}
\Sigma_T^W(\mu_W^2) &= \Sigma_T^W(M_W^2) + (\mu_W^2 - M_W^2) \left. \frac{\partial \Sigma_T^W(k^2)}{\partial k^2} \right|_{k^2=M_W^2} + c_T^W + \mathcal{O}(\alpha^3), \\
\Sigma_T^{ZZ}(\mu_Z^2) &= \Sigma_T^{ZZ}(M_Z^2) + (\mu_Z^2 - M_Z^2) \left. \frac{\partial \Sigma_T^{ZZ}(k^2)}{\partial k^2} \right|_{k^2=M_Z^2} + \mathcal{O}(\alpha^3), \\
\frac{1}{\mu_Z^2} \Sigma_T^{AZ}(\mu_Z^2) &= \frac{1}{\mu_Z^2} \Sigma_T^{AZ}(0) + \frac{1}{M_Z^2} \Sigma_T^{AZ}(M_Z^2) - \frac{1}{M_Z^2} \Sigma_T^{AZ}(0) + \mathcal{O}(\alpha^2).
\end{aligned} \tag{2.52}$$

We have added the constant term  $c_T^W = \frac{\alpha}{\pi}(M_W^2 - \mu_W^2)$ , which originates from the non-analytic terms from photon exchange (more details in Ref. [10]). The first five counterterms of Eq. (2.51) can be thus replaced by

$$\begin{aligned}
\delta\mu_W^2 &= \Sigma_T^W(M_W^2) + (\mu_W^2 - M_W^2) \left. \frac{\partial \Sigma_T^W(k^2)}{\partial k^2} \right|_{k^2=M_W^2} + c_T^W, \\
\delta\mu_Z^2 &= \Sigma_T^{ZZ}(M_Z^2) + (\mu_Z^2 - M_Z^2) \left. \frac{\partial \Sigma_T^{ZZ}(k^2)}{\partial k^2} \right|_{k^2=M_Z^2}, \\
\delta\mathcal{Z}_W &= - \left. \frac{\partial \Sigma_T^W(k^2)}{\partial k^2} \right|_{k^2=M_W^2}, \quad \delta\mathcal{Z}_{ZZ} = - \left. \frac{\partial \Sigma_T^{ZZ}(k^2)}{\partial k^2} \right|_{k^2=M_Z^2}, \\
\delta\mathcal{Z}_{AZ} &= - \frac{2}{M_Z^2} \Sigma_T^{AZ}(M_Z^2) + \left( \frac{\mu_Z^2}{M_Z^2} - 1 \right) \delta\mathcal{Z}_{ZA}.
\end{aligned} \tag{2.53}$$

In the CMS the radiative correction to the muon decay (Eq. (2.46)) can be rewritten as

$$\Delta r = -\delta\mathcal{Z}_{AA} + \frac{\Sigma_T^W(0) - \delta\mu_W^2}{\mu_W^2} - 2 \frac{\delta s_w}{s_w} + \frac{c_w}{s_w} \delta\mathcal{Z}_{ZA} + \frac{\alpha}{4\pi s_w^2} \left( 6 + \frac{7 - 4s_w^2}{2s_w^2} \ln \frac{\mu_W^2}{\mu_Z^2} \right). \tag{2.54}$$

Even though the CMS introduces complex masses and couplings, making the Cutkosky cutting rules invalid, it preserve the unitarity of the theory at NLO, as proven in Ref. [84].



# Chapter 3

## Calculation of the amplitudes

A general decay width is obtained integrating the squared amplitude of the process,

$$\overline{\sum} |\mathcal{M}(p; p_1, \dots, p_n)|^2, \quad (3.1)$$

over the phase-space volume times a flux factor:

$$\Gamma_n = \frac{(2\pi)^{4-3n}}{2m} \int \left[ \prod_{i=1}^n d^4 p_i \delta(p_i^2 - m_i^2) \theta(p_i^0) \right] \delta^{(4)} \left( p - \sum_{i=1}^n p_i \right) \overline{\sum} |\mathcal{M}(p; p_1, \dots, p_n)|^2, \quad (3.2)$$

where  $p$  and  $m$  are the momentum and the mass of the decaying particle, and  $p_i$  and  $m_i$  are the momenta and the masses of the  $n$  outgoing particles, respectively. The symbol  $\overline{\sum}$  takes into account the average of the initial spins and colours and the sum over all possible final polarizations and colours. In Eq. (3.2) the on-shell conditions are imposed on the momenta, the energy is required to be positive, and the four-momentum is conserved.

An approximated value of  $\Gamma_n$  can be estimated calculating the leading order (LO) prediction. More accurate values can be obtained by considering higher orders in perturbation theory. The next-to-leading order (NLO) corrections comprise the real emission of a gluon (QCD corrections) or photon (EW corrections), and one-loop diagrams (virtual corrections) together with the corresponding counterterms.

The aim of this thesis is to calculate the NLO QCD and EW corrections to the top-quark partial decay width, for both the cases of a semileptonic,  $t \rightarrow b \nu_\ell \ell^+$ , and a hadronic,  $t \rightarrow b q \bar{q}'$ , decay. In the following we will omit the term 'partial' for the decay width into a specific final state, unless an ambiguity of the text would explicitly required. In this work the top and the bottom quarks are massive, while the other fermions appearing in the process are considered massless. Moreover, with  $t \rightarrow b u \bar{d}$  we will refer to both  $t \rightarrow b u \bar{d}$  and  $t \rightarrow b c \bar{s}$  processes. The details of the calculation are presented in the following chapters.

There are different methods to evaluate the necessary matrix elements, e.g. the usual Dirac formalism or spinorial formalisms. In this thesis a spinorial technique, the Weyl–van-der-Waerden formalism, as e.g. formulated in Ref. [85], has been used and is briefly described in Sect. 3.1. The result for the Born amplitude is shown in Sect. 3.2 and the squared matrix elements for the real emission are listed in Sect. 3.3. Section 3.4 describes how to calculate the virtual contributions and the corresponding counterterms.

### 3.1 The Weyl–van-der-Waerden formalism

The main idea of the Weyl–van-der-Waerden (WvdW) formalism is to reduce all higher-dimensional Lorentz structures (i.e. Dirac matrices, polarization vectors, four-vectors) to the two-dimensional irreducible representations  $D(\frac{1}{2}, 0)$  and  $D(0, \frac{1}{2})$ . While with the conventional approaches the number of terms grows quadratically with the number of diagrams (squared amplitudes and completeness relations), with the WvdW formalism the squaring of the amplitudes is performed numerically. A sum over the different helicity contributions is required, but the calculation can be simplified employing discrete symmetries.

In the following the basic concept of the WvdW spinor technique, used in our calculation, is presented. More details on the formalism can be found in Ref. [85], which we follow closely.

#### Spinors

The WvdW spinors,  $\psi_A$  and  $\psi^{\dot{A}}$ , belong to the representations  $D(\frac{1}{2}, 0)$  and  $D(0, \frac{1}{2})$ , respectively, and are called covariant and contravariant. Their complex conjugation (denoted by dotting) is defined as

$$\psi_{\dot{A}} = (\psi_A)^*, \quad \psi^A = (\psi^{\dot{A}})^*, \quad (3.3)$$

and their indices can be lowered and raised,

$$\psi^A = \epsilon^{AB} \psi_B, \quad \psi^{\dot{A}} = \epsilon^{\dot{A}\dot{B}} \psi_{\dot{B}}, \quad \psi_A = \psi^B \epsilon_{BA}, \quad \psi_{\dot{A}} = \psi^{\dot{B}} \epsilon_{\dot{B}\dot{A}}, \quad (3.4)$$

using the antisymmetric matrix

$$\epsilon_{AB} = \epsilon_{\dot{A}\dot{B}} = \epsilon^{AB} = \epsilon^{\dot{A}\dot{B}} = \begin{pmatrix} 0 & +1 \\ -1 & 0 \end{pmatrix}. \quad (3.5)$$

This allows to define a Lorentz-invariant spinor product

$$\begin{aligned} \langle \phi \psi \rangle &= \phi_A \psi^A = \phi_A \epsilon^{AB} \psi_B = \phi_1 \psi_2 - \phi_2 \psi_1 = -\langle \psi \phi \rangle, \\ \langle \phi \psi \rangle^* &= \phi_{\dot{A}} \psi^{\dot{A}} = \phi_{\dot{A}} \epsilon^{\dot{A}\dot{B}} \psi_{\dot{B}} = (\phi_1 \psi_2 - \phi_2 \psi_1)^* = -\langle \psi \phi \rangle^*. \end{aligned} \quad (3.6)$$

#### Four-vectors

The four-vector  $k^\mu$  can be rewritten in the  $D(\frac{1}{2}, \frac{1}{2}) = D(\frac{1}{2}, 0) \otimes D(0, \frac{1}{2})$  representation as

$$K_{\dot{A}B} = k^\mu \sigma_{\mu, \dot{A}B} = \begin{pmatrix} k^0 + k^3 & k^1 + ik^2 \\ k^1 - ik^2 & k^0 - k^3 \end{pmatrix}, \quad (3.7)$$

where  $\sigma_{\mu, \dot{A}B} = (\sigma^0, -\boldsymbol{\sigma})$ ,  $\boldsymbol{\sigma}$  are the standard Pauli matrices, and  $\sigma^0 = \mathbb{1}$ . The Minkowski product between two vectors  $k^\mu$  and  $p^\mu$  is given by

$$2k \cdot p = 2k_\mu g^{\mu\nu} p_\nu = K_{\dot{A}B} P^{\dot{A}B}, \quad (3.8)$$

where the hermiticity of the  $\boldsymbol{\sigma}$  matrices and the relations

$$\sigma_{\dot{A}B}^\mu = \sigma_{B\dot{A}}^\mu, \quad \sigma^{\mu, \dot{A}B} = \sigma^{\mu, B\dot{A}}, \quad \sigma_{\dot{A}B}^\mu \sigma^{\nu, \dot{A}B} = 2g^{\mu\nu}, \quad (3.9)$$

have been used. The decomposition of  $K_{\dot{A}B}$  into spinors reads for time-like vectors ( $k^2 > 0$ )

$$K_{\dot{A}B} = \sum_{i=1,2} \kappa_{i,\dot{A}} \kappa_{i,B} \quad \text{with} \quad \kappa_{i,A} = \sqrt{\lambda_i} n_{i,A}, \quad (3.10)$$

where  $n_{i,A}$  are the normalized eigenvectors and  $\lambda_i$  the eigenvalues, defined as

$$n_{1,A} = \begin{pmatrix} e^{-i\phi} \cos \frac{\theta}{2} \\ \sin \frac{\theta}{2} \end{pmatrix}, \quad n_{2,A} = \begin{pmatrix} \sin \frac{\theta}{2} \\ -e^{+i\phi} \cos \frac{\theta}{2} \end{pmatrix}, \quad \lambda_{1,2} = k^0 \pm |\mathbf{k}|. \quad (3.11)$$

Here  $\theta$  and  $\phi$  represent the polar and the azimuthal angles of  $\mathbf{k}$ , respectively. In case of a light-like vector ( $k^2 = 0$ ) the eigenvalue  $\lambda_2$  vanishes and

$$K_{\dot{A}B} = \kappa_{1,\dot{A}} \kappa_{1,B}, \quad \kappa_{1,A} = \sqrt{2k^0} n_{1,A}. \quad (3.12)$$

### Spin- $\frac{1}{2}$ particles

The Dirac spinors  $\Psi$  transform in the direct sum representation  $D(\frac{1}{2}, 0) \oplus D(0, \frac{1}{2})$  and can be decomposed into a pair of covariant and contravariant spinors:

$$\Psi = \begin{pmatrix} \phi_A \\ \psi^{\dot{A}} \end{pmatrix}. \quad (3.13)$$

In particular, after solving the Dirac equation for massive particles, we obtain the solutions  $\Psi = \exp\{\mp i k x\} \Psi_k^{(\pm)}$ , where  $\Psi_k^{(\pm)}$  is defined, depending on the helicity  $\sigma$ , for the massive and massless cases in Table 3.1.

	Massless		Massive	
	$\sigma = +$	$\sigma = -$	$\sigma = +$	$\sigma = -$
IF	$\Psi_{k,1}^{(+)} = \begin{pmatrix} \kappa_{1,A} \\ 0 \end{pmatrix}$	$\Psi_{k,2}^{(+)} = \begin{pmatrix} 0 \\ \kappa_1^{\dot{A}} \end{pmatrix}$	$\Psi_{k,1}^{(+)} = \begin{pmatrix} \kappa_{1,A} \\ -\kappa_2^{\dot{A}} \end{pmatrix}$	$\Psi_{k,2}^{(+)} = \begin{pmatrix} \kappa_{2,A} \\ \kappa_1^{\dot{A}} \end{pmatrix}$
IA	$\bar{\Psi}_{k,2}^{(-)} = (\kappa_1^A, 0)$	$\bar{\Psi}_{k,1}^{(-)} = (0, \kappa_{1,\dot{A}})$	$\bar{\Psi}_{k,2}^{(-)} = (\kappa_1^A, -\kappa_{2,\dot{A}})$	$\bar{\Psi}_{k,1}^{(-)} = (\kappa_2^A, \kappa_{1,\dot{A}})$
OF	$\bar{\Psi}_{k,1}^{(+)} = (0, \kappa_{1,\dot{A}})$	$\bar{\Psi}_{k,2}^{(+)} = (\kappa_1^A, 0)$	$\bar{\Psi}_{k,1}^{(+)} = (-\kappa_2^A, \kappa_{1,\dot{A}})$	$\bar{\Psi}_{k,2}^{(+)} = (\kappa_1^A, \kappa_{2,\dot{A}})$
OA	$\Psi_{k,2}^{(-)} = \begin{pmatrix} 0 \\ \kappa_1^{\dot{A}} \end{pmatrix}$	$\Psi_{k,1}^{(-)} = \begin{pmatrix} \kappa_{1,A} \\ 0 \end{pmatrix}$	$\Psi_{k,2}^{(-)} = \begin{pmatrix} -\kappa_{2,A} \\ \kappa_1^{\dot{A}} \end{pmatrix}$	$\Psi_{k,1}^{(-)} = \begin{pmatrix} \kappa_{1,A} \\ +\kappa_2^{\dot{A}} \end{pmatrix}$

Table 3.1: Helicity eigenstates for spin- $\frac{1}{2}$  massless and massive particles.  $\sigma$  is the helicity, IF stands for incoming fermion, IA for incoming antifermion, OF for outgoing fermion, and OA for outgoing antifermion.

## Spin-1 particles

We distinguish two cases:

### - Massive particles:

They are described by three orthogonal polarization vectors,  $\varepsilon_{\pm}^{\mu}(k)$  and  $\varepsilon_0^{\mu}$ , that transform under Lorentz transformations as four-vectors.

For incoming spin-1 particles the polarization vectors are

$$\begin{aligned}\varepsilon_{+,AB}(k) &= \sqrt{2} n_{2,\dot{A}} n_{1,B}, & \varepsilon_{-,AB}(k) &= \sqrt{2} n_{1,\dot{A}} n_{2,B}, \\ \varepsilon_{0,AB}(k) &= \frac{1}{m} (\kappa_{1,\dot{A}} \kappa_{1,B} - \kappa_{2,\dot{A}} \kappa_{2,B}),\end{aligned}\tag{3.14}$$

while in the case of outgoing spin-1 particles they are

$$\begin{aligned}\varepsilon_{+,AB}^*(k) &= \sqrt{2} n_{1,\dot{A}} n_{2,B}, & \varepsilon_{-,AB}^*(k) &= \sqrt{2} n_{2,\dot{A}} n_{1,B}, \\ \varepsilon_{0,AB}^*(k) &= \frac{1}{m} (\kappa_{1,\dot{A}} \kappa_{1,B} - \kappa_{2,\dot{A}} \kappa_{2,B}),\end{aligned}\tag{3.15}$$

where  $n_{i,A}$  and  $\kappa_{i,A}$  are defined in Eqs. (3.10) and (3.11), respectively, and  $m$  is the mass of the particle.

### - Massless particles:

In case of massless particles, the longitudinal polarization does not exist. For this reason a new degree of freedom appears for  $\varepsilon_{\pm}^{\mu}(k)$  in the form of an arbitrary gauge. In more detail, the polarization vectors read

$$\begin{aligned}\varepsilon_{+,AB}(k) &= \frac{\sqrt{2} g_{+,\dot{A}} k_B}{\langle g_+ k \rangle^*}, & \varepsilon_{-,AB}(k) &= \frac{\sqrt{2} k_{\dot{A}} g_{-,B}}{\langle g_- k \rangle}, \\ \varepsilon_{+,AB}^*(k) &= \frac{\sqrt{2} k_{\dot{A}} g_{+,B}}{\langle g_+ k \rangle}, & \varepsilon_{-,AB}^*(k) &= \frac{\sqrt{2} g_{-,\dot{A}} k_B}{\langle g_- k \rangle^*},\end{aligned}\tag{3.16}$$

where  $g_{\pm,A}$  are arbitrary spinors, with  $\langle g_{\pm} k \rangle \neq 0$ , called *gauge spinors*. Of course, gauge-invariant quantities do not depend on the choice of  $g_{\pm,A}$ . In our calculation the gauge spinors

$$g_{\pm,A} = g_A = P_{A\dot{B}} k^{\dot{B}} = \sum_{i=1,2} \kappa_{i,A} \langle \kappa_i k \rangle^* \tag{3.17}$$

have been chosen, and consequently

$$\langle gk \rangle = 2pk. \tag{3.18}$$

Following the prescriptions listed above, we are now able to write down the Feynman rules in terms of the WvdW formalism. In App. C, the propagators and the vertices used in this work are listed. The calculation of the different matrix elements is described in the following sections.

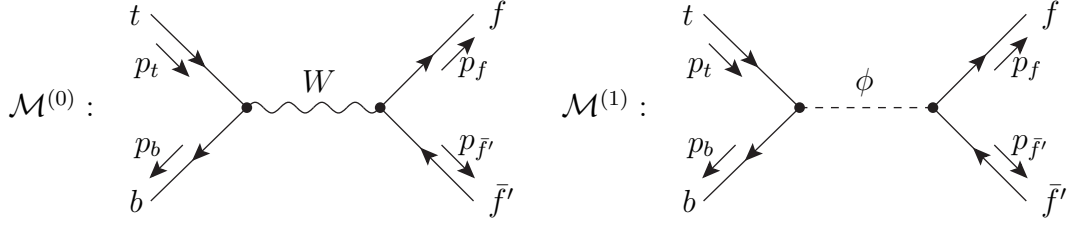


Figure 3.1: LO diagrams for the process  $t(p_t) \rightarrow b(p_b) f(p_f) \bar{f}(p_{\bar{f}})$ .

## 3.2 Born Amplitudes

For the Born amplitude of the processes represented in Fig. 3.1, we need to define the different spinors

$$\Psi_t = \begin{pmatrix} \phi_A \\ \psi^{\dot{A}} \end{pmatrix}, \quad \bar{\Psi}_b = (\phi'^A, \psi'_{\dot{A}}), \quad \bar{\Psi}_f = (\alpha^A, \beta_{\dot{A}}), \quad \Psi_{\bar{f}} = \begin{pmatrix} \alpha'_{\dot{A}} \\ \beta'^A \end{pmatrix}, \quad (3.19)$$

following Table 3.1. With some algebra (see App. C), the LO matrix element is

$$\mathcal{M}^{(0)} = \frac{K}{D_0} \langle \psi' \beta \rangle \langle \psi \beta' \rangle^*, \quad (3.20)$$

with

$$K = 2 \frac{e^2}{2s_w^2} \quad \text{and} \quad D_0 = (p_t - p_b)^2 - \mu_W^2. \quad (3.21)$$

The triple scalar-fermion-fermion vertex is proportional to the fermion's masses. In this thesis the fermions stemming from the  $W$ -boson decay are considered as massless. For this reason  $\mathcal{M}^{(1)}$  is zero.

Since the  $W$  boson is an unstable particle, a complex mass  $\mu_W$  is used in the calculation (see Sect. 2.3). The Born amplitude can be calculated taking the squared absolute value of the LO matrix element  $\mathcal{M}_0$ , summed over all possible polarizations and colours ( $N_c = 1$  for the semileptonic decay and  $N_c = 3$  for the hadronic decay), and taking the average over the initial spin and colours:

$$\overline{\sum} |\mathcal{M}_0|^2 = \frac{1}{2} \cdot \frac{1}{3} \cdot N_c \cdot \sum_{pol} |\mathcal{M}^{(0)}|^2. \quad (3.22)$$

## 3.3 Real corrections

The contribution given by the real corrections is presented in four different cases, depending on the type of corrections (QCD for the emission of a gluon or EW for the emission of a photon) and on the decay products of the  $W$  boson (leptonic or hadronic decay). In the following we illustrate the analytical results of the amplitudes for the real emission (denoted by the subscript 1). The issue of soft and collinear singularities appearing during the integration, and the phase-space integration itself are described in more detail in Chaps. 4 and 5, respectively.

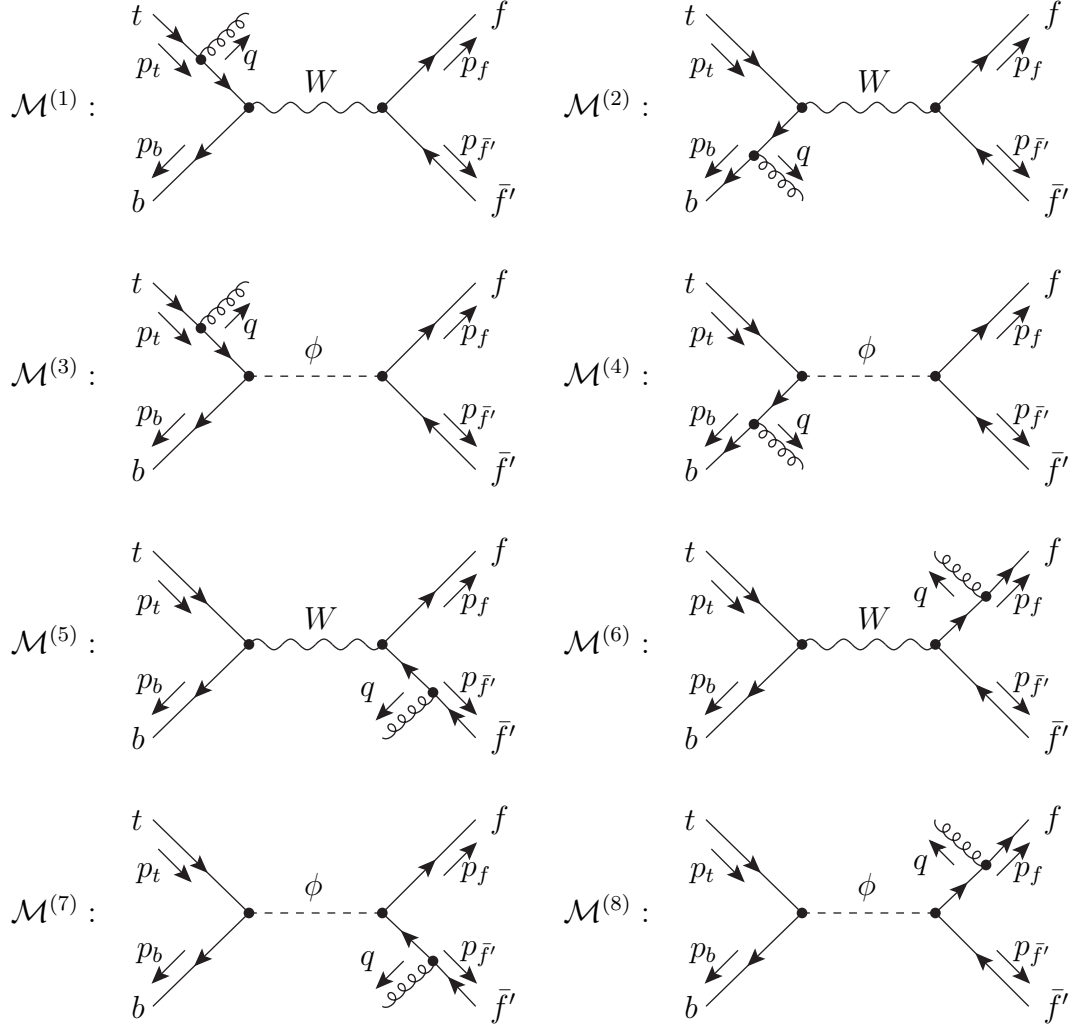


Figure 3.2: Diagrams contributing to the process  $t(p_t) \rightarrow b(p_b) f(p_f) \bar{f}'(p_{\bar{f}'}) g(q)$  in lowest order.

### QCD corrections to $t(p_t) \rightarrow b(p_b) \nu_\ell(p_\nu) \ell(p_\ell)$

A gluon can be emitted either by the  $t$  or the  $b$  quarks, as shown in the first four diagrams of Fig. 3.2, with  $f = \nu_\ell$  and  $\bar{f}' = \ell^+$ .

The matrix elements  $\mathcal{M}^{(3)}$  and  $\mathcal{M}^{(4)}$  are zero, due to the fact that the lepton and the neutrino are massless, therefore only two matrix elements have to be calculated:

$$\begin{aligned} \mathcal{M}^{(1)} &= \frac{A}{D_1 D_2} \langle \psi' \beta \rangle [\langle \phi \beta' \rangle^* \langle \psi | \lambda | \phi \rangle + \langle \psi \beta' \rangle^* \langle \psi | \lambda | \psi \rangle - \langle q \beta' \rangle^* \langle \psi | \lambda | q \rangle - m_t \langle \beta' | \lambda | \phi \rangle], \\ \mathcal{M}^{(2)} &= -\frac{A}{D_2 D_3} \langle \psi \beta' \rangle^* [\langle \phi' \beta \rangle \langle \phi' | \lambda | \psi' \rangle + \langle \psi' \beta \rangle \langle \psi' | \lambda | \psi' \rangle + \langle q \beta \rangle \langle q | \lambda | \psi' \rangle - m_b \langle \phi' | \lambda | \beta \rangle], \end{aligned} \quad (3.23)$$

where the spinors are defined in Eq. (3.19), and

$$D_1 = (p_e + p_\nu)^2 - \mu_W^2, \quad D_2 = 2p_t q, \quad D_3 = 2p_b q, \quad A = 2 \frac{e^2}{2s_w^2} \sqrt{4\pi\alpha_s} t^a, \quad (3.24)$$

with  $t^a$  the colour factor, with  $\sum_a t^a t^a = C_F \mathbb{1}$  and  $C_F = \frac{4}{3}$ . In Eq. (3.23) the spinorial product

$$\langle \psi | \lambda | \phi \rangle = \psi^{\dot{A}} \varepsilon_{\lambda, \dot{A} B} \phi^B \quad (3.25)$$

is defined,  $m_t$  and  $m_b$  are the top and the bottom quark masses, and  $q$  is the gluon momentum. To calculate the contribution given by the real amplitude we need to square the sum of the two matrix elements,

$$\overline{\sum} |\mathcal{M}_1|^2 = \frac{1}{2} \cdot \frac{1}{3} \cdot 3 \cdot \sum_{pol} |\mathcal{M}^{(1)} + \mathcal{M}^{(2)}|^2. \quad (3.26)$$

### QCD corrections to $t(p_t) \rightarrow b(p_b) u(p_u) \bar{d}(p_d)$

For the hadronic decay of the  $W$  boson, the QCD corrections have to take into account not only the emission of the gluon from the  $t$  and  $b$  quarks, but also the cases when the gluon is emitted by the  $u$  and  $\bar{d}$  quarks (Fig. 3.2, with  $f = u$  and  $\bar{f}' = \bar{d}$ ). The matrix elements  $\mathcal{M}^{(3)}$ ,  $\mathcal{M}^{(4)}$ ,  $\mathcal{M}^{(7)}$ , and  $\mathcal{M}^{(8)}$  are zero, due to the  $\phi u \bar{d}$ -vertex. Thus two further matrix elements have to be calculated,

$$\begin{aligned} \mathcal{M}^{(5)} &= \frac{A}{D_4 D_5} \langle \psi' \beta \rangle [\langle \psi \alpha' \rangle^* \langle \beta' | \lambda | \alpha' \rangle + \langle \psi \beta' \rangle^* \langle \beta' | \lambda | \beta' \rangle + \langle \psi q \rangle^* \langle \beta' | \lambda | q \rangle], \\ \mathcal{M}^{(6)} &= -\frac{A}{D_5 D_6} \langle \psi \beta' \rangle^* [\langle \psi' \alpha \rangle \langle \alpha | \lambda | \beta \rangle + \langle \psi' \beta \rangle \langle \beta | \lambda | \beta \rangle + \langle \psi' q \rangle \langle q | \lambda | \beta \rangle], \end{aligned} \quad (3.27)$$

with  $A$  defined in Eq. (3.24), and

$$D_4 = 2p_d q, \quad D_5 = (p_t - p_b)^2 - \mu_W^2, \quad D_6 = 2p_u q. \quad (3.28)$$

The final squared amplitude for the real emission of a gluon is

$$\overline{\sum} |\mathcal{M}_1|^2 = \frac{1}{2} \cdot \frac{1}{3} \cdot 9 \cdot \left[ \sum_{pol} |\mathcal{M}^{(1)} + \mathcal{M}^{(2)}|^2 + \sum_{pol} |\mathcal{M}^{(5)} + \mathcal{M}^{(6)}|^2 \right], \quad (3.29)$$

where  $\mathcal{M}^{(1)}$  and  $\mathcal{M}^{(2)}$  are the same as in Eq. (3.23), for  $f = u$  and  $f' = \bar{d}$ . The amplitude of Eq. (3.29) is written as an incoherent sum of two different contributions, because their interference is zero due to colour conservation.

## EW corrections to $t(p_t) \rightarrow b(p_b) \nu_\ell(p_\nu) \ell^+(p_\ell)$

The same approach used for the QCD corrections can be applied in the EW case. Here the possible diagrams are shown in Fig. 3.3 (with  $f = \nu_\ell$ ,  $\bar{f}' = \ell^+$  and excluding  $\mathcal{M}^{(11)}$ ), and the corresponding matrix elements are

$$\begin{aligned}
\mathcal{M}^{(1)} &= \frac{Q_t B}{D_1 D_2} \langle \psi' \beta \rangle [\langle \phi \beta' \rangle^* \langle \psi | \lambda | \phi \rangle + \langle \psi \beta' \rangle^* \langle \psi | \lambda | \psi \rangle - \langle q \beta' \rangle^* \langle \psi | \lambda | q \rangle - m_t \langle \beta' | \lambda | \phi \rangle], \\
\mathcal{M}^{(2)} &= -\frac{Q_b B}{D_2 D_3} \langle \psi \beta' \rangle^* [\langle \phi' \beta \rangle \langle \phi' | \lambda | \psi' \rangle + \langle \psi' \beta \rangle \langle \psi' | \lambda | \psi' \rangle + \langle q \beta \rangle \langle q | \lambda | \psi' \rangle - m_b \langle \phi' | \lambda | \beta \rangle], \\
\mathcal{M}^{(3)} &= \frac{Q_e B}{D_4 D_5} \langle \psi' \beta \rangle [\langle \psi \alpha' \rangle^* \langle \beta' | \lambda | \alpha' \rangle + \langle \psi \beta' \rangle^* \langle \beta' | \lambda | \beta' \rangle + \langle \psi q \rangle^* \langle \beta' | \lambda | q \rangle], \\
\mathcal{M}^{(4)} &= -\frac{B}{2D_2 D_5} \left\{ \langle \psi' \beta \rangle \langle \psi \beta' \rangle^* [2\langle \phi | \lambda | \phi \rangle + 2\langle \psi | \lambda | \psi \rangle - 2\langle \phi' | \lambda | \phi' \rangle - 2\langle \psi' | \lambda | \psi' \rangle - \langle q | \lambda | q \rangle] \right. \\
&\quad + \langle \beta' | \lambda | \beta \rangle [-\langle \psi' \phi \rangle \langle \psi \phi \rangle^* + \langle \psi' \phi' \rangle \langle \psi \phi' \rangle^* + 2\langle \psi' q \rangle \langle \psi q \rangle^*] \\
&\quad \left. - \langle \psi | \lambda | \psi' \rangle [\langle \alpha \beta \rangle \langle \alpha \beta' \rangle^* + \langle \alpha' \beta \rangle \langle \alpha' \beta' \rangle^* + 2\langle \beta q \rangle \langle \beta' q \rangle^*] \right\}, \\
\mathcal{M}^{(5)} &= \frac{B}{2D_2 D_5} \langle \beta' | \lambda | \beta \rangle [m_t \langle \psi' \phi \rangle + m_b \langle \phi' \psi \rangle^*], \\
\mathcal{M}^{(6)} &= \mathcal{M}^{(7)} = \mathcal{M}^{(8)} = \mathcal{M}^{(9)} = \mathcal{M}^{(10)} = 0.
\end{aligned} \tag{3.30}$$

The triple scalar-fermion-fermion vertex is proportional to the fermion's masses, i.e. the matrix elements  $\mathcal{M}^{(6-10)}$  are zero. In Eq. (3.30),  $Q_a$  is the charge of the particle  $a$ , the denominators  $D_i$ , with  $u \rightarrow \nu_\ell$  and  $\bar{d} \rightarrow \ell^+$ , have been defined in Eqs. (3.24) and (3.28), and

$$B = -2e \frac{e^2}{2s_w^2}. \tag{3.31}$$

The amplitude of the real EW corrections is therefore given by

$$\overline{\sum} |\mathcal{M}_1|^2 = \frac{1}{2} \cdot \frac{1}{3} \cdot 3 \cdot \sum_{pol} \left| \sum_{i=1}^5 \mathcal{M}^{(i)} \right|^2. \tag{3.32}$$

## EW corrections to $t(p_t) \rightarrow b(p_b) u(p_u) \bar{d}(p_d)$

This case is similar to the previous one. There is only one additional diagram contributing ( $\mathcal{M}^{(11)}$  in Fig. 3.3, with  $f = u$  and  $\bar{f}' = \bar{d}$ ), whose matrix element is

$$\mathcal{M}^{(11)} = -\frac{Q_u B}{D_5 D_6} \langle \psi \beta' \rangle^* [\langle \psi' \alpha \rangle \langle \alpha | \lambda | \beta \rangle + \langle \psi' \beta \rangle \langle \beta | \lambda | \beta \rangle + \langle \psi' q \rangle \langle q | \lambda | \beta \rangle]. \tag{3.33}$$

The final squared matrix element is given by

$$\overline{\sum} |\mathcal{M}_1|^2 = \frac{1}{2} \cdot \frac{1}{3} \cdot 3 \cdot \sum_{pol} \left| \sum_{i=1}^{11} \mathcal{M}^{(i)} \right|^2, \tag{3.34}$$

where the matrix elements from (1) to (10) are described in Eq. (3.30), with  $f = u$  and  $f' = \bar{d}$ .

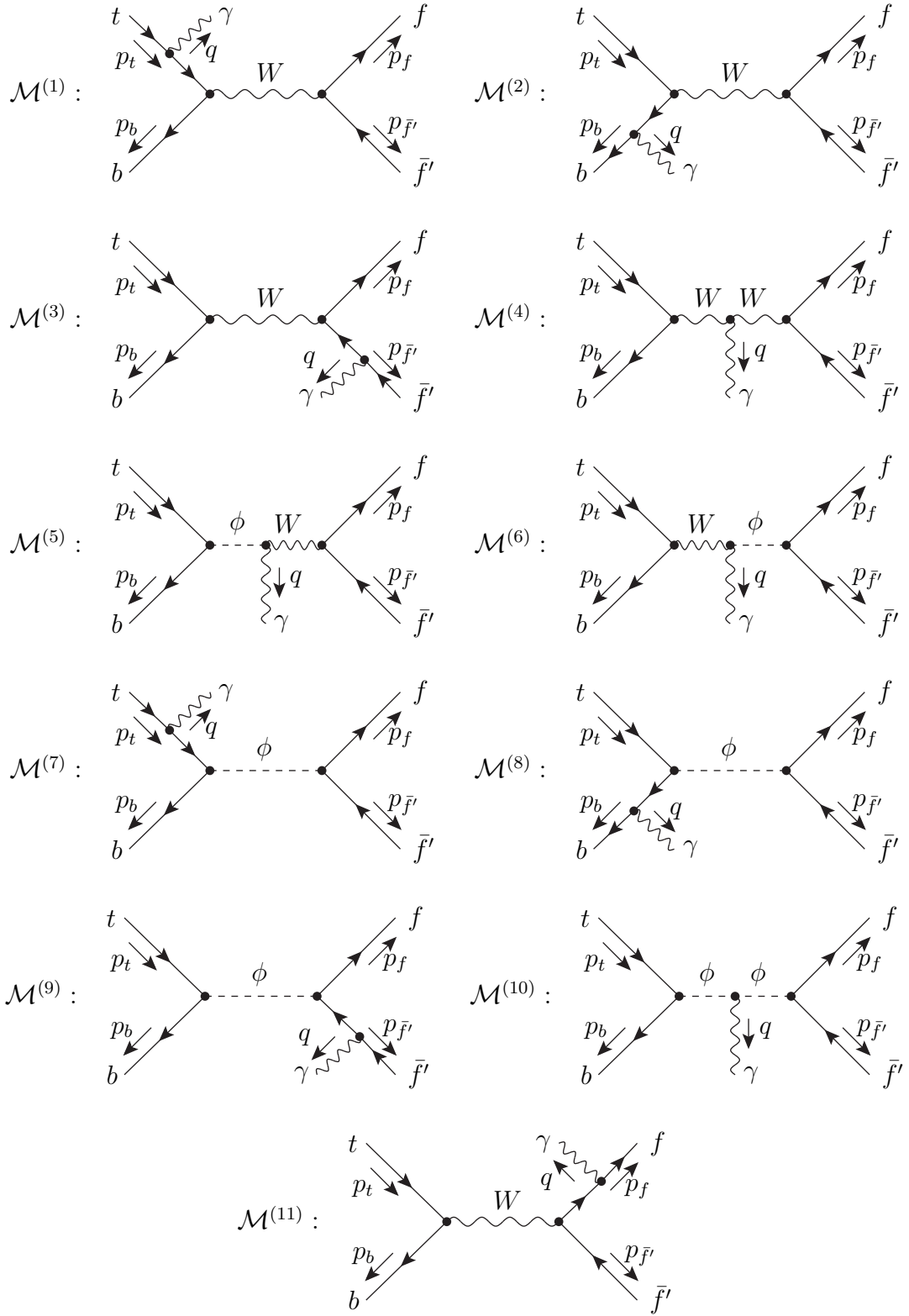


Figure 3.3: Diagrams contributing to the process  $t(p_t) \rightarrow b(p_b) f(p_f) \bar{f}(p_{\bar{f}}) \gamma(q)$  in lowest order.

### 3.4 Virtual corrections and counterterms

To calculate the virtual corrections to  $t(p_t) \rightarrow b(p_b) f(p_f) \bar{f}'(p_{\bar{f}'})$ , we need to evaluate the one-loop contributions to the process. In case of QCD corrections the number of diagrams is small: The gluon can be exchanged only between quarks belonging to the same generation (colour conservation). On the other hand, if one wants to calculate the EW corrections to the same process, the number of diagrams largely increases, as can be clearly seen in Figs. 3.4, 3.5 and 3.6<sup>1</sup>, making the evaluation laborious and difficult. For this reason an automation is important. This can be done, for example, using the fact that the virtual matrix element  $\mathcal{M}_V$  can be decomposed into a finite number of *standard matrix elements* (SME)  $\mathcal{M}_i$  multiplied by polarization-independent form factors  $F_i$  [22],

$$\mathcal{M}_V = \sum_i \mathcal{M}_i F_i. \quad (3.35)$$

The SME contain the information about the Dirac structure, the polarization, and the chirality of the particles involved in the process, while the form factors incorporate all other factors (propagators, couplings and tensors integrals). The SME appearing for the top-quark decay width at the one-loop level are

$$\begin{aligned} \mathcal{M}_1^{\sigma,\tau} &= \bar{u}(p_b) \gamma_\alpha \omega_\sigma u(p_t) \bar{u}(p_f) \gamma^\alpha \omega_\tau v(p_{\bar{f}'}), \\ \mathcal{M}_2^{\sigma,\tau} &= \bar{u}(p_b) \not{p}_f \omega_\sigma u(p_t) \bar{u}(p_f) \not{p}_t \omega_\tau v(p_{\bar{f}'}), \\ \mathcal{M}_3^{\sigma,\tau} &= \bar{u}(p_b) \gamma_\alpha \gamma_\beta \gamma_\delta \omega_\sigma u(p_t) \bar{u}(p_f) \gamma^\alpha \gamma^\beta \gamma^\delta \omega_\tau v(p_{\bar{f}'}), \\ \mathcal{M}_4^{\sigma,\tau} &= \bar{u}(p_b) \gamma_\alpha \gamma_\beta \not{p}_f \omega_\sigma u(p_t) \bar{u}(p_f) \gamma^\alpha \gamma^\beta \not{p}_t \omega_\tau v(p_{\bar{f}'}), \\ \mathcal{M}_5^{\sigma,\tau} &= \bar{u}(p_b) \gamma_\alpha \not{p}_f \omega_\sigma u(p_t) \bar{u}(p_f) \gamma^\alpha \omega_\tau v(p_{\bar{f}'}), \\ \mathcal{M}_6^{\sigma,\tau} &= \bar{u}(p_b) \omega_\sigma u(p_t) \bar{u}(p_f) \not{p}_t \omega_\tau v(p_{\bar{f}'}), \\ \mathcal{M}_7^{\sigma,\tau} &= \bar{u}(p_b) \gamma_\alpha \gamma_\beta \omega_\sigma u(p_t) \bar{u}(p_f) \gamma^\alpha \gamma^\beta \not{p}_t \omega_\tau v(p_{\bar{f}'}), \end{aligned} \quad (3.36)$$

where  $\omega_\pm = \frac{1 \pm \gamma_5}{2}$  are the chirality projection operators ( $\sigma$  and  $\tau$  are the chirality of the  $t$  quark and the  $f$  fermion, respectively) and  $u(p_t)$ ,  $\bar{u}(p_f)$  and  $v(p_{\bar{f}'})$  are the spinors of the incoming and outgoing fermions or antifermions. Therefore, it is possible to implement the SME into a code using the WvdW formalism and to automatize the calculation of the corresponding form factors. For this purpose, we use an in-house code written by S. Dittmaier, which makes use of the COLLIER library (see Ref. [86]) for the calculation of the one-loop integrals.

As stated in Sect. 2.2, the loop integrals comprise UV divergences. They cancel against the UV divergences arising from the counterterms diagrams. The contribution of the counterterms factorizes for the top-quark decay into the LO matrix element and a factor  $\delta_{\text{ct}}$ , which depends on the final state and on the type of corrections:

$$\mathcal{M}_{\text{ct}} = \mathcal{M}_0 \delta_{\text{ct}}. \quad (3.37)$$

---

<sup>1</sup>The diagrams containing a  $\phi f f'$  vertex, with  $m_f = m_{f'} = 0$ , do not contribute to the process and are not included in Figs. 3.4, 3.5 and 3.6.

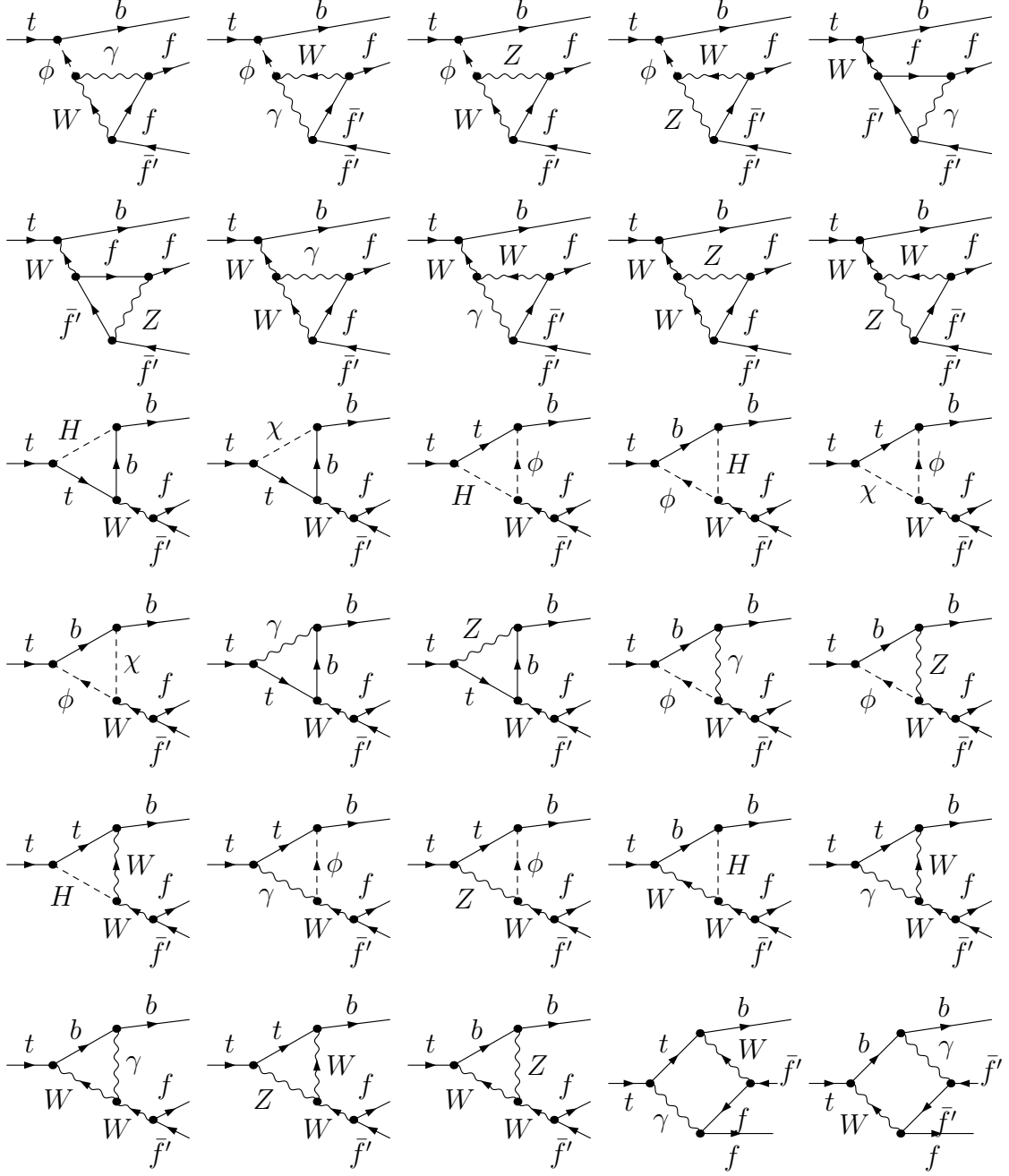


Figure 3.4: Virtual diagrams contributing to the process  $t(p_t) \rightarrow b(p_b) f(p_f) \bar{f}(p_{\bar{f}})$ .

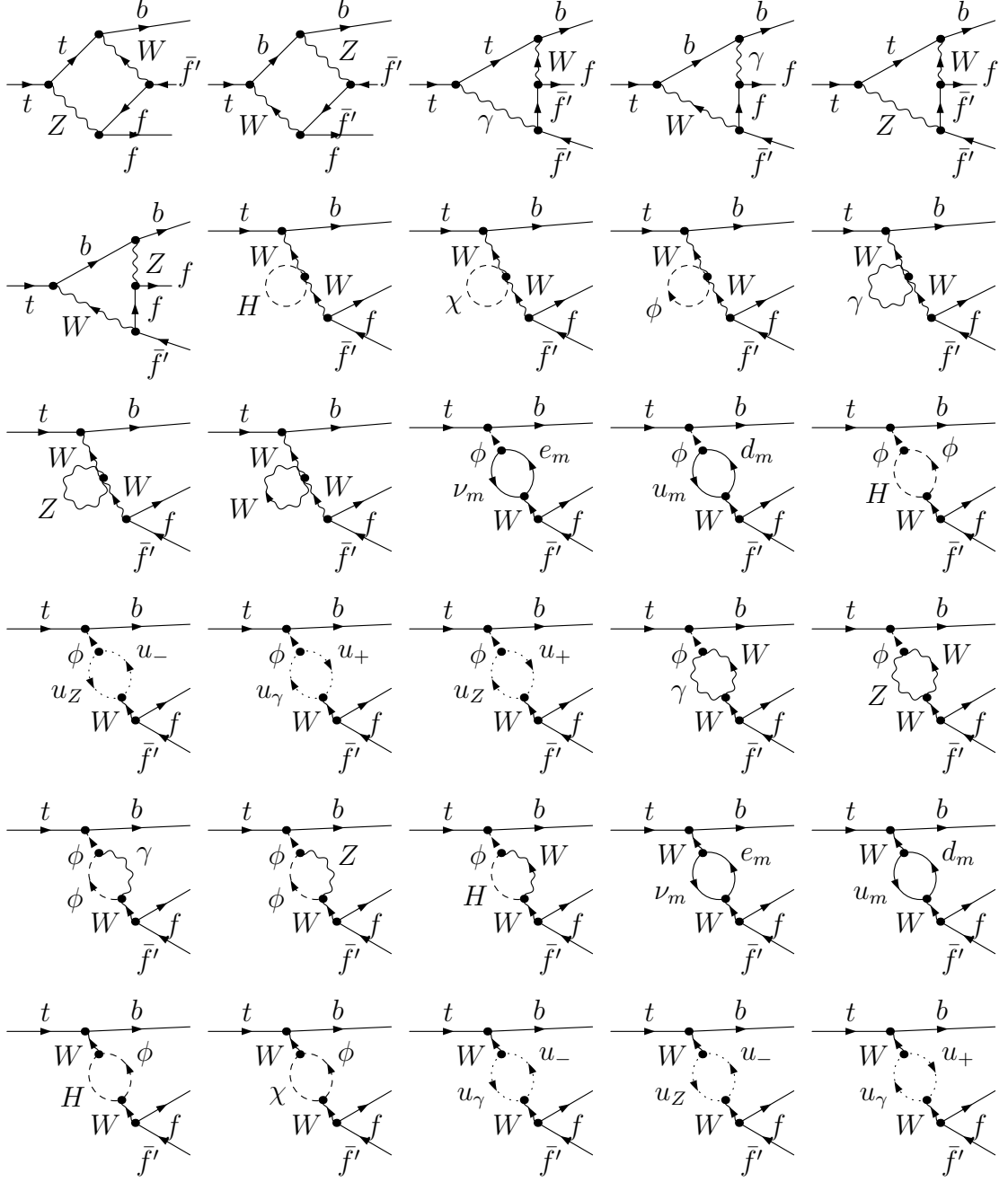


Figure 3.5: Virtual diagrams contributing to the process  $t(p_t) \rightarrow b(p_b) f(p_f) \bar{f}(p_{\bar{f}})$ .

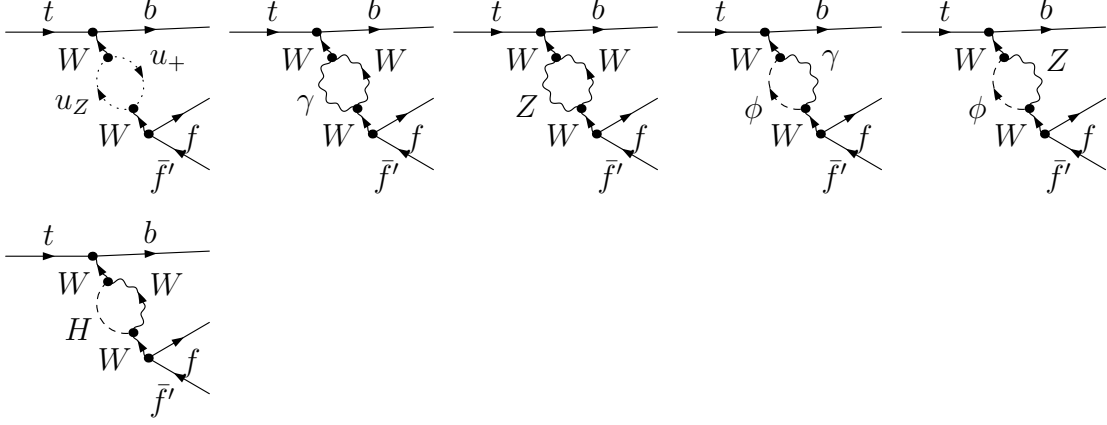


Figure 3.6: Virtual diagrams contributing to the process  $t(p_t) \rightarrow b(p_b) f(p_f) \bar{f}(p_{\bar{f}})$ .

In our processes  $\delta_{\text{ct}}$  reads

$$\begin{aligned}
\delta_{\text{ct,lept}}^{\text{QCD}} &= \frac{1}{2} [\delta\mathcal{Z}_t + \delta\mathcal{Z}_b], \\
\delta_{\text{ct,hadr}}^{\text{QCD}} &= \frac{1}{2} [\delta\mathcal{Z}_t + \delta\mathcal{Z}_b + \delta\mathcal{Z}_u + \delta\mathcal{Z}_d], \\
\delta_{\text{ct,lept}}^{\text{EW}} &= 2\delta\mathcal{Z}_e - 2\frac{\delta s_w}{s_w} + \frac{1}{2} [\delta\mathcal{Z}_t + \delta\mathcal{Z}_b + \delta\mathcal{Z}_{ee} + \delta\mathcal{Z}_\nu] + \frac{\delta\mu_W^2}{s_{34} - \mu_W^2} - \Delta r, \\
\delta_{\text{ct,hadr}}^{\text{EW}} &= 2\delta\mathcal{Z}_e - 2\frac{\delta s_w}{s_w} + \frac{1}{2} [\delta\mathcal{Z}_t + \delta\mathcal{Z}_b + \delta\mathcal{Z}_u + \delta\mathcal{Z}_d] + \frac{\delta\mu_W^2}{s_{34} - \mu_W^2} - \Delta r. \tag{3.38}
\end{aligned}$$

The IR divergences are treated using mass regulators, both for the soft and the collinear cases, and cancel when the integrated real contribution is added. More details are given in Chap. 4.



# Chapter 4

## The one-cutoff phase-space slicing method

In the case of processes containing massless particles the calculation of loop diagrams gives rise to terms proportional to  $\ln(m^2/Q^2)$ , where  $Q$  is the typical scale of the process, which diverge in the limit of the mass  $m \rightarrow 0$ . These divergences are called *mass* or *infrared* (IR) *divergences*. They cancel when the virtual contribution is added to the real one, after phase-space integration and for sufficiently inclusive observables, according to the Kinoshita–Lee–Nauenberg (KLN) theorem [87, 88].

The IR divergences can be classified in two different types: the *soft* and the *collinear singularities*. In the virtual corrections, the soft singularities typically occur if a gluon or a photon with a small momentum  $q$  is exchanged between the external particles with momenta  $p_f$ , while the collinear singularities arise in a loop diagram if a massless external particle splits into two massless internal particles [89]. In the real corrections the singularities arise during the numerical phase-space integration: If the momentum of the emitted massless particle is very small ( $q \rightarrow 0$ ), the divergences are soft, otherwise, if the gluon/photon is radiated almost parallel to the high-energetic fermion ( $2p_f q \rightarrow 0$ ), the divergences are called collinear. The singularities are regularized in this work through the so-called *mass regularization* [90, 91], which introduces an infinitesimal photon (gluon) mass<sup>1</sup>  $m_\gamma$  ( $m_g$ ) and small fermion masses<sup>2</sup>  $m_f$ . Such masses appear in the intermediate steps of the calculation as logarithmic terms, which cancel after combining virtual and real contributions. To isolate these mass singularities from the real correction we use an extension of the *one-cutoff phase-space slicing method* (OCSM) [37–41].

The main idea of the phase-space slicing method is to introduce technical cut parameters to separate the resolved region of the real emission phase space from the unresolved region, which contains the soft and collinear divergences. While the former part can be numerically integrated by Monte Carlo methods, in the latter the matrix elements and the phase-space measure have to be approximated to carry out part of the integration analytically. The separation between the two regions can be performed in two different ways. One possibility is to apply two cuts:

---

<sup>1</sup>The gluon mass is needed and thus introduced here only for “QED-like” IR singularities, to avoid the issue of the difference between the zero-mass and small-mass theories described in Ref. [92].

<sup>2</sup>After the introduction of a regulator mass, we will refer to the massless particle as a *light particle*.

the first on the energy of the emitted gluon/photon, to isolate the soft divergences, and the second on the angle between the gluon/photon and the emitting fermion, isolating the collinear divergences. This method is known in the literature as the *two-cutoff slicing* [39, 93]. Another procedure, the one-cutoff slicing method, isolates both types of singularities making use of only one cut. This technique has the advantage to be Lorentz invariant and thus to be equally applicable in any reference frame. Moreover, the OCSM is technically convenient, since, in contrast to other standard procedures such as the *dipole subtraction method* [42–45], it offers the possibility to avoid negative weights during the integration process (useful to generate unweighted events with a Monte Carlo program). For these reasons, we base the calculation performed in this thesis on the OCSM. The dipole subtraction approach has been instead implemented in an independent calculation as a check of the results (see Sect. 6.1).

The OCSM has been extensively studied in the literature, in the massless [37, 38] or massive [39–41] cases. It should be noted that performing an expansion of the results obtained with the full mass dependence is not feasible due to the hierarchy between the cut imposed by the slicing method and the light fermion masses. This forbids to simply take the massless limit of the massive case to deal with processes involving light particles (fundamental when using mass regularization). Moreover, so far there is no prescription in the literature for the OCSM in the particular case of a decay process with more than two particles in the final state.

To cover these lacks, in this work we developed an extension of the OCSM. Our method employs the idea, described in Ref. [44] for the dipole-subtraction formalism, of using a function that has the appropriate asymptotic behavior both in the soft and in the collinear limits. This allows us to perform analytical integrations also for the cases of light particles. Moreover, we take into consideration some boundary regions appearing only in the case of more than two particles in the final state. The details are presented in the following sections.

## 4.1 Overview of the method

We consider the real emission of a massless vector boson from a generic process. In this section only the photonic case is discussed, but this method can be easily extended to gluon emission. A summary with the complete results used in this work is reported in Sect. 4.2.3.

We define the Lorentz-invariant quantity

$$s_{f\gamma} \equiv 2p_f q, \quad (4.1)$$

where  $p_f$  is the momentum of a fermion  $f$  and  $q$  is the photon momentum. Furthermore, the resolution parameter  $\Delta s$ , which is an arbitrary cut, is introduced to divide the phase space into two regions, whose sum does not depend on  $\Delta s$ . This property can be used during the calculation as a check on correctness.

The correction given by the real emission of a photon is calculated by integrating the squared matrix element  $|\mathcal{M}_1|^2$  (given in Sect. 3.3), summed over all photon polarizations  $\lambda_\gamma$ , over the corresponding phase space  $d\Phi_1$ . It is possible to identify two different regions:

$$\int d\Phi_1 \sum_{\lambda_\gamma} |\mathcal{M}_1|^2 = I_S + I_H. \quad (4.2)$$

- The *hard region*, where  $s_{f\gamma} > \Delta s$  for all fermions  $f$  appearing in the process:

$$I_H = \int d\Phi_1 \sum_{\lambda_\gamma} |\mathcal{M}_1|^2 \prod_f \Theta(s_{f\gamma} - \Delta s). \quad (4.3)$$

There are neither soft nor collinear singularities, and the integration can be performed numerically via Monte Carlo methods (see Chapter 5).

- The *singular region*, where  $I_S$  is defined:  $s_{f\gamma} < \Delta s$  for at least one of the fermions  $f$ .

If only one invariant  $s_{f\gamma} < \Delta s$ , the fermion  $f$  and the photon are collinear. If instead at least two invariants are smaller than  $\Delta s$ , the photon is soft. These two types of divergences can overlap.

In the singular region some of the integrals are calculated analytically in the limit  $\Delta s \rightarrow 0$ . The details are presented in Sect. 4.2. The remaining integrals are integrated numerically, as described in Sect. 4.3.

## 4.2 Singular region

Integrating the singular region analytically ( $I_S$  in Eq. (4.2)), the main idea is to find a function that has the same asymptotic behavior as the squared matrix element for the real corrections, in the soft and collinear limits. This method, described in Ref. [44] for the dipole-subtraction formalism, is adapted here to the OCSM.

When the emitted photon becomes soft ( $q \rightarrow 0$ ), the *soft-photon approximation* (see App.B) can be used: The squared real matrix element becomes proportional to the square of the LO matrix element  $\mathcal{M}_0$ ,

$$\sum_{\lambda_\gamma} |\mathcal{M}_1|^2 \underset{q \rightarrow 0}{\sim} -e^2 |\mathcal{M}_0|^2 \sum_{f,f'} Q_f Q_{f'} \frac{p_f p_{f'}}{(p_f q)(p_{f'} q)}, \quad (4.4)$$

where  $Q_f$  and  $Q_{f'}$  are the charges of the fermions  $f$  and  $f'$ , respectively, and  $e$  is the electric unit charge. A similar factorization occurs in the case of a collinear photon emission, in the limit of vanishing fermion masses

$$\sum_{\lambda_\gamma} |\mathcal{M}_1|^2 \underset{p_f q \rightarrow 0}{\sim} Q_f^2 e^2 g_{f,\tau}(p_f, q) |\mathcal{M}_0|^2. \quad (4.5)$$

The function  $g_{f,\tau}$  depends on the spin-flip variable  $\tau = \pm$  and is different for incoming or outgoing fermions. Its explicit form can be found in Ref. [44].

Taking advantage of this factorization property, we construct a function  $|\mathcal{M}_{sub}|^2$  such that

$$|\mathcal{M}_{sub}|^2 \sim \sum_{\lambda_\gamma} |\mathcal{M}_1|^2 \quad \text{for } q \rightarrow 0 \quad \text{or } p_f q \rightarrow 0. \quad (4.6)$$

For this purpose we make use of the auxiliary functions  $g_{ff',\tau}(p_f, p_{f'}, q)$  of Ref. [44],

$$|\mathcal{M}_{sub}|^2 = -e^2 \sum_{\substack{f \neq f' \\ \tau = \pm}} Q_f \sigma_f Q_{f'} \sigma_{f'} g_{ff',\tau}(p_f, p_{f'}, q) |\mathcal{M}_0(\tilde{\Phi}_{0,ff'})|^2. \quad (4.7)$$

These functions are simple enough to be analytically integrated over the photon phase space and have the appropriate asymptotic behavior both in the soft and in the collinear limits. We consider in this work only the unpolarized case: We sum over the spins and obtain the radiator function

$$g_{ff'} = g_{ff',+} + g_{ff',-}. \quad (4.8)$$

The sign factor in Eq. (4.7) is  $\sigma_f = +1$  for incoming fermions and outgoing anti-fermions, and  $\sigma_f = -1$  for outgoing fermions and incoming anti-fermions. With this convention charge conservation reads

$$\sum_f \sigma_f Q_f = 0. \quad (4.9)$$

Note that the matrix elements on the left-hand side and those on the right-hand side of Eqs. (4.4) and (4.5) are defined on different phase spaces ( $\Phi_1$  and  $\Phi_0$ , respectively). For this reason we need to apply a mapping that projects the momenta of  $\Phi_1$  to  $\Phi_0$ , in such a way that the whole phase space is spanned and the mass-shell relations are fulfilled. The projected momenta are denoted by a tilde and span the phase space  $\tilde{\Phi}_{0,ff'}$ , which we label  $\tilde{\Phi}_0$  for all pairs of fermions  $ff'$  (the explicit mapping of  $\Phi_1 \rightarrow \tilde{\Phi}_0$  can be found in Sect. 4.3).

For the analytical phase-space integration, the factorization property of the integral  $\int d\Phi_1$  in the singular limit is used:

$$\int d\Phi_1 = \int d\tilde{\Phi}_0 \otimes \int d[q], \quad (4.10)$$

where  $\int d[q]$  is connected to the photon phase space. It is then possible to rewrite

$$\int d\Phi_1 \sum_{\lambda_\gamma} |\mathcal{M}_1|^2 \sim \int d\tilde{\Phi}_0 |\mathcal{M}_0(\tilde{\Phi}_0)|^2 S \quad \text{for } p_f q \rightarrow 0 \quad \text{or} \quad q \rightarrow 0, \quad (4.11)$$

where

$$S = -\frac{\alpha}{2\pi} \sum_{f \neq f'} Q_f \sigma_f Q_{f'} \sigma_{f'} G_{ff'}(P_{ff'}^2) \quad (4.12)$$

and

$$G_{ff'}(P_{ff'}^2) = 8\pi^2 \int d[q] g_{ff'}(p_f, p_{f'}, q) \Theta_f \Theta_{f'}. \quad (4.13)$$

In the previous equations  $\alpha = e^2/(4\pi)$  is the fine-structure constant,  $P_{ff'}^2$  depends on the momenta of the fermions  $f$  and  $f'$ , and the cut functions are defined by

$$\Theta_f \Theta_{f'} = \Theta(s_{f\gamma} - \Delta s) \Theta(\Delta s - s_{f'\gamma}) + \Theta(\Delta s - s_{f\gamma}) \Theta(s_{f'\gamma} - \Delta s) + \Theta(\Delta s - s_{f\gamma}) \Theta(\Delta s - s_{f'\gamma}). \quad (4.14)$$

The radiator functions  $g_{ff'}$  appearing in the definition of  $|\mathcal{M}_{sub}|^2$  (see Eq. (4.7)) are defined only for pairs of fermions (called *emitter* and *spectator* following the idea of Ref. [44]). As a consequence, the cuts of Eq. (4.14) identify the singular domain of the functions  $G_{ff'}(P_{ff'}^2)$  only for pairs of different fermions  $f$  and  $f'$ , ignoring in which region of the phase space any other fermion  $f''$  appearing in the process is located. This means that the instance where  $s_{f\gamma} > \Delta s$  and  $s_{f'\gamma} > \Delta s$  is considered part of the hard region and it is not analytically integrated. However, the case where  $s_{f''\gamma} < \Delta s$ , even though  $s_{f\gamma} > \Delta s$  and  $s_{f'\gamma} > \Delta s$ , is by definition part of the singular region where  $I_S$  is defined and it is not taken into account when calculating

$G_{ff'}(P_{ff'}^2)$ . For this reason, we introduce another phase-space region, named *quasi-soft region* (QS) in the following, that includes these kind of contributions:

$$I_S = \int d\tilde{\Phi}_0 |\mathcal{M}_0(\tilde{\Phi}_0)|^2 S + I_{QS}. \quad (4.15)$$

The integrand of the quantity  $I_{QS}$  is calculated using the soft photon/gluon approximation and it is splitted into various contributions to avoid double counting. Then a numerical integration is performed, as described in more detail in Sect. 4.3.

Particular attention has to be paid while evaluating the collinear limit, as explained in Refs. [44, 45]. Collinear singularities appear only in the case of small masses, which give rise to terms of the form  $\alpha \ln(m_f^2/Q^2)$ . In our process only the collinearity with respect to the final-state radiation occurs. For the EW corrections to the semileptonic top-quark decay width we can distinguish two kinds of observables, depending on the type of fermion emitting the collinear photon:

- *Collinear-safe observables*: The fermion  $f$  is a positron. Both the positron and the photon are detected as a shower in the EM calorimeter of the experiments. Since it is impossible to separate them if they are collinear, they are treated like a single quasi-particle of momentum  $\tilde{p}_f = p_f + q$  (*photon recombination* [94]). This procedure guarantees that the quantity

$$z_{ff'} = \frac{p_f p_{f'}}{p_f p_{f'} + p_f q} \quad (4.16)$$

can be integrated over its whole range. Events that differ only in the value of  $z_{ff'}$  fill the histogram bins in a way that is independent of  $z_{ff'}$ . The contribution of the form  $\alpha \ln(m_f^2/Q^2)$  cancels completely after adding the virtual corrections, as granted by the KLN theorem.

- *Non-collinear-safe observables*: The fermion  $f$  is a muon and is detected in the muon chambers, while the photon is detected in the EM calorimeter. This means that collinearly radiated muons and photons can be experimentally distinguished introducing a dependence on the variable  $z_{ff'}$  of Eq. (4.16). To make this dependence explicit, in our calculation the following splitting is introduced:

$$p_f = z_{ff'} \tilde{p}_f, \quad p_{f'} = \tilde{p}_{f'} \quad \text{and} \quad q = (1 - z_{ff'}) \tilde{p}_f. \quad (4.17)$$

The previous equations define the momenta of the events associated with  $|\mathcal{M}_{sub}|^2$  of Eq. (4.7) treated as  $(N+1)$ -particle events. These transformations allow to use selection functions, such as event selections or  $\theta$ -functions for cuts, which now implicitly depend on  $z_{ff'}$  itself, constraining its integration.

In the integration soft singularities occur when  $z_{ff'} \rightarrow 1$ . Following Ref. [45] we write

$$\begin{aligned} \int d\Phi_1 |\mathcal{M}_{sub,ff'}(\Phi_1)|^2 = & -\frac{\alpha}{2\pi} Q_f \sigma_f Q_{f'} \sigma_{f'} \int d\tilde{\Phi}_{0,ij} \int_0^1 dz \\ & \times \left\{ G_{ff'}(P_{ff'}^2) \delta(1 - z_{ff'}) + [\bar{\mathcal{G}}_{ff'}(P_{ff'}^2, z_{ff'})]_+ \right\} \\ & \times |\mathcal{M}_0(\tilde{p}_f, \tilde{p}_{f'})|^2 \Theta_{cut}(p_f = z_{ff'} \tilde{p}_f, q = (1 - z_{ff'}) \tilde{p}_f, p_{f'} = \tilde{p}_{f'}), \end{aligned} \quad (4.18)$$

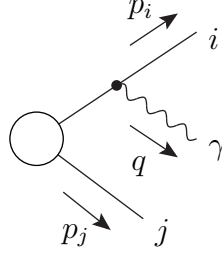


Figure 4.1: Generic diagram with a final emitter  $i$  and a final spectator  $j$ .

where  $\Theta_{cut}$  is a step function acting on the  $(N + 1)$ -particles phase space. In the term in the curly brackets on the right-hand side of Eq. (4.18) we have isolated the singularities, employing the  $[\dots]_+$  prescription

$$\bar{\mathcal{G}}_{ff'}(P_{ff'}^2, z_{ff'}) = G_{ff'}(P_{ff'}^2)\delta(1 - z_{ff'}) + [\bar{\mathcal{G}}_{ff'}(P_{ff'}^2, z_{ff'})]_+. \quad (4.19)$$

This procedure simplifies the integration in the non-collinear-safe region.  $G_{ff'}(P_{ff'}^2)$  corresponds to the quantity calculated in the collinear-safe case and  $[\bar{\mathcal{G}}_{ff'}(P_{ff'}^2, z_{ff'})]_+$  is a regular term that can be calculated setting  $m_\gamma = 0$ .

In case of an hadronic decay of the top quark, it is experimentally impossible to separate two collinear partons. For this reason only the case of collinear-safe observables appears. It is, however, important to define IR-safe jet observables, which are obtained by recombining the collinear partons through a *jet algorithms* [95].

In the following sections we explicitly show how to calculate  $G_{ff'}(P_{ff'}^2)$  and  $[\bar{\mathcal{G}}_{ff'}(P_{ff'}^2, z_{ff'})]_+$  for different pairs of fermions  $f$  and  $f'$ , distinguishing between the possible combinations of initial/final and spectator/emitter particles. We use the notation introduced in Ref. [44].

### 4.2.1 Final-state spectator and final-state emitter

In the case of a final-state spectator  $j$  and a final-state emitter  $i$  (Fig. 4.1), we introduce the abbreviations

$$P_{ij} = p_i + p_j + q, \quad \overline{P}_{ij}^2 = P_{ij}^2 - m_i^2 - m_j^2 - m_\gamma^2, \quad \lambda_{ij} = \lambda(P_{ij}^2, m_i^2, m_j^2), \quad (4.20)$$

where

$$\lambda(x, y, z) = x^2 + y^2 + z^2 - 2xy - 2xz - 2yz \quad (4.21)$$

is the Källén function and

$$\lambda_{ij} = \overline{P}_{ij}^4 - 4m_i^2 m_j^2, \quad \text{for } m_\gamma = 0. \quad (4.22)$$

The unpolarized radiator function is given by [44]

$$g_{ij}(p_i, p_j, q) = \frac{1}{(p_i q) R_{ij}(y_{ij})} \left[ \frac{2}{1 - z_{ij}(1 - y_{ij})} - 1 - z_{ij} - \frac{m_i^2}{p_i q} \right], \quad (4.23)$$

where the following variables are used:

$$y_{ij} = \frac{p_i q}{p_i p_j + p_i q + p_j q} = \frac{2p_i q}{\overline{P}_{ij}^2}, \quad z_{ij} = \frac{p_i p_j}{p_i p_j + p_j q}. \quad (4.24)$$

Throughout this section, we refer to them using the shorthand notation  $y$  and  $z$ .

The photon phase space can be written as

$$\int [dq(P_{ij}^2, y, z)] = \frac{1}{4(2\pi)^2} \frac{\overline{P}_{ij}^4}{\sqrt{\lambda_{ij}}} \int_{y_1}^{y_2} dy (1-y) \int_{z_1(y)}^{z_2(y)} dz \quad (4.25)$$

and consequently

$$G_{ij}(P_{ij}^2) = \frac{\overline{P}_{ij}^4}{2\sqrt{\lambda_{ij}}} \int_{y_1}^{y_2} dy (1-y) \int_{z_1(y)}^{z_2(y)} dz g_{ij}(p_i, p_j, q) \Theta_f \Theta_{f'}. \quad (4.26)$$

The boundary values of  $y$  and  $z$  are

$$\begin{aligned} y_1 &= \frac{2m_i m_\gamma}{\overline{P}_{ij}^2}, \quad y_2 = 1 - \frac{2m_j(\sqrt{P_{ij}^2} - m_j)}{\overline{P}_{ij}^2}, \\ z_{1,2}(y) &= \frac{(1-y)(2m_i^2 + \overline{P}_{ij}^2 y) \mp \sqrt{y^2 - y_1^2} \sqrt{\lambda_{ij}} R_{ij}(y)}{2(1-y)(m_i^2 + m_\gamma^2 + \overline{P}_{ij}^2 y)}, \end{aligned} \quad (4.27)$$

where

$$R_{ij}(y) = \frac{\sqrt{(2m_j^2 + \overline{P}_{ij}^2 - \overline{P}_{ij}^2 y)^2 - 4P_{ij}^2 m_j^2}}{\sqrt{\lambda_{ij}}}. \quad (4.28)$$

In order to integrate Eq. (4.26),  $y$  and  $z$  have to fulfill the  $\Theta_f \Theta_{f'}$  condition of Eq. (4.14), which sets the following boundaries:

$$\text{SOFT:} \quad \begin{cases} z > 1 - \Delta z, & \text{for } s_{j\gamma} < \Delta s, \\ y < \Delta y, & \text{for } s_{i\gamma} < \Delta s, \end{cases} \quad (4.29)$$

$$\text{COLLINEAR 1: } \gamma \text{ collinear to } i \quad \begin{cases} z < 1 - \Delta z, & \text{for } s_{j\gamma} > \Delta s, \\ y < \Delta y, & \text{for } s_{i\gamma} < \Delta s, \end{cases} \quad (4.30)$$

$$\text{COLLINEAR 2: } \gamma \text{ collinear to } j \quad \begin{cases} z > 1 - \Delta z, & \text{for } s_{j\gamma} < \Delta s, \\ y > \Delta y, & \text{for } s_{i\gamma} > \Delta s, \end{cases} \quad (4.31)$$

where

$$\Delta y \equiv \frac{\Delta s}{\overline{P}_{ij}^2} \quad \text{and} \quad \Delta z \equiv \frac{\Delta y}{1-y}. \quad (4.32)$$

This means that the integral we need to calculate is of the form

$$\begin{aligned}
G_{ij}(P_{ij}^2) &= \int_{y_a}^{y_b} dy \int_{z_a(y)}^{z_b(y)} dz \frac{\overline{P}_{ij}^2 (1-y)}{\sqrt{\lambda_{ij}} y R_{ij}(y)} \left[ \frac{2}{1-z(1-y)} - 1 - z - \frac{2m_i^2}{\overline{P}_{ij}^2 y} \right] \\
&= \frac{\overline{P}_{ij}^2}{\sqrt{\lambda_{ij}}} \int_{y_a}^{y_b} dy \left\{ \frac{2}{y R_{ij}(y)} \ln \left( \frac{1-(1-y)z_a(y)}{1-(1-y)z_b(y)} \right) \right. \\
&\quad \left. + (z_a(y) - z_b(y)) \frac{(1-y)}{y R_{ij}(y)} \left[ 1 + \frac{(z_a(y) + z_b(y))}{2} + \frac{2m_i^2}{\overline{P}_{ij}^2 y} \right] \right\}, \tag{4.33}
\end{aligned}$$

where the integration boundaries,  $y_a$ ,  $y_b$ ,  $z_a(y)$ , and  $z_b(y)$ , will be discussed in the following for each case. Sometimes it is convenient to use the result given in Eq. (4.10) of Ref. [44] for the subtraction method, i.e. the total integration over the intervals  $[z_1(y), z_2(y)]$  and  $[y_1, y_2]$ , defined in Eq. (4.27):

$$\begin{aligned}
G_{ij}^{(\text{sub})}(P_{ij}^2) &= \frac{3}{2} + \frac{a_3^2}{2} + \ln \left( a_3 \frac{m_\gamma^2}{m_i^2} \right) - 2 \ln(1 - a_3^2) + \frac{\overline{P}_{ij}^2}{\sqrt{\lambda_{ij}}} \left\{ \ln(a_1) \ln \left( \frac{m_\gamma^2 m_j^2}{\lambda_{ij} a_2} \right) \right. \\
&\quad \left. + 4 \text{Li}_2 \left( -\sqrt{\frac{a_2}{a_1}} \right) - 4 \text{Li}_2(-\sqrt{a_1 a_2}) + 2 \text{Li}_2(a_1) - \frac{\pi^2}{3} + \frac{1}{2} \ln^2(a_1) \right\}, \tag{4.34}
\end{aligned}$$

where

$$a_1 = \frac{\overline{P}_{ij}^2 + 2m_i^2 - \sqrt{\lambda_{ij}}}{\overline{P}_{ij}^2 + 2m_i^2 + \sqrt{\lambda_{ij}}}, \quad a_2 = \frac{\overline{P}_{ij}^2 - \sqrt{\lambda_{ij}}}{\overline{P}_{ij}^2 + \sqrt{\lambda_{ij}}} \quad \text{and} \quad a_3 = \frac{m_i}{\sqrt{\overline{P}_{ij}^2 - m_j}}. \tag{4.35}$$

### Emitter $i = b$ and spectator $j$ , with $m_j \rightarrow 0$

Due to the small mass of the spectator, the hierarchy between the parameters is

$$m_\gamma^2 \ll m_j^2 \ll \Delta s \ll m_b^2, P_{bj}^2. \tag{4.36}$$

With these conditions,  $y_1 < \Delta y < y_2$ ,  $z_2 > (1 - \Delta z)$  and  $(1 - \Delta z) < z_1$  for  $y_- < y < y_+$ , where

$$y_- = \frac{m_b^2 \Delta y}{\overline{P}_{bj}^2} + \mathcal{O}(\Delta y^2), \quad y_+ = 1 - \Delta y \left( 1 + \frac{m_b^2}{\overline{P}_{bj}^2} \right) + \mathcal{O}(\Delta y^2), \tag{4.37}$$

and  $y_1$ ,  $y_2$ ,  $z_1$  and  $z_2$  are defined in Eq. (4.27). Moreover we have  $y_2 > y_+$  and

$$\begin{cases} y_- > \Delta y, & \text{for } \overline{P}_{bj}^2 < m_b^2, \\ y_- < \Delta y, & \text{for } \overline{P}_{bj}^2 > m_b^2. \end{cases} \tag{4.38}$$

For this integration two cases can be distinguished:

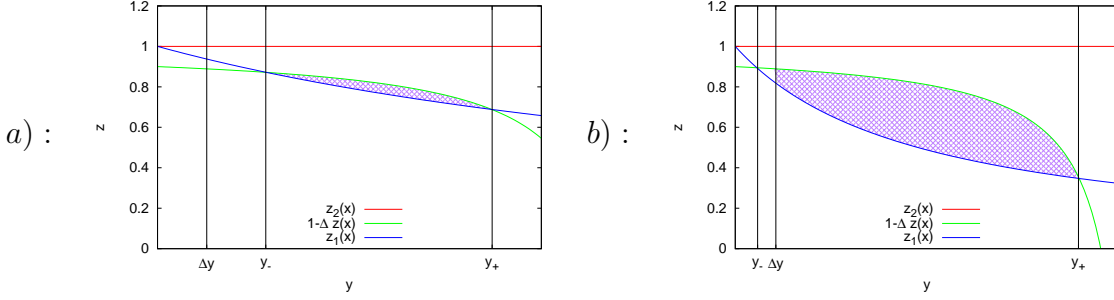


Figure 4.2: Boundary of the integration for the case  $b$ -quark emitter and light fermion  $j$  spectator, with  $\Delta y = 0.1$  and  $m_b = 4.78 \text{ GeV}$ . In case  $a)$  we have  $\overline{P}_{bj}^2 = 28 \text{ GeV}^2 < m_b^2$ , while in case  $b)$  we have  $\overline{P}_{bj}^2 = 40 \text{ GeV}^2 > m_b^2$ .

- $\overline{P}_{bj}^2 < m_b^2$ : To calculate the  $\Theta_f \Theta_{f'}$  contribution we consider the massless limit  $m_j \rightarrow 0$  of the complete integration in Eq. (4.34),

$$G_{bj}^{(\text{sub})}(P_{bj}^2) = \frac{3}{2} - \frac{\pi^2}{3} + 2\text{Li}_2\left(\frac{m_b^2}{P_{bj}^2}\right) + \ln\left(\frac{m_b m_\gamma^2 \sqrt{P_{bj}^2}}{\overline{P}_{bj}^4}\right) + \ln\left(\frac{m_b^2}{P_{bj}^2}\right) \ln\left(\frac{m_\gamma^2}{m_b \sqrt{P_{bj}^2}}\right) + \frac{m_b^2}{2P_{bj}^2}. \quad (4.39)$$

We subtract to  $G_{bj}^{(\text{sub})}(P_{bj}^2)$  the integral (c) between  $[y_-, y_+]$  and  $[z_1, 1 - \Delta z]$ ,

$$G_{bj}|_{(c)}(P_{bj}^2) = \frac{\overline{P}_{bj}^2}{\sqrt{\lambda_{bj}}} \int_{y_-}^{y_+} dy \left\{ \frac{2}{y R_{bj}(y)} \ln\left(\frac{1 - (1 - y)z_1}{1 - (1 - y)(1 - \Delta z)}\right) + (z_1 - (1 - \Delta z)) \frac{(1 - y)}{y R_{bj}(y)} \left[ 1 + \frac{(z_1 + (1 - \Delta z))}{2} + \frac{2m_b^2}{\overline{P}_{bj}^2 y} \right] \right\} \quad (4.40)$$

$$= -\frac{\pi^2}{3} + \ln\left(\frac{m_b^2}{P_{bj}^2}\right) \ln\left(\frac{P_{bj}^2 m_b^2 \Delta s^2}{\overline{P}_{bj}^8}\right) - 2\text{Li}_2\left(-\frac{m_b^2}{\overline{P}_{bj}^2}\right) - \ln^2\left(\frac{m_b^2}{\overline{P}_{bj}^2}\right) + \ln\left(\frac{\sqrt{P_{bj}^2} \Delta s^2 m_b^3}{\overline{P}_{bj}^8}\right) + \frac{m_b^2}{2P_{bj}^2} + \frac{3}{2}, \quad (4.41)$$

which is the black area pictorially shown in Fig. 4.2 a). The final contribution for  $i = b$ , the light fermion  $j$  and  $\overline{P}_{bj}^2 < m_b^2$  case is

$$G_{bj}(P_{bj}^2) = 2 \ln\left(\frac{m_\gamma \overline{P}_{bj}^2}{m_b \Delta s}\right) + \ln\left(\frac{m_b^2}{P_{bj}^2}\right) \ln\left(\frac{\overline{P}_{bj}^4 m_\gamma^2}{m_b \sqrt{P_{bj}^2} \Delta s^2}\right). \quad (4.42)$$

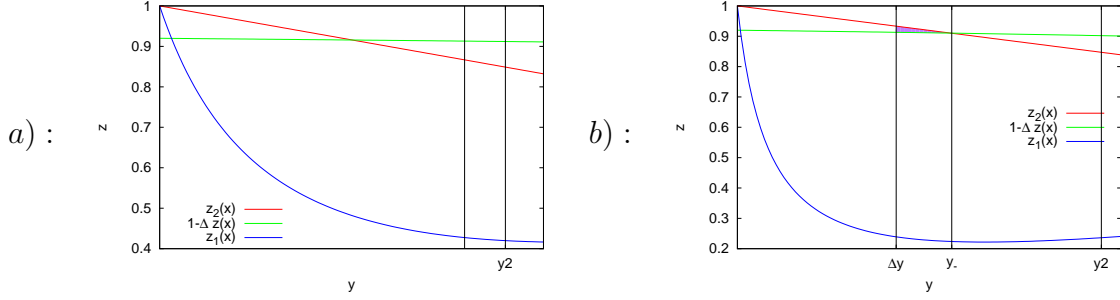


Figure 4.3: Boundary of the integration for the case light fermion  $i$  emitter and  $b$ -quark spectator, with  $\Delta y = 0.1$  and  $m_b = 4.78 \text{ GeV}$ . In case  $a$ ) we have  $\overline{P}_{ib}^2 = 18 \text{ GeV}^2 < m_b^2$ , while in case  $b$ ) we have  $\overline{P}_{ib}^2 = 35 \text{ GeV}^2 > m_b^2$ .

- $\overline{P}_{bj}^2 > m_b^2$ : We proceed similarly to the previous case, subtracting from Eq. (4.39) the integral (d) between  $[\Delta y, y_+]$  and  $[z_1, 1 - \Delta z]$  (the black area shown in Fig. 4.2 b)). We find

$$G_{bj}(P_{bj}^2)|_{(d)} = -\frac{\pi^2}{6} + \ln\left(\frac{m_b^2}{P_{bj}^2}\right) \ln\left(\frac{P_{bj}^2 \Delta s^2}{m_b^2 \overline{P}_{bj}^4}\right) + \ln\left(\frac{\sqrt{P_{bj}^2 \Delta s^2}}{m_b \overline{P}_{bj}^4}\right) - \frac{1}{2} + \frac{m_b^2}{2P_{bj}^2} + \frac{2m_b^2}{\overline{P}_{bj}^2}. \quad (4.43)$$

The contribution for  $i = b$ , the light fermion  $j$  and  $\overline{P}_{bj}^2 > m_b^2$  is

$$G_{bj}(P_{bj}^2) = 2 - \frac{\pi^2}{6} + 2\text{Li}_2\left(\frac{m_b^2}{P_{bj}^2}\right) + 2 \ln\left(\frac{m_\gamma m_b}{\Delta s}\right) + \ln\left(\frac{m_b^2}{P_{bj}^2}\right) \ln\left(\frac{\overline{P}_{bj}^4 m_\gamma^2 m_b}{P_{bj}^2 \sqrt{P_{bj}^2 \Delta s^2}}\right) - \frac{2m_b^2}{\overline{P}_{bj}^2}. \quad (4.44)$$

### Emitter $i$ and spectator $j = b$ , with $m_i \rightarrow 0$

The SOFT (Eq. (4.29)) and COLLINEAR 1 (Eq. (4.30)) conditions cover the domain  $[y_-, \Delta y]$  and  $[z_1, z_2]$ , which we call (a). We have  $z_1 < (1 - \Delta z)$  for  $y > y_-$  and  $z_2 > (1 - \Delta z)$  for  $y < y_+$ , where

$$y_- = \frac{m_i^2}{\overline{P}_{ib}^2} \Delta y, \quad y_+ = \frac{\overline{P}_{ib}^2}{m_b^2} \Delta y, \quad \text{and} \quad \begin{cases} y_+ < \Delta y, & \text{for } \overline{P}_{ib}^2 < m_b^2, \\ y_+ > \Delta y, & \text{for } \overline{P}_{ib}^2 > m_b^2. \end{cases} \quad (4.45)$$

Two different cases are encountered in the integration:

- $\overline{P}_{ib}^2 < m_b^2$ : To calculate the  $\Theta_f \Theta_{f'}$  contribution (a) needs to be evaluated, as shown in Fig. 4.3 a). To simplify the calculation, we first solve the integral for the region  $y \in [\Delta y, y_2]$  and  $z \in [z_1, z_2]$  (that we call (b)), where we can safely set  $m_\gamma = 0$ ,

$$G_{ib}(P_{ib}^2)|_{(b)} = \frac{\pi^2}{3} + \frac{1}{2} \ln\left(\frac{m_i^2 m_\gamma^4}{\Delta s^3}\right) - \ln^2\left(\frac{\Delta s P_{ib}^2}{\overline{P}_{ib}^4}\right) + \ln\left(\frac{m_i^2 P_{ib}^2}{\overline{P}_{ib}^4}\right) \ln\left(\frac{m_\gamma^2 \sqrt{P_{ib}^2}}{m_i \overline{P}_{ib}^2}\right). \quad (4.46)$$

Here the substitution

$$x = y_2 - y + \frac{\sqrt{\lambda_{ib}} R_{ib}}{\bar{P}_{ib}^2} \quad (4.47)$$

has been used. We then subtract Eq. (4.46) from the complete integral, i.e. Eq. (4.34), which corresponds to the region (a) + (b):

$$\begin{aligned} G_{ib}^{(\text{sub})}(P_{ib}^2) &= \frac{3}{2} - \frac{\pi^2}{3} + 4\text{Li}_2\left(-\frac{m_b}{\sqrt{P_{ib}^2}}\right) + \ln\left(\frac{m_i m_\gamma^2}{(\sqrt{P_{ib}^2} - m_b)^3}\right) \\ &\quad + \ln\left(\frac{m_i^2 P_{ib}^2}{\bar{P}_{ib}^4}\right) \ln\left(\frac{m_\gamma^2 \sqrt{P_{ib}^2}}{m_i \bar{P}_{ib}^2}\right). \end{aligned} \quad (4.48)$$

The final result is given by

$$G_{ib}(P_{ib}^2)|_{(a)} = \frac{3}{2} - \frac{2\pi^2}{3} + \frac{1}{2} \ln\left(\frac{m_i^2 m_\gamma^4}{\Delta s^3}\right) - \ln^2\left(\frac{\Delta s P_{ib}^2}{\bar{P}_{ib}^4}\right) + \ln\left(\frac{m_i^2 P_{ib}^2}{\bar{P}_{ib}^4}\right) \ln\left(\frac{m_\gamma^2 \sqrt{P_{ib}^2}}{m_i \bar{P}_{ib}^2}\right). \quad (4.49)$$

Until now we assumed collinear safety with respect to radiation off the lepton. In the case of non-collinear-safe observables, particular attention has to be taken in the region where the collinear photon is emitted by the light fermion (COLLINEAR 1 (C1)):

$$G_{ib}(P_{ib}^2)|_{C1} = \frac{\bar{P}_{ib}^4}{2\sqrt{\lambda_{ib}}} \left[ \int_{y_-}^{y_+} dy (1-y) \int_{z_1}^{1-\Delta z} dz + \int_{y_+}^{\Delta y} dy (1-y) \int_{z_1}^{z_2} dz \right] g_{ib}(p_i, p_b, q). \quad (4.50)$$

We need to interchange the order of the integration of the previous equation to leave the integration over  $z$  open. This allows us to get the extra term  $[\bar{\mathcal{G}}_{ib}(P_{ib}^2, z)]_+$  described in Eq. (4.18). The inversion of the parameterization of Eq. (4.50) reads

$$\begin{cases} y_{1+} \sim \frac{\bar{P}_{ib}^2}{m_b^2} z & \text{for } y < \frac{m_i}{m_b}, \\ y_{1-} \sim \frac{m_i^2 (1-z)}{\bar{P}_{ib}^2 z} & \text{for } y > \frac{m_i}{m_b}, \end{cases} \quad y_2 \sim \frac{\bar{P}_{ib}^2}{m_b^2} (1-z) \quad \text{and} \quad y_\Delta \sim 1 - \frac{\Delta y}{1-z}, \quad (4.51)$$

setting  $m_\gamma = 0$  and using

$$z_1 \sim \frac{m_i^2}{m_i^2 + \bar{P}_{ib}^2 y} + \frac{m_b^2}{\bar{P}_{ib}^2} y, \quad z_2 \sim 1 - \frac{m_b^2}{\bar{P}_{ib}^2} y, \quad (4.52)$$

after the assumption

$$\mathcal{O}\left(\frac{m_i^2}{\bar{P}_{ib}^2}\right) < y < \Delta y. \quad (4.53)$$

We define

$$\bar{\mathcal{G}}_{ib}^i(P_{ib}^2, z) = \frac{\bar{P}_{ib}^4}{2\sqrt{\lambda_{ib}}} \int_{y_a(z)}^{y_b(z)} dy (1-y) g_{ib} \quad (4.54)$$

and identify four different contributions

$$\bar{\mathcal{G}}_{ib}(P_{ib}^2, z) = \begin{cases} \bar{\mathcal{G}}_{ib}^{(1)}(P_{ib}^2, z) & \text{with } y_a(z) = y_{1-}(z), y_b(z) = y_{1+}(z), \quad \text{for } z \in [z_0, z_-], \\ \bar{\mathcal{G}}_{ib}^{(2)}(P_{ib}^2, z) & \text{with } y_a(z) = y_{1-}(z), y_b(z) = \Delta y, \quad \text{for } z \in [z_-, z_A], \\ \bar{\mathcal{G}}_{ib}^{(3)}(P_{ib}^2, z) & \text{with } y_a(z) = y_{1-}(z), y_b(z) = y_2(z), \quad \text{for } z \in [z_A, z_B], \\ \bar{\mathcal{G}}_{ib}^{(4)}(P_{ib}^2, z) & \text{with } y_a(z) = y_{1-}(z), y_b(z) = y_\Delta(z), \quad \text{for } z \in [z_B, z_C], \end{cases} \quad (4.55)$$

where

$$\begin{aligned} z_0 &= 2 \frac{m_i m_b}{\bar{P}_{ib}^2}, \quad z_- = \frac{m_b^2}{\bar{P}_{ib}^2} \Delta y, \quad z_A = 1 - \frac{m_b^2}{\bar{P}_{ib}^2} \Delta y, \\ z_B &= 1 - \Delta y - \frac{\bar{P}_{ib}^2}{m_b^2} \Delta y^2, \quad z_C = 1 - \Delta y - \frac{m_i^2}{\bar{P}_{ib}^2} \Delta y^2. \end{aligned} \quad (4.56)$$

It is possible to observe that the soft divergences appear at the endpoint  $z \rightarrow 1$ , and that  $z_A \sim z_B \sim z_C \sim 1$ . This means that  $\bar{\mathcal{G}}_{ib}^{(3)}(P_{ib}^2, z)$  and  $\bar{\mathcal{G}}_{ib}^{(4)}(P_{ib}^2, z)$  do not contribute to  $[\bar{\mathcal{G}}_{ib}(P_{ib}^2, z)]_+$ . Consequently, for our purposes it is sufficient to calculate

$$\bar{\mathcal{G}}_{ib}^{(1)}(P_{ib}^2, z) = 0 \quad \text{and} \quad \bar{\mathcal{G}}_{ib}^{(2)}(P_{ib}^2, z) = \frac{1+z^2}{1-z} \ln \left( \frac{z \Delta s}{m_i^2(1-z)} \right) - \frac{2z}{1-z}. \quad (4.57)$$

-  $\bar{P}_{ib}^2 > m_b^2$ : In this case we need to add to Eq. (4.49) the quantity

$$\begin{aligned} G_{ib}(P_{ib}^2)|_{(f)} &= \int_{\Delta y}^{y_-} dy \frac{2\bar{P}_{ib}^2}{y\sqrt{\lambda_{ib}}R_{ib}(y)} \ln \left( \frac{1 - (1-y)(1-\Delta z)}{1 - (1-y)z_2} \right) \\ &= \frac{\pi^2}{6} + 2 \ln \left( \frac{m_b^2}{\bar{P}_{ib}^2} \right) \ln \left( \frac{P_{ib}^2}{\bar{P}_{ib}^2} \right) + 2\text{Li}_2 \left( -\frac{m_b^2}{\bar{P}_{ib}^2} \right), \end{aligned} \quad (4.58)$$

which originates from the COLLINEAR 2 (C2) condition, as shown in Fig. 4.3 b).

Concerning the non-collinear-safe observables, the C1 contribution is given by

$$G_{ib}(P_{ib}^2)|_{C1} = \frac{\bar{P}_{ib}^4}{2\sqrt{\lambda_{ib}}} \int_{y_-}^{\Delta y} dy (1-y) \int_{z_1}^{1-\Delta z} dz g_{ib}(p_i, p_b, q). \quad (4.59)$$

When inverted, leaving the integration over  $z$  open, Eq. (4.59) gives rise to

$$\bar{\mathcal{G}}_{ib}(P_{ib}^2, z) = \begin{cases} \bar{\mathcal{G}}_{ib}^{(1)}(P_{ib}^2, z) & \text{with } y_a(z) = y_{1-}(z), y_b(z) = y_{1+}(z), \quad \text{for } z \in [z_0, z_-], \\ \bar{\mathcal{G}}_{ib}^{(2)}(P_{ib}^2, z) & \text{with } y_a(z) = y_{1-}(z), y_b(z) = \Delta y, \quad \text{for } z \in [z_-, z_D], \\ \bar{\mathcal{G}}_{ib}^{(3)}(P_{ib}^2, z) & \text{with } y_a(z) = y_{1-}(z), y_b(z) = y_\Delta(z), \quad \text{for } z \in [z_D, z_C], \end{cases} \quad (4.60)$$

where  $\bar{\mathcal{G}}_{ib}^i(P_{ib}^2, z)$  is defined in Eq. (4.54),  $y_{1-}(z)$ ,  $y_{1+}(z)$ ,  $y_\Delta(z)$  in Eq. (4.51),  $z_0$ ,  $z_-$ ,  $z_C$  in Eq. (4.56) and

$$z_D = 1 - \Delta y - \Delta y^2. \quad (4.61)$$

With the same arguments as in the case  $\overline{P}_{ib}^2 < m_b^2$ , only

$$\bar{\mathcal{G}}_{ib}^{(1)}(P_{ib}^2, z) = 0 \quad \text{and} \quad \bar{\mathcal{G}}_{ib}^{(2)}(P_{ib}^2, z) = \frac{1+z^2}{1-z} \ln\left(\frac{z\Delta s}{m_i^2(1-z)}\right) - \frac{2z}{1-z} \quad (4.62)$$

contribute to  $[\bar{\mathcal{G}}_{ib}(P_{ib}^2, z)]_+$ .

Summarizing, the soft+collinear contribution for the light fermion  $i$  and  $j = b$  is

$$\begin{aligned} G_{ib}(P_{ib}^2) &= \frac{3}{2} - \frac{2\pi^2}{3} + \frac{1}{2} \ln\left(\frac{m_i^2 m_\gamma^4}{\Delta s^3}\right) - \ln^2\left(\frac{\Delta s P_{ib}^2}{\overline{P}_{ib}^4}\right) + \ln\left(\frac{m_i^2 P_{ib}^2}{\overline{P}_{ib}^4}\right) \ln\left(\frac{m_\gamma^2 \sqrt{P_{ib}^2}}{m_i \overline{P}_{ib}^2}\right) \\ &+ \Theta(\overline{P}_{ib}^2 - m_b^2) \left\{ \frac{\pi^2}{6} + 2\text{Li}_2\left(-\frac{m_b^2}{\overline{P}_{ib}^2}\right) + 2 \ln\left(\frac{m_b^2}{\overline{P}_{ib}^2}\right) \ln\left(\frac{P_{ib}^2}{\overline{P}_{ib}^2}\right) \right\}, \end{aligned} \quad (4.63)$$

with the non-collinear-safe contribution given by

$$[\bar{\mathcal{G}}_{ib}(P_{ib}^2, z)]_+ = \left[ \frac{1+z^2}{1-z} \ln\left(\frac{z\Delta s}{m_i^2(1-z)}\right) - \frac{2z}{1-z} \right]_+. \quad (4.64)$$

### Emitter $i = u$ and spectator $j = d$ and vice versa

In the case where the  $W$  boson is decaying hadronically, the photon can be emitted by both the light quarks stemming from the decay (we refer to them as  $u$  and  $d$ ).  $G_{ud}(P_{ud}^2)$  and  $G_{du}(P_{du}^2)$  can be easily calculated taking the massless limit of the case of a light emitter  $i$  and  $j = b$ , replacing  $i \rightarrow u$  and  $b \rightarrow d$ , and vice versa. The final result is

$$G_{ij}(P_{ij}^2) = \frac{3}{2} - \frac{\pi^2}{2} + \frac{1}{2} \ln\left(\frac{m_i^2 m_\gamma^4}{\Delta s^3}\right) - \ln^2\left(\frac{\Delta s}{P_{ij}^2}\right) + \frac{1}{2} \ln\left(\frac{m_i^2}{P_{ij}^2}\right) \ln\left(\frac{m_\gamma^4}{m_i^2 P_{ij}^2}\right), \quad (4.65)$$

being  $\overline{P}_{ij}^2 = P_{ij}^2$ , and  $m_i$  and  $m_j$  the divergences regulators.

### 4.2.2 Final-state emitter and initial-state spectator, and vice versa

In the cases of a final-state emitter  $i$  and an initial-state spectator  $a$ , and of an initial-state emitter  $a$  and a final state spectator  $i$  (represented on the left- and on the right-hand side of Fig. 4.4, respectively), the following variables and abbreviations are used:

$$P_{ia} = P_{ai} = p_i - p_a + q, \quad s_{ia} = s_{ai} = -\overline{P}_{ia}^2 = -P_{ia}^2 + m_i^2 + m_a^2 + m_\gamma^2 > 0, \quad (4.66)$$

and

$$\lambda_{ia} = \lambda_{ai} = \lambda(P_{ia}^2, m_i^2, m_a^2) = s_{ia}^2 - 4m_i^2 m_a^2. \quad (4.67)$$

The radiator functions are [44]

$$\begin{aligned} g_{ia}(p_i, p_a, q) &= \frac{1}{(p_i q) x} \left[ \frac{2}{2-x-z} - 1 - z - \frac{m_i^2}{p_i q} \right], \\ g_{ai}(p_a, p_i, q) &= \frac{1}{(p_a q) x} \left[ \frac{2}{2-x-z} - R_{ia}(x)(1+x) - \frac{x m_a^2}{p_i q} \right], \end{aligned} \quad (4.68)$$

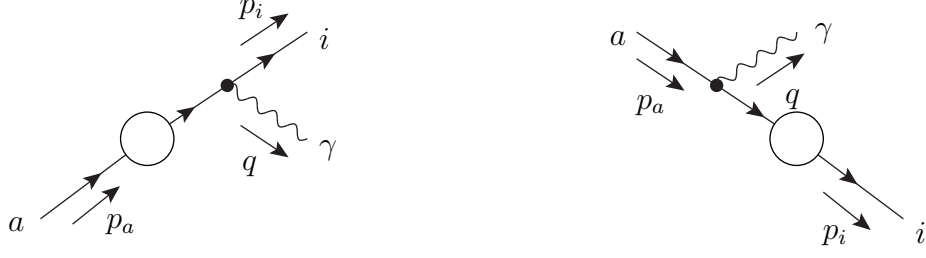


Figure 4.4: Generic diagram with a final-state emitter  $i$  and an initial-state spectator  $a$  on the left, and with an initial-state emitter  $a$  and a final-state spectator  $i$  on the right.

where  $x$  and  $z$  are the shorthands for

$$x_{ia} = x_{ai} = \frac{p_a p_i + p_a q - p_i q}{p_a p_i + p_a q}, \quad z_{ia} = z_{ai} = \frac{p_a p_i}{p_a p_i + p_a q}, \quad (4.69)$$

and

$$R_{ia}(x) = R_{ai}(x) = \frac{\sqrt{(-s_{ia} + 2m_a^2 x)^2 - 4P_{ia}^2 m_a^2 x^2}}{\sqrt{\lambda_{ia}}}. \quad (4.70)$$

The kinematic and angular constraints lead to the conditions  $x \in [x_1, x_2]$  and  $z \in [z_1, z_2]$ , where

$$\begin{cases} x_1 = \frac{s_{ia}}{2m_a(m_a - \sqrt{P_{ia}^2})}, \\ x_2 = 1 - \frac{2m_i m_\gamma}{s_{ia}}, \end{cases}$$

and

$$z_{1,2}(x) = \frac{s_{ia}(1-x) + 2m_i^2 x \mp \sqrt{(1-x)^2 - \frac{4m_i^2 m_\gamma^2}{s_{ia}^2}} x^2 \sqrt{\lambda_{ia}} R_{ia}(x)}{2[(1-x)s_{ia} + (m_i^2 + m_\gamma^2)x]}. \quad (4.71)$$

The final integrals, which have to be calculated, are

$$\begin{aligned} G_{ia}(P_{ia}^2) &= \frac{s_{ia}^2}{2\sqrt{\lambda_{ia}} R_{ia}(x)} \int_{x_1}^{x_2} dx \int_{z_1(x)}^{z_2(x)} dz g_{ia}(p_i, p_a, q) \Theta_f \Theta_{f'}, \\ G_{ai}(P_{ia}^2) &= \frac{s_{ia}^2}{2\sqrt{\lambda_{ia}} R_{ia}(x)} \int_{x_1}^{x_2} dx \int_{z_1(x)}^{z_2(x)} dz g_{ai}(p_a, p_i, q) \Theta_f \Theta_{f'}, \end{aligned} \quad (4.72)$$

where the regions contributing to  $\Theta_f \Theta_{f'}$  (Eq. (4.14)) are

$$\text{SOFT: } \begin{cases} z > 1 - \Delta z & \text{for } s_{a\gamma} < \Delta s, \\ x > \frac{1}{1 + \Delta x} & \text{for } s_{i\gamma} < \Delta s, \end{cases} \quad (4.73)$$

$$\text{COLLINEAR 1: } \gamma \text{ collinear to } i \quad \begin{cases} z < 1 - \Delta z & \text{for } s_{a\gamma} > \Delta s, \\ x > \frac{1}{1 + \Delta x} & \text{for } s_{i\gamma} < \Delta s, \end{cases} \quad (4.74)$$

$$\text{COLLINEAR 2: } \gamma \text{ collinear to } a \quad \begin{cases} z > 1 - \Delta z & \text{for } s_{a\gamma} < \Delta s, \\ x < \frac{1}{1 + \Delta x} & \text{for } s_{i\gamma} > \Delta s, \end{cases} \quad (4.75)$$

with

$$\Delta x \equiv \frac{\Delta s}{s_{ia}}, \quad \Delta z \equiv x \Delta x \quad \text{and} \quad x_1 < \frac{1}{1 + \Delta x} < x_2. \quad (4.76)$$

### Emitter $i = b$ and spectator $a = t$ , and vice versa

For the final-state emitter  $i = b$  and the initial-state spectator  $a = t$  (and vice versa) we can see that  $1 - \Delta z > z_2$ . This means that we have neither SOFT (Eq. (4.73)) nor COLLINEAR 2 (Eq. (4.75)) contributions, due to the large mass of the top quark. The only contribution left is given by the case where the photon is collinear to the  $b$  quark. Therefore we calculate the integrals

$$\begin{aligned} G_{bt}(P_{bt}^2) &= \frac{s_{bt}}{\sqrt{\lambda_{bt}}} \int_{\frac{1}{1+\Delta x}}^{x_2} dx \frac{1}{R_{bt}(x)(1-x)} \left\{ 2 \ln \left( \frac{2-x-z_1}{2-x-z_2} \right) \right. \\ &\quad \left. + (z_1 - z_2) \left[ 1 + \frac{(z_1 + z_2)}{2} + \frac{2m_b^2 x}{s_{bt}(1-x)} \right] \right\} \\ &= 2 \ln \left( \frac{m_\gamma m_b}{\Delta s} \right) + 2 - \frac{s_{bt}}{\sqrt{\lambda_{bt}}} \left\{ \frac{\pi^2}{3} - \frac{1}{2} \ln^2(b_1) \right. \\ &\quad \left. + \ln(b_1) \ln \left( \frac{\Delta s^2(m_t^2 + m_b^2 + s_{bt})}{m_\gamma^2 \lambda_{bt}} \right) - 2\text{Li}_2(b_1) \right\} \end{aligned} \quad (4.77)$$

and

$$\begin{aligned} G_{tb}(P_{tb}^2) &= \frac{s_{bt}}{\sqrt{\lambda_{bt}}} \int_{\frac{1}{1+\Delta x}}^{x_2} dx \frac{1}{R_{bt}(x)} \left\{ \frac{2}{1-x} \ln \left( \frac{(1-z_1)(2-x-z_2)}{(1-z_2)(2-x-z_1)} \right) \right. \\ &\quad \left. - R_{bt}(x)(1+x) \ln \left( \frac{1-z_2}{1-z_1} \right) - \frac{2m_t^2 x^2}{s_{bt}} \left[ \frac{1}{1-z_2} - \frac{1}{1-z_1} \right] \right\} \\ &= 2 \ln \left( \frac{m_\gamma m_b}{\Delta s} \right) - \frac{s_{bt}}{\sqrt{\lambda_{bt}}} \left\{ 2 \ln \left( \frac{b_1}{c_0} \right) \ln \left( \frac{m_\gamma \sqrt{\lambda_{bt}}}{m_t \Delta s} \right) + \frac{1}{2} \ln(c_0 b_1) \ln \left( \frac{b_1}{c_0} \right) \right. \\ &\quad \left. - \ln \left( \frac{s_{bt} + m_b^2 + m_t^2}{m_t^2} \right) \ln(b_1) + \ln(c_0) - 2\text{Li}_2(c_0) + 2\text{Li}_2(b_1) \right\}, \end{aligned} \quad (4.78)$$

using, respectively, Eq. (4.28) and Eq. (4.34) of Ref. [44], where we have identified  $(1 - x_0)$  with  $\Delta x$ , in the limit  $\Delta x \rightarrow 0$ , and

$$b_1 = \frac{2m_b^2 + s_{bt} - \sqrt{\lambda_{bt}}}{2m_b^2 + s_{bt} + \sqrt{\lambda_{bt}}}, \quad c_0 = \frac{s_{bt} - \sqrt{\lambda_{bt}}}{s_{bt} + \sqrt{\lambda_{bt}}}. \quad (4.79)$$

### Emitter $i$ and spectator $a = t$ , with $m_i \rightarrow 0$

The mass of the emitter is small, we therefore consider the hierarchy

$$m_\gamma^2 \ll m_i^2 \ll \Delta s \ll m_t^2, s_{it} \quad (4.80)$$

between the parameters. It is possible to show that  $1 - \Delta z < z_2$  for  $x > x_3$  and that  $1 - \Delta z > z_1$  for  $x < x_4$ , where

$$x_3 = 1 - \frac{s_{it}^2 \Delta x}{m_t^4}, \quad x_4 = 1 - \frac{m_i^2}{s_{it}} \Delta x, \quad \text{and} \quad x_1 < \frac{1}{1 + \Delta x} < x_3 < x_4 < x_2. \quad (4.81)$$

Only the SOFT (Eq. (4.73)) and COLLINEAR 1 (Eq. (4.74)) contributions survive. Therefore, the integral that has to be calculated is

$$G_{it}(P_{it}^2) = \frac{s_{it}}{\sqrt{\lambda_{it}}} \int_{1-\Delta x}^{x_2} dx \frac{1}{R_{it}(x)(1-x)} \left\{ 2 \ln \left( \frac{2-x-z_1}{2-x-z_2} \right) + (z_1 - z_2) \left[ 1 + \frac{(z_1 + z_2)}{2} + \frac{2m_i^2 x}{s_{it}(1-x)} \right] \right\} \quad (4.82)$$

$$= \frac{1}{2} \ln \left( \frac{m_\gamma^4 m_i^2}{\Delta s^3} \right) + \frac{3}{2} - \frac{2\pi^2}{3} - 2 \ln \left( \frac{\Delta s}{s_{it}} \right) \ln \left( \frac{s_{it} + m_t^2}{s_{it}} \right) - \frac{1}{2} \ln^2 \left( \frac{m_i^2}{s_{it}} \right) - \ln^2 \left( \frac{\Delta s}{s_{it}} \right) + \ln \left( \frac{m_\gamma^2}{s_{it}} \right) \ln \left( \frac{(s_{it} + m_t^2) m_i^2}{s_{it}^2} \right) - \frac{1}{2} \ln^2 \left( \frac{s_{it} + m_t^2}{s_{it}} \right). \quad (4.83)$$

The contribution to the non-collinear-safe observables is obtained by interchanging the order of the integrations of the COLLINEAR 1 region ,

$$G_{it}(P_{it}^2)|_{C1} = \frac{s_{it}^2}{2\sqrt{\lambda_{it}} R_{it}(x)} \left[ \int_{\frac{1}{1+\Delta x}}^{x_3} dx \int_{z_1}^{z_2} dz + \int_{x_3}^{x_4} dx \int_{z_1}^{1-\Delta z} dz \right] g_{it}(p_i, p_t, q), \quad (4.84)$$

and leaving the integration over  $z$  open. The only part that contributes to the plus distribution is

$$\begin{aligned} [\bar{G}_{it}(P_{it}^2, z)]_+ &= \left[ \frac{s_{it}^2}{2\sqrt{\lambda_{it}} R_{it}(x)} \int_{\frac{1}{1+\Delta x}}^{x_1(z)} dx g_{it}(p_i, p_t, q) \right]_+ \\ &= \left[ \frac{1+z^2}{1-z} \ln \left( \frac{z \Delta s}{m_i^2(1-z)} \right) - \frac{2z}{1-z} \right]_+. \end{aligned} \quad (4.85)$$

### Emitter $a = t$ and spectator $i$ , with $m_i \rightarrow 0$

Since the light particle is the spectator, we can extract the soft+collinear contribution from Eq. (4.78), replacing  $b \rightarrow i$  and taking the limit  $m_i \rightarrow 0$ ,

$$G_{ti}(P_{ti}^2) = 2 \ln \left( \frac{m_\gamma s_{it}}{m_t \Delta s} \right) - \ln \left( \frac{s_{it} + m_t^2}{m_t^2} \right) \ln \left( \frac{m_\gamma^2 s_{it}^2}{m_t \sqrt{s_{it} + m_t^2} \Delta s^2} \right). \quad (4.86)$$

### 4.2.3 Summary of the singular contributions

We list in the following the results obtained performing the analytical integration described in Eq. (4.12) for the various final states and corrections to the top-quark decay.

- **Leptonic decay, QCD corrections:**

When the  $W$  boson is decaying leptonically, only the  $t$  and the  $b$  quarks can emit a gluon. Thus the singular integral contributing to the first term on the right-hand side of Eq. (4.15) is given by

$$S = \frac{\alpha_s}{2\pi} C_F (G_{tb} + G_{bt}), \quad (4.87)$$

where the colour factor is  $C_F = \frac{4}{3}$ .

- **Leptonic decay, EW corrections:**

The photon can be emitted either from the  $t$  or the  $b$  quarks or from the charged lepton. Following Eq. (4.12) we have

$$S = -\frac{\alpha}{2\pi} [-Q_t Q_b (G_{tb} + G_{bt}) + Q_t Q_\ell (G_{t\ell} + G_{\ell t}) - Q_\ell Q_b (G_{\ell b} + G_{b\ell})]. \quad (4.88)$$

- **Hadronic decay, QCD corrections:**

In this case the gluon can be emitted from all the quarks appearing in the process. There is no interference between the diagrams where the gluon is emitted by  $u$  or  $d$  and by  $t$  or  $b$ . More specifically, due to colour conservation, the trace over the colour factors of the interfering diagrams is zero. For this reason the singular integral reads

$$S = \frac{\alpha_s}{2\pi} C_F [(G_{tb} + G_{bt}) + (G_{ud} + G_{du})]. \quad (4.89)$$

- **Hadronic decay, EW corrections:**

Any of the particles appearing in the process can emit a photon, therefore

$$S = -\frac{\alpha}{2\pi} [-Q_t Q_b (G_{tb} + G_{bt}) + Q_t Q_d (G_{td} + G_{dt}) - Q_d Q_b (G_{db} + G_{bd}) - Q_t Q_u (G_{tu} + G_{ut}) + Q_u Q_b (G_{ub} + G_{bu}) - Q_u Q_d (G_{ud} + G_{du})]. \quad (4.90)$$

Since the integrals  $G_{ff'}(P_{ff'}^2)$  always appear in pairs, it is useful to summarize the results in a more compact form:

$$G_{tb} + G_{bt} = 2 \ln \left( \frac{m_\gamma^2 m_b^2}{\Delta s^2} \right) + 2 - \frac{s_{bt}}{\sqrt{\lambda_{bt}}} \left\{ \frac{\pi^2}{3} - 2 \ln(c_0) \ln \left( \frac{m_\gamma \sqrt{\lambda_{bt}}}{m_t \Delta s} \right) - \frac{1}{2} \ln^2(c_0) + \ln(c_0) - 2 \text{Li}_2(c_0) \right\}, \quad (4.91)$$

$$G_{ti} + G_{it} = \frac{1}{2} \ln \left( \frac{m_\gamma^8 m_i^2 s_{it}^4}{\Delta s^7 m_t^4} \right) + \frac{3}{2} - \frac{2\pi^2}{3} - 2 \ln \left( \frac{\Delta s}{s_{it}} \right) \ln \left( \frac{m_t^2}{s_{it}} \right) - \ln^2 \left( \frac{\Delta s}{s_{it}} \right) + \ln \left( \frac{m_\gamma^2}{s_{it}} \right) \ln \left( \frac{m_t^2 m_i^2}{s_{it}^2} \right) - \frac{1}{2} \ln^2 \left( \frac{s_{it}}{m_t^2} \right) - \frac{1}{2} \ln^2 \left( \frac{m_i^2}{s_{it}} \right), \quad (4.92)$$

$$G_{bi} + G_{ib} = \frac{3}{2} - \frac{2\pi^2}{3} + \frac{1}{2} \ln \left( \frac{m_\gamma^8 m_b^4 m_i^2}{\Delta s^7} \right) - \ln^2 \left( \frac{\Delta s}{\bar{P}_{bi}^2} \right) + \frac{1}{2} \ln \left( \frac{m_b^2}{\bar{P}_{bi}^2} \right) \ln \left( \frac{m_\gamma^4 m_b^2 \bar{P}_{bi}^2}{\Delta s^4} \right) + \frac{1}{2} \ln \left( \frac{m_i^2}{\bar{P}_{bi}^2} \right) \ln \left( \frac{m_\gamma^4}{m_i^2 \bar{P}_{bi}^2} \right) + \Theta(m_b^2 - \bar{P}_{bi}^2) \ln \left( \frac{m_b^2}{\bar{P}_{bi}^2} \right) \left[ \ln \left( \frac{m_b^2}{\bar{P}_{bi}^2} \right) - 2 \right] + \Theta(\bar{P}_{bi}^2 - m_b^2) \left[ 2 - \frac{2m_b^2}{\bar{P}_{bi}^2} \right], \quad (4.93)$$

$$G_{ud} + G_{du} = 3 - \pi^2 + \ln \left( \frac{m_u m_d m_\gamma^4}{\Delta s^3} \right) - 2 \ln^2 \left( \frac{\Delta s}{\bar{P}_{ud}^2} \right) + \frac{1}{2} \ln \left( \frac{m_d^2}{\bar{P}_{ud}^2} \right) \ln \left( \frac{m_\gamma^4}{m_d^2 \bar{P}_{ud}^2} \right) + \frac{1}{2} \ln \left( \frac{m_u^2}{\bar{P}_{ud}^2} \right) \ln \left( \frac{m_\gamma^4}{m_u^2 \bar{P}_{ud}^2} \right), \quad (4.94)$$

where  $i = u, d, \ell$ , depending on the  $W$ -boson decay mode ( $m_i \rightarrow 0$ ), and  $c_0$  is defined in Eq. (4.79).

### 4.3 Quasi-soft region

To integrate the singular region of the phase space, described in Eq. (4.15) by the integral  $I_S$ , we introduced in the previous sections the one-cutoff phase-space slicing method. We noticed, however, that not all the domain of  $I_S$  is covered by the integrals described in Eqs. (4.91)-(4.94): The regions where  $s_{f\gamma}$  is bigger than  $\Delta s$  for a pair emitter-spectator, but smaller than  $\Delta s$  for a third fermion (the so-called quasi-soft region), have not yet been examined.

To better explain it, we consider the explicit example of  $t(p_t) \rightarrow b(p_b) \nu_\ell(p_\nu) \ell^+(p_\ell) + \gamma(q)$ . This method can be easily extended to all other cases. Following Eqs. (4.15) and (4.88) for the emission of a photon in a semileptonic top-quark decay, the singular integral reads

$$I_S = \frac{\alpha}{2\pi} \int d\tilde{\Phi}_0 |\mathcal{M}_0(\tilde{\Phi}_{0,ff'})|^2 [Q_t Q_b (G_{tb} + G_{bt}) - Q_t Q_\ell (G_{t\ell} + G_{\ell t}) + Q_\ell Q_b (G_{\ell b} + G_{b\ell})] + I_{QS}. \quad (4.95)$$

$s_{t\gamma} < \Delta s$				$s_{t\gamma} > \Delta s$			
$s_{b\gamma} < \Delta s$		$s_{b\gamma} > \Delta s$		$s_{b\gamma} < \Delta s$		$s_{b\gamma} > \Delta s$	
$s_{\ell\gamma} < \Delta s$	$s_{\ell\gamma} > \Delta s$	$s_{\ell\gamma} < \Delta s$	$s_{\ell\gamma} > \Delta s$	$s_{\ell\gamma} < \Delta s$	$s_{\ell\gamma} > \Delta s$	$s_{\ell\gamma} < \Delta s$	$s_{\ell\gamma} > \Delta s$
$F_{tb} + F_{bt}$	$F_{tb} + F_{bt}$	$F_{tb} + F_{bt}$	$F_{tb} + F_{bt}$	$F_{tb} + F_{bt}$	$F_{tb} + F_{bt}$	$I_{QS,1}^{\text{EW,lept}}$	$I_H$
$F_{t\ell} + F_{\ell t}$	$F_{t\ell} + F_{\ell t}$	$F_{t\ell} + F_{\ell t}$	$F_{t\ell} + F_{\ell t}$	$F_{t\ell} + F_{\ell t}$	$I_{QS,2}^{\text{EW,lept}}$	$F_{t\ell} + F_{\ell t}$	
$F_{\ell b} + F_{b\ell}$	$F_{\ell b} + F_{b\ell}$	$F_{\ell b} + F_{b\ell}$	$I_{QS,3}^{\text{EW,lept}}$	$F_{\ell b} + F_{b\ell}$	$F_{\ell b} + F_{b\ell}$	$F_{\ell b} + F_{b\ell}$	

Table 4.1: Different contributions to the real EW correction phase space for the process  $t(p_t) \rightarrow b(p_b) \nu_\ell(p_\nu) \ell^+(p_\ell)$ .

The full phase space is integrated only if all the contributions shown in Table 4.1 are taken into account, where

$$F_{ff'} = \frac{\alpha}{2\pi} \int d\tilde{\Phi}_0 |\mathcal{M}_0(\tilde{\Phi}_{0,ff'})|^2 Q_f Q_{f'} G_{ff'}. \quad (4.96)$$

We emphasize that the functions  $G_{ff'}$  have to fulfill the  $\Theta_f \Theta_{f'}$  condition of Eq. (4.14). This implies that, for example in the case  $s_{t\gamma} > \Delta s$  and  $s_{b\gamma} > \Delta s$  for the pair emitter-spectator  $tb$ , the quantity  $F_{tb} + F_{bt} = 0$ , ignoring the behavior of  $s_{\ell\gamma}$ . The contribution given by the quasi-soft region if  $s_{\ell\gamma} < \Delta s$  (in red in Table 4.1) is thus needed,

$$I_{QS,1}^{\text{EW,lept}} = \frac{\alpha}{2\pi} \int_{\substack{s_{t\gamma}, s_{b\gamma} > \Delta s \\ s_{\ell\gamma} < \Delta s}} d\Phi_1 |\mathcal{M}_0(\tilde{\Phi}_0)|^2 Q_t Q_b (g_{tb} + g_{bt}). \quad (4.97)$$

Although its integral domain has support only in regions with a volume of  $\mathcal{O}(\Delta s)$ , there is an enhancement in the integrand in the limit where  $s_{t\gamma}$  and  $s_{b\gamma}$  are close to the border  $\Delta s$ , i.e. close to the soft limit. The soft-photon approximation (App. B) can therefore be used and the sum  $(g_{tb} + g_{bt})$  can be expressed by the eikonal factors, yielding

$$I_{QS,1}^{\text{EW,lept}} = -\frac{\alpha}{2\pi} Q_t Q_b \int_{\substack{s_{t\gamma}, s_{b\gamma} > \Delta s \\ s_{\ell\gamma} < \Delta s}} d\Phi_1 |\mathcal{M}_0(\tilde{\Phi}_0)|^2 \left( \frac{m_t^2}{(p_t q)^2} + \frac{m_b^2}{(p_b q)^2} - \frac{2p_t p_b}{(p_b q)(p_t q)} \right). \quad (4.98)$$

In this work the following generic mapping  $\tilde{\Phi}_0$  is used:

$$\tilde{p}_f^\mu = p_f^\mu + q^\mu - \frac{y_{ff'}}{1 - y_{ff'}} p_{f'}^\mu, \quad \tilde{p}_{f'}^\mu = \frac{1}{1 - y_{ff'}} p_{f'}^\mu, \quad \tilde{q} = 0, \quad (4.99)$$

where

$$y_{ff'} = \frac{s_{f\gamma}}{s_{ff'} + s_{f\gamma} + s_{f'\gamma}}. \quad (4.100)$$

The situation for the other two quasi-soft integrals is similar:

$$\begin{aligned} I_{QS,2}^{\text{EW,lept}} &= +\frac{\alpha}{2\pi} Q_t Q_\ell \int_{\substack{s_{t\gamma}, s_{\ell\gamma} > \Delta s \\ s_{b\gamma} < \Delta s}} d\Phi_1 |\mathcal{M}_0(\tilde{\Phi}_0)|^2 \left( \frac{m_t^2}{(p_t q)^2} - \frac{2p_t p_\ell}{(p_\ell q)(p_t q)} \right), \\ I_{QS,3}^{\text{EW,lept}} &= -\frac{\alpha}{2\pi} Q_b Q_\ell \int_{\substack{s_{b\gamma}, s_{\ell\gamma} > \Delta s \\ s_{t\gamma} < \Delta s}} d\Phi_1 |\mathcal{M}_0(\tilde{\Phi}_0)|^2 \left( \frac{m_b^2}{(p_b q)^2} - \frac{2p_b p_\ell}{(p_\ell q)(p_b q)} \right). \end{aligned} \quad (4.101)$$

The same procedure can be extended to the EW corrections of the hadronic decay

$$\begin{aligned}
I^{\text{EW,hadr}} &= \sum_{i=1}^6 I_{QS,i}^{\text{EW,hadr}}, \\
I_{QS,1}^{\text{EW,hadr}} &= -\frac{\alpha}{2\pi} Q_t Q_b \int_{\substack{s_{t\gamma}, s_{b\gamma} > \Delta s \\ s_{d\gamma} \vee s_{u\gamma} < \Delta s}} d\Phi_1 |\mathcal{M}_0(\tilde{\Phi}_0)|^2 \left( \frac{m_t^2}{(p_t q)^2} + \frac{m_b^2}{(p_b q)^2} - \frac{2p_t p_b}{(p_b q)(p_t q)} \right), \\
I_{QS,2}^{\text{EW,hadr}} &= +\frac{\alpha}{2\pi} Q_t Q_d \int_{\substack{s_{t\gamma}, s_{d\gamma} > \Delta s \\ s_{b\gamma} \vee s_{u\gamma} < \Delta s}} d\Phi_1 |\mathcal{M}_0(\tilde{\Phi}_0)|^2 \left( \frac{m_t^2}{(p_t q)^2} - \frac{2p_t p_d}{(p_d q)(p_t q)} \right), \\
I_{QS,3}^{\text{EW,hadr}} &= -\frac{\alpha}{2\pi} Q_b Q_d \int_{\substack{s_{b\gamma}, s_{d\gamma} > \Delta s \\ s_{t\gamma} \vee s_{u\gamma} < \Delta s}} d\Phi_1 |\mathcal{M}_0(\tilde{\Phi}_0)|^2 \left( \frac{m_b^2}{(p_b q)^2} - \frac{2p_b p_d}{(p_d q)(p_b q)} \right), \\
I_{QS,4}^{\text{EW,hadr}} &= -\frac{\alpha}{2\pi} Q_t Q_u \int_{\substack{s_{t\gamma}, s_{u\gamma} > \Delta s \\ s_{b\gamma} \vee s_{d\gamma} < \Delta s}} d\Phi_1 |\mathcal{M}_0(\tilde{\Phi}_0)|^2 \left( \frac{m_t^2}{(p_t q)^2} - \frac{2p_t p_u}{(p_u q)(p_t q)} \right), \\
I_{QS,5}^{\text{EW,hadr}} &= +\frac{\alpha}{2\pi} Q_b Q_u \int_{\substack{s_{b\gamma}, s_{u\gamma} > \Delta s \\ s_{t\gamma} \vee s_{d\gamma} < \Delta s}} d\Phi_1 |\mathcal{M}_0(\tilde{\Phi}_0)|^2 \left( \frac{m_b^2}{(p_b q)^2} - \frac{2p_b p_u}{(p_u q)(p_b q)} \right), \\
I_{QS,6}^{\text{EW,hadr}} &= -\frac{\alpha}{2\pi} Q_u Q_d \int_{\substack{s_{u\gamma}, s_{d\gamma} > \Delta s \\ s_{t\gamma} \vee s_{b\gamma} < \Delta s}} d\Phi_1 |\mathcal{M}_0(\tilde{\Phi}_0)|^2 \left( -\frac{2p_u p_d}{(p_u q)(p_d q)} \right), \tag{4.102}
\end{aligned}$$

where  $s_{f\gamma} \vee s_{f'\gamma} < \Delta s$  stands for  $s_{f\gamma} < \Delta s$  or  $s_{f'\gamma} < \Delta s$ .

The QCD corrections of the hadronic decay in the quasi-soft region are

$$\begin{aligned}
I^{\text{QCD,hadr}} &= \sum_{i=1}^2 I_{QS,i}^{\text{QCD,hadr}}, \\
I_{QS,1}^{\text{QCD,hadr}} &= -\frac{\alpha}{2\pi} \int_{\substack{s_{tg}, s_{bg} > \Delta s \\ s_{dg} \vee s_{ug} < \Delta s}} d\Phi_1 |\mathcal{M}_0(\tilde{\Phi}_0)|^2 \left( \frac{m_t^2}{(p_t q)^2} + \frac{m_b^2}{(p_b q)^2} - \frac{2p_t p_b}{(p_b q)(p_t q)} \right), \\
I_{QS,2}^{\text{QCD,hadr}} &= -\frac{\alpha}{2\pi} \int_{\substack{s_{ug}, s_{dg} > \Delta s \\ s_{tg} \vee s_{bg} < \Delta s}} d\Phi_1 |\mathcal{M}_0(\tilde{\Phi}_0)|^2 \left( -\frac{2p_u p_d}{(p_u q)(p_d q)} \right). \tag{4.103}
\end{aligned}$$

In case of QCD corrections to the leptonic decay this approach is not necessary, since there are only two possible emitting particles.

The integrals listed in Eqs. (4.98), (4.101), (4.102), and (4.103) can be numerically integrated, after applying appropriate mappings (see Chap. 5).

# Chapter 5

## Phase-space integration

The numerical integrations of the amplitudes described in the previous chapters have been performed with **VEGAS** [96], a program for multi-dimensional integration based on Monte Carlo techniques. A brief overview of the **VEGAS** integrator is given in Sect. 5.1.

For the phase-space integration, we follow the methods and the notation introduced in Refs. [9, 97]. They will be explained in a general way in Sect. 5.2, while a more detailed description of the specific cases of the  $1 \rightarrow 3$  and the  $1 \rightarrow 4$  particle phase spaces will be presented in Sects. 5.3 and 5.4, respectively.

### 5.1 VEGAS

**VEGAS** [96] is an algorithm for an adaptive multi-dimensional Monte Carlo integration, which allows to integrate a function  $f(\vec{x})$  over the  $n$ -dimensional unit cube  $\Omega$  ( $0 \leq x \leq 1$ ),

$$I = \int_{\Omega} d^n x f(\vec{x}). \quad (5.1)$$

The integration proceeds as follows:

- The integrand is evaluated at  $N$  random points  $\vec{x}_i$ , forming a weighted average

$$I \simeq S = \frac{1}{N} \sum_{i=1}^N \frac{f(\vec{x}_i)}{p(\vec{x}_i)}, \quad (5.2)$$

with an approximate uncertainty  $\sigma$ , where

$$\sigma^2 = \frac{1}{(N-1)N} \sum_{i=1}^N \frac{f(\vec{x}_i)^2}{p(\vec{x}_i)} - S^2 \quad (5.3)$$

and  $p(\vec{x}_i)$  is the density of the random points.

- A cumulative estimate  $\bar{S}$  of the integrand is calculated,

$$\bar{S} = \bar{\sigma}^2 \sum_{\alpha} \frac{S_{\alpha}}{\sigma_{\alpha}^2}, \quad (5.4)$$

after performing  $m$  estimates  $\{S_\alpha\}_{\alpha=1}^m$ . The approximate uncertainty in  $\bar{S}$  is

$$\frac{1}{\bar{\sigma}^2} = \sum_{\alpha} \frac{1}{\sigma_{\alpha}^2}, \quad (5.5)$$

where  $\sigma_{\alpha}^2$  is described in Eq. (5.3).

- The  $\chi^2$  per degree of freedom (*dof*),

$$\frac{\chi^2}{dof} = \frac{1}{m-1} \sum_{\alpha=1}^m \frac{(S_{\alpha} - \bar{S})^2}{\sigma_{\alpha}^2}, \quad (5.6)$$

is computed to check if the various estimates  $S_{\alpha}$  are consistent within the errors.

An important issue is the choice of the random integration points: **VEGAS** tries to estimate the shape of the function  $f(\vec{x})$  through  $\alpha$  iterations. During the first iteration, the algorithm uses a grid to divide the integration volume into hypercubes, where it distributes the randomly chosen points uniformly. During this procedure, it acquires information about the function, defining a new adapted density

$$p'(\vec{x}) = \frac{|f(\vec{x})|}{\int_{\Omega} d^n \vec{x} f(\vec{x})}. \quad (5.7)$$

In the subsequent iterations the integrator uses  $p'(\vec{x})$  to sample the regions where the random points become concentrated. This adaptive step allows to reduce  $\sigma_{\alpha}^2$ .

The **VEGAS** algorithm can in addition be employed, during the computation of the integral of  $f(\vec{x})$ , to compute differential distributions.

## 5.2 Phase-space parameterizations

In order to evaluate the top-quark width  $\Gamma_n$ , the squared matrix element for  $n$  particles in the final state (calculated explicitly in Chap. 3), has to be integrated over the entire phase-space volume multiplied by the flux factor (see Eq. (3.2)). During the integration it is possible to run into problematic regions which can cause numerical instabilities, e.g. the peaking behavior of Breit-Wigner resonances and of the propagators of massless particles. The efficiency of the Monte Carlo integration can be improved upon adapting the integration. This can be done flattening the peaking structures of the integrand through suitable mappings that mimic its behavior [97].

To explain how to construct the mappings, we first rewrite Eq. (3.2) as

$$\Gamma_n = \int_V d\Phi \rho(p_i(\Phi)) f(p_i(\Phi)). \quad (5.8)$$

In the previous equation,  $V$  is the volume of the new set of variables,  $\rho$  is the density of points in their phase space,  $p_i(\Phi)$  represents the relation between the phase-space variables  $\Phi$  and the momenta  $p_1, \dots, p_n$ , and

$$f(p_i(\Phi)) = N_c \frac{(2\pi)^{4-3n}}{2m_t} \sum \overline{|\mathcal{M}(p_t; p_1, \dots, p_n)|^2}. \quad (5.9)$$

We perform the phase-space integration with the **VEGAS** algorithm, which uses random numbers  $r_a \in [0, 1]$  (see Sect. 5.1) as variables. Therefore, we need to parametrize  $\Phi$  in terms of  $\mathbf{r} = (r_a)$ . This can be done in the following way:

$$\Gamma_n = \int_0^1 d\mathbf{r} \frac{f(p_i(\mathbf{h}(\mathbf{r})))}{g(p_i(\mathbf{h}(\mathbf{r})))}, \quad (5.10)$$

assuming  $\Phi = \mathbf{h}(\mathbf{r})$  and  $g$ , which is the probability density of the events generated in the phase space, defined as

$$\frac{1}{g(p_i(\mathbf{h}(\mathbf{r})))} = \rho(p_i(\Phi)) \left| \frac{\partial \mathbf{h}(\mathbf{r})}{\partial \mathbf{r}} \right|_{\mathbf{r}=\mathbf{h}^{-1}(\Phi)}. \quad (5.11)$$

In practice the  $1 \rightarrow n$  particle phase space is decomposed into subsequent  $1 \rightarrow 2$  decays, interconnected by intermediate particles, as described in the following.

First of all we consider an isotropic decay of a particle with momentum  $p^*$  into two particles of momenta  $p_i^*$  and  $p_j^*$ , and masses  $m_i$  and  $m_j$ , respectively. The star indicates that the particles are in the rest frame of the decaying particle, with momenta

$$p^* = \begin{pmatrix} \sqrt{\bar{s}_{ij}} \\ 0 \\ 0 \\ 0 \end{pmatrix}, \quad p_i^* = \begin{pmatrix} \frac{\bar{s}_{ij} + m_i^2 - m_j^2}{2\sqrt{\bar{s}_{ij}}} \\ 0 \\ 0 \\ \frac{\lambda(\bar{s}_{ij}, m_i^2, m_j^2)}{2\sqrt{\bar{s}_{ij}}} \end{pmatrix}, \quad p_j^* = p^* - p_i^*, \quad (5.12)$$

where  $\bar{s}_{ij} = p^{*2} = (p_i^* + p_j^*)^2$  and  $\lambda$  is the Källén function defined in Eq. (4.21). The  $1 \rightarrow 2$  particle phase-space integration can be written as

$$\begin{aligned} \int d\Phi_d(\bar{s}_{ij}, m_i^2, m_j^2) &= \frac{\lambda(\bar{s}_{ij}, m_i^2, m_j^2)}{8\bar{s}_{ij}} \int_0^{2\pi} d\phi^* \int_{-1}^1 d\cos\theta^*, \\ &= \frac{1}{g_d(\bar{s}_{ij}, m_i^2, m_j^2)} \int_0^1 dr_1 \int_0^1 dr_2, \end{aligned} \quad (5.13)$$

where the density is given by

$$g_d(\bar{s}_{ij}, m_i^2, m_j^2) = \frac{2\bar{s}_{ij}}{\lambda(\bar{s}_{ij}, m_i^2, m_j^2) \pi}, \quad (5.14)$$

and  $\phi^*$  and  $\theta^*$  are azimuthal and the polar angles in the rest frame of the decaying particle, respectively. These angles are parametrized as

$$\phi^* = 2\pi r_1 \quad \text{and} \quad \cos\theta^* = 2r_2 - 1. \quad (5.15)$$

The decay is isotropic, thus, we apply a rotation to orient the momenta of the outgoing particle into a generic coordinate system

$$p_i' = \mathcal{R}(\phi^*, \cos\theta^*) p_i^*, \quad (5.16)$$

with the rotation matrix

$$\mathcal{R}(\phi^*, \cos \theta^*) = \begin{pmatrix} 1 & 0 & 0 & 0 \\ 0 & \cos \phi^* & \sin \phi^* & 0 \\ 0 & -\sin \phi^* & \cos \phi^* & 0 \\ 0 & 0 & 0 & 1 \end{pmatrix} \begin{pmatrix} 1 & 0 & 0 & 0 \\ 0 & \cos \theta^* & 0 & \sin \theta^* \\ 0 & 0 & 1 & 0 \\ 0 & -\sin \theta^* & 0 & \cos \theta^* \end{pmatrix}. \quad (5.17)$$

If  $p^* \neq p_t$ , one more rotation with  $\mathcal{R}(\phi, \cos \theta)$ , and a boost are needed, so that the particle is located along the axis of the previous  $1 \rightarrow 2$  decay. The boost is described by the transformation

$$\begin{pmatrix} p_0 \\ \mathbf{p} \end{pmatrix} = \mathcal{B}(p_0, -\mathbf{p}) \begin{pmatrix} p'_0 \\ \mathbf{p}' \end{pmatrix} = \begin{pmatrix} \gamma p'_0 + \mathbf{b} \mathbf{p}' \\ \mathbf{p}' + \mathbf{b} \frac{\mathbf{b} \mathbf{p}'}{1-\gamma} + \mathbf{b} p'_0 \end{pmatrix} \quad (5.18)$$

with  $\mathbf{b} = \mathbf{p}/m$ ,  $\gamma = p_0/m$  and  $m = \sqrt{p^2}$ .

To integrate the complete phase space, we define the Lorentz-invariant variables  $\bar{s}_{ij} = (p_i + p_j)^2$  that are related to Eq. (4.1) by

$$\bar{s}_{ij} = m_i^2 + m_j^2 + s_{ij}. \quad (5.19)$$

It is important to find the best way to map  $\bar{s}_{ij}$ , so that its density  $g_s$  simulates the behavior of the original integrand in the regions where the latter is large. This can be achieved by the following transformation:

$$\int_{\bar{s}_{\min}}^{\bar{s}_{\max}} d\bar{s}_{ij} = \int_0^1 \frac{dr}{g_s(\bar{s}_{ij}(r), m^2, \bar{s}_{\min}, \bar{s}_{\max})}, \quad (5.20)$$

where

$$\frac{1}{g_s(\bar{s}_{ij}(r), m^2, \bar{s}_{\min}, \bar{s}_{\max})} = \frac{d\bar{s}_{ij}(r, m^2, \bar{s}_{\min}, \bar{s}_{\max})}{dr}, \quad (5.21)$$

and  $\bar{s}_{\min}$  and  $\bar{s}_{\max}$  are the minimum and maximum values that  $\bar{s}_{ij}$  can reach depending on the kinematics. In the previous equations we have identified the quantity  $h(r)$ , introduced in Eq. (5.10), with  $\bar{s}_{ij}$ .

For our purposes, we use two of the mappings proposed in Ref. [97]:

- Decaying particle with finite mass  $m$  and vanishing width  $\Gamma$ ,

$$\begin{aligned} \bar{s}_{ij} &= \exp [r \ln(\bar{s}_{\max} - m^2) + (1 - r) \ln(\bar{s}_{\min} - m^2)] + m^2, \\ g_s &= \frac{1}{[\ln(\bar{s}_{\max} - m^2) - \ln(\bar{s}_{\min} - m^2)] (\bar{s}_{ij} - m^2)}. \end{aligned} \quad (5.22)$$

- Decaying particle (vector boson  $V$ ) with mass  $m = M_V$  and width  $\Gamma_V \neq 0$ ,

$$\begin{aligned} \bar{s}_{ij} &= M_V \Gamma_V \tan [y_1 + (y_2 - y_1) r] + M_V^2, \\ g_s &= \frac{M_V \Gamma_V}{(y_2 - y_1) [(\bar{s}_{ij} - M_V^2)^2 + M_V^2 \Gamma_V^2]}, \end{aligned} \quad (5.23)$$

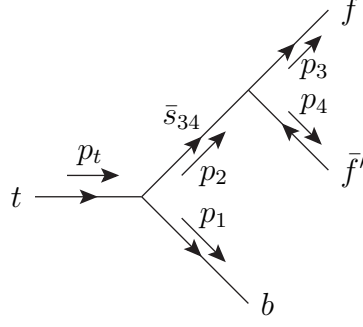


Figure 5.1: Diagram illustrating the phase-space mapping for the process  $t \rightarrow b f \bar{f}'$ .

with

$$y_{1,2} = \arctan \left( \frac{\bar{s}_{\min, \max} - M_V^2}{M_V \Gamma_V} \right). \quad (5.24)$$

In the following paragraphs the different mappings will be described in more detail.

### 5.3 $1 \rightarrow 3$ particle phase space

As an example we consider the mapping for the process  $t(p_t) \rightarrow b(p_1) f(p_3) \bar{f}'(p_4)$ . This can be constructed by two consecutive decays, as shown in Fig. 5.1.

The  $1 \rightarrow 3$  particle phase-space integral can be written as

$$\int d\Phi_3 = \int_{\bar{s}_{34, \min}}^{\bar{s}_{34, \max}} d\bar{s}_{34} \int d\phi_d(p_t^2, m_b^2, \bar{s}_{34}) \int d\phi_d(\bar{s}_{34}, m_3^2, m_4^2). \quad (5.25)$$

The fermions  $f$  and  $\bar{f}'$  form a lepton-neutrino pair if the decay is leptonic, or a quark-antiquark pair in the case of a hadronic  $W$  decay.  $\sqrt{\bar{s}_{34}}$  represents the virtuality of the  $W$  boson. In both cases, these final-state particles are considered to be light. Thus  $\bar{s}_{34, \min} = 0$  and  $\bar{s}_{34, \max} = (m_t - m_b)^2$ . For the first decay,  $t(p_t) \rightarrow b(p_1) W(p_2)$ , the top quark, which is assumed to be unpolarized, is at rest and its decay is isotropic. Without loss of generality, the angles  $\phi$  and  $\theta$  can be fixed to

$$\phi_{12}^* = 0 \quad \text{and} \quad \cos \theta_{12}^* = 1, \quad (5.26)$$

and the density  $g_d$  reads

$$g_d(m_t^2, m_b^2, \bar{s}_{34}) = \frac{2m_t^2}{\pi \lambda(m_t^2, m_b^2, \bar{s}_{34})}. \quad (5.27)$$

For the second decay,  $W(p_2) \rightarrow f(p_3) \bar{f}'(p_4)$ , we define

$$\phi_{34}^* = 2\pi r_1 \quad \text{and} \quad \cos \theta_{34}^* = 2r_2 - 1, \quad (5.28)$$

and obtain

$$g_d(\bar{s}_{34}, 0, 0) = \frac{2}{\pi}. \quad (5.29)$$

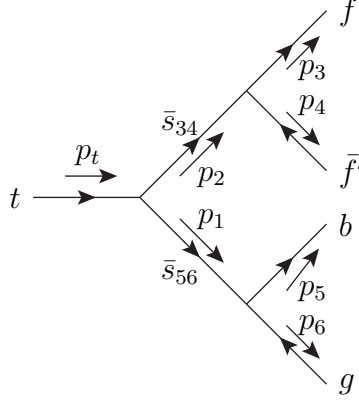


Figure 5.2: Diagram illustrating the phase-space mapping for the process  $t \rightarrow b f \bar{f}'$  with a gluon emitted by the  $b$  quark.

Since the square of the  $W$ -boson propagator is proportional to a Breit-Wigner distribution (i.e.  $\Gamma_W \neq 0$ ), we map  $\bar{s}_{34}$  as described in Eq. (5.23):

$$\bar{s}_{34} = M_W^2 + M_W \Gamma_W \tan [y_1 + (y_2 - y_1) r_3], \quad (5.30)$$

where  $y_1$  and  $y_2$  are given in Eq. (5.24), and consequently

$$g_s = \frac{M_W \Gamma_W}{(y_2 - y_1) [(\bar{s}_{34} - M_W^2)^2 + M_W^2 \Gamma_W^2]}. \quad (5.31)$$

Finally, we can write the phase-space integral for the top width in terms of the parameters  $r_a$  needed in VEGAS,

$$\begin{aligned} \Gamma_3(t \rightarrow b f \bar{f}') &= \frac{1}{8(2\pi)^3} \frac{N_c}{2m_t} \int_0^1 \prod_{a=1}^3 dr_a \frac{\lambda(m_t^2, m_b^2, \bar{s}_{34})}{4m_t^2} (y_2 - y_1) [(\bar{s}_{34} - M_W^2)^2 + M_W^2 \Gamma_W^2] \\ &\times \sum |\mathcal{M}(p_t; p_2, p_3, p_4)|^2. \end{aligned} \quad (5.32)$$

The only resonance appearing in this process is due to the  $W$  boson, which is flattened by the mapping, allowing for an efficient and well-converging integration.

## 5.4 1 $\rightarrow$ 4 particle phase space

For the case of a 1  $\rightarrow$  4 particle phase space, we refer to the process  $t \rightarrow b f \bar{f}' + g/\gamma$ , where a gluon or a photon is emitted. It is important to notice that the massless vector boson can be emitted by different particles and that this changes the peaking structure of the integrand. For this reason we consider the two phase-space mappings ( $PSM = 1, 2$ ) described in the following.

- $PSM = 1$ :  $t(p_t) \rightarrow b(p_5) f(p_3) \bar{f}'(p_4) g(p_6)$  where the boson (as an example we consider a gluon) is emitted by the  $b$  quark, as represented in Fig. 5.2. The invariant masses of

the two intermediate particles are  $\bar{s}_{56} = p_1^2 = (p_5 + p_6)^2$  and  $\bar{s}_{34} = p_2^2 = (p_3 + p_4)^2$ . The phase-space integral is

$$\int^{(1)} d\phi_4 = \int_{\bar{s}_{56,\min}}^{\bar{s}_{56,\max}} d\bar{s}_{56} \int_{\bar{s}_{34,\min}}^{\bar{s}_{34,\max}} d\bar{s}_{34} \int d\phi_d(p_t, \bar{s}_{56}, \bar{s}_{34}) \int d\phi_d(p_1, m_b^2, m_3^2) \int d\phi_d(p_2, m_3^2, m_4^2), \quad (5.33)$$

where  $f$  and  $\bar{f}'$  are considered massless, and the superscript on the symbol of the integral denotes the type of mapping. Following the OCSM (see Sect. 4.1), to integrate only over the hard region, the momenta need to fulfil the conditions

$$s_{b\gamma} = \bar{s}_{56} - m_b^2 > \Delta s, \quad s_{t\gamma} = 2p_t \cdot p_6 > \Delta s. \quad (5.34)$$

The former cuts are Lorentz invariant and can therefore be applied directly in the mapping (boundary of the integration). We have  $\bar{s}_{56,\min} = m_b^2 + \Delta s$ ,  $\bar{s}_{56,\max} = m_t^2$ ,  $\bar{s}_{34,\min} = 0$  and  $\bar{s}_{34,\max} = (m_t - \sqrt{\bar{s}_{56}})^2$ . The integration over the invariant mass of the  $W$  boson  $\sqrt{\bar{s}_{34}}$  requires a Breit-Wigner mapping (Eqs. (5.30) and (5.31)).

The propagator of the  $b$  quark is proportional to  $1/(\bar{s}_{56} - m_b^2)^2$ . Because of the coupling structure, only the quantity  $1/(\bar{s}_{56} - m_b^2)$  develops a pole in the IR limit. Thus we rewrite

$$\begin{aligned} \int_{m_b^2 + \Delta s}^{m_t^2} \frac{d\bar{s}_{56}}{(\bar{s}_{56} - m_b^2)} &= \int_{\ln(\Delta s)}^{\ln(m_t^2 - m_b^2)} d \ln(\bar{s}_{56} - m_b^2) \\ &= \int_0^1 dr_1 \ln \left( \frac{\bar{s}_{56,\max} - m_b^2}{\bar{s}_{56,\min} - m_b^2} \right), \end{aligned} \quad (5.35)$$

and map  $\bar{s}_{56}$  in a more efficient way, using Eq. (5.22), as

$$\begin{aligned} \bar{s}_{56} &= \exp \left[ r_1 \ln(\bar{s}_{56,\max} - m_b^2) + (1 - r_1) \ln(\bar{s}_{56,\min} - m_b^2) \right] + m_b^2, \\ g_s &= \frac{1}{[\ln(\bar{s}_{56,\max} - m_b^2) - \ln(\bar{s}_{56,\min} - m_b^2)] (\bar{s}_{56} - m_b^2)}. \end{aligned} \quad (5.36)$$

The three decays can be linked following the same procedure described in Sect. 5.3.

Finally the complete phase-space integral can be written as

$$\begin{aligned} \Gamma_4^{(1)}(t \rightarrow b f \bar{f}' + g/\gamma) &= \frac{1}{64(2\pi)^5} \frac{N_c}{2m_t} \int_0^1 \prod_{a=1}^6 dr_a \ln \left( \frac{m_t^2 - m_b^2}{\Delta s} \right) (\bar{s}_{56} - m_b^2)^2 \\ &\times \frac{\lambda(p_t^2, \bar{s}_{56}, \bar{s}_{34})(y_2 - y_1)[(\bar{s}_{56} - M_W^2)^2 + M_W^2 \Gamma_W^2]}{\bar{s}_{56} M_W \Gamma_W m_t^2} \sum |\mathcal{M}(p_t; p_3, p_4, p_5, p_6)|^2 \Theta_{\Delta s}, \end{aligned} \quad (5.37)$$

where

$$y_{1,2} = \arctan \left( \frac{\bar{s}_{56,\min,\max} - M_W^2}{M_W \Gamma_W} \right). \quad (5.38)$$

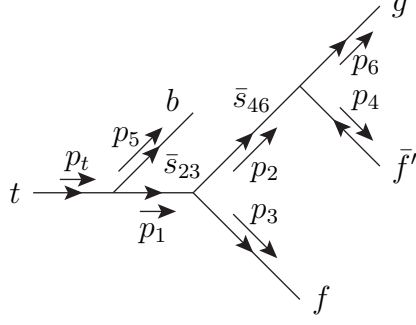


Figure 5.3: Diagram illustrating the phase-space mapping for the process  $t \rightarrow b f \bar{f}'$  with a gluon emitted by the fermion  $\bar{f}'$ .

In Eq. (5.37),  $\Theta_{\Delta s}$  is a function that ensures the right domain of integration, e.g. in the hard region (Sect. 4.1) we have

$$\Theta_{\Delta s} = \prod_f \Theta(s_{f\gamma} - \Delta s). \quad (5.39)$$

For the quasi-soft region  $\Theta_{\Delta s}$  is defined case-by-case by the subscripts of the integrals reported in Sect. 4.3. The variables  $r_a$  are related to the kinematical quantities as follows:

$$\begin{aligned} \bar{s}_{34} &= M_W^2 + M_W \Gamma_W \tan[y_1 + (y_2 - y_1)r_2], \\ \phi_{34} &= 2\pi r_3 \quad \text{and} \quad \cos \theta_{34} = 2r_4 - 1, \\ \phi_{56} &= 2\pi r_5 \quad \text{and} \quad \cos \theta_{56} = 2r_6 - 1. \end{aligned} \quad (5.40)$$

Moreover, we recall that

$$\phi_{12} = 0, \quad \cos \theta_{12} = 1, \quad (5.41)$$

where  $\phi_{ij}$  and  $\theta_{ij}$  are the azimuthal and polar angles between particle  $i$  and particle  $j$ , respectively.

This mapping is, in the case of the QCD correction for a leptonic  $W$ -boson decay, sufficient to deliver a stable numerical integration, since the gluon can only be emitted by the  $b$  and the  $t$  quarks. In all other cases the gluon/photon can be emitted by the light fermions, too. Therefore, we need to define another mapping.

- $PSM = 2$ : The boson is emitted by one of the light fermions.

Consider the process  $t(p_t) \rightarrow b(p_5) f(p_3) \bar{f}'(p_4) g(p_6)$ , where the gluon is emitted by  $\bar{f}'$  (see Fig. 5.3). As in the previous case, we build the  $1 \rightarrow 4$  phase space considering three subsequent  $1 \rightarrow 2$  decays and the invariants  $\bar{s}_{23} = p_1^2 = (p_2 + p_3)^2$  and  $\bar{s}_{46} = p_2^2 = (p_4 + p_6)^2$ . The phase-space integral is

$$\int^{(2)} d\phi_4 = \int_{\bar{s}_{23,\min}}^{\bar{s}_{23,\max}} d\bar{s}_{23} \int_{\bar{s}_{46,\min}}^{\bar{s}_{46,\max}} d\bar{s}_{46} \int d\phi_d(p_t, \bar{s}_{23}, m_b^2) \int d\phi_d(p_1, \bar{s}_{46}, m_f^2) \int d\phi_d(p_2, m_{f'}^2, 0), \quad (5.42)$$

where  $m_f$  and  $m_{f'}$  are the vanishing masses of the final-state fermions, so that  $\bar{s}_{23,\min} = \Delta s$ ,  $\bar{s}_{23,\max} = (m_t - m_b)^2$ ,  $\bar{s}_{46,\min} = \Delta s$ , and  $\bar{s}_{46,\max} = \bar{s}_{23}$ .

We parametrize, as in the previous case, the  $W$ -boson virtuality  $\bar{s}_{23}$  following Eq. (5.23), and the virtuality  $\bar{s}_{46}$  of the emitting fermion  $f'$  following Eq. (5.22). Moreover, the cuts  $s_{f'g} = \bar{s}_{46} > \Delta s$  (already implemented in the phase space) and  $s_{fg} = 2p_3 \cdot p_6 > \Delta s$  are imposed to identify the hard region, where  $I_H$  is defined (Eq. (4.3)).

The optimized integral, in terms of the random numbers  $r_a$ , reads

$$\begin{aligned} \Gamma_4^{(2)}(t \rightarrow bf\bar{f}' + g/\gamma) &= \frac{1}{64(2\pi)^5} \frac{N_c}{2m_t} \int_0^1 \prod_{a=1}^6 dr_a [\ln(\bar{s}_{23}) - \ln(\Delta s)] (\bar{s}_{23} - \bar{s}_{46}) \bar{s}_{46} \\ &\times \frac{\lambda(p_t^2, \bar{s}_{23}, m_b^2)(y_2 - y_1)[(\bar{s}_{23} - M_W^2)^2 + M_W^2 \Gamma_W^2]}{\bar{s}_{23} M_W \Gamma_W m_t^2} \sum |\mathcal{M}(p_t; p_3, p_4, p_5, p_6)|^2 \Theta_{\Delta s}, \end{aligned} \quad (5.43)$$

with

$$y_{1,2} = \arctan \left( \frac{\bar{s}_{23,\min,\max} - M_W^2}{M_W \Gamma_W} \right), \quad (5.44)$$

and

$$\begin{aligned} \bar{s}_{23} &= M_W^2 + M_W \Gamma_W \tan[y_1 + (y_2 - y_1)r_1], \\ \bar{s}_{46} &= \exp\{r_2 \ln(\bar{s}_{46,\max}) + (1 - r_2) \ln(\bar{s}_{46,\min})\}, \\ \phi_{12} &= 0 \quad \text{and} \quad \cos \theta_{12} = 1, \\ \phi_{23} &= 2\pi r_3 \quad \text{and} \quad \cos \theta_{23} = 2r_4 - 1, \\ \phi_{46} &= 2\pi r_5 \quad \text{and} \quad \cos \theta_{46} = 2r_6 - 1. \end{aligned}$$

## Different mappings for the real corrections

We analyze now how to combine the different mappings in the specific cases of interest.

- **QCD real corrections to the semileptonic decay:**  $t(p_t) \rightarrow b(p_5) \nu_\ell(p_3) \ell^+(p_4) g(p_6)$ .

The only diagrams contributing to this process are those in which the gluon is emitted by the  $t$  and  $b$  quarks. It is worth to notice that the virtuality of the  $W$  boson is the same in both diagrams,  $\bar{s}_{34} = (p_3 + p_4)^2$ . This implies that in both cases we can flatten the Breit-Wigner shaped propagator of the  $W$ -boson using the mapping  $PSM = 1$ , Eq. (5.33), allowing for an efficient integration.

- **EW corrections to the semileptonic decay:**  $t(p_t) \rightarrow b(p_5) \nu_\ell(p_3) \ell^+(p_4) \gamma(p_6)$ .

The photon can be emitted not only from the  $t$  and  $b$  quarks, but also from the charged lepton and the  $W$  boson. When the photon is emitted by the  $b$  or  $t$  quark (as the gluon in the QCD case),  $PSM = 1$  leads to an appropriate mapping; when it is emitted by  $\ell^+$  or  $W^+$ , instead, the second mapping ( $PSM = 2$ ) is better suited. For this reason we need a combination of the two mappings. This can be done using a partition of

unity, i.e. rewriting the  $1 \rightarrow 4$  particle phase-space integration as the sum of two integrals, weighted by ratios of invariants ( $s_{b\gamma}$  and  $s_{\ell\gamma}$ ):

$$\int d\Phi_4 = \int^{(1)} d\Phi_4 \frac{s_{\ell\gamma}}{s_{\ell\gamma} + s_{b\gamma}} + \int^{(2)} d\Phi_4 \frac{s_{b\gamma}}{s_{\ell\gamma} + s_{b\gamma}}. \quad (5.45)$$

This approach allows to disentangle the resonance structure, which then can be dealt with separately. Thus, the EW corrections to the semileptonic decay read

$$\int d\Phi_4 \overline{\sum} |\mathcal{M}(p_t; p_3, p_4, p_5, p_6)|^2 = \int^{(1)} d\Phi_4 \frac{s_{\ell\gamma}}{s_{\ell\gamma} + s_{b\gamma}} \overline{\sum} |\mathcal{M}|^2 + \int^{(2)} d\Phi_4 \frac{s_{b\gamma}}{s_{\ell\gamma} + s_{b\gamma}} \overline{\sum} |\mathcal{M}|^2. \quad (5.46)$$

- **QCD real corrections to the hadronic decay:**  $t(p_t) \rightarrow b(p_5) u(p_3) \bar{d}(p_4) g(p_6)$ .

For the real contribution, the gluon can be emitted by each of the four quarks involved in the process. The matrix element is usually the sum of all possible contributions, but in the specific case of QCD corrections, there is no interference term between the emission from  $t/b$  and  $u/d$ , due to colour conservation. Therefore the real matrix element squared can be decomposed, as described for Eq. (3.29), according to

$$\overline{\sum} |\mathcal{M}(p_t; p_3, p_4, p_5, p_6)|^2 = \overline{\sum} |\mathcal{M}_t + \mathcal{M}_b|^2 + \overline{\sum} |\mathcal{M}_u + \mathcal{M}_d|^2, \quad (5.47)$$

where  $\mathcal{M}_i$  is the matrix element for the process where the gluon is emitted by the quark  $i$ . This allows us to perform two independent integrations:

- $t/b$  contribution: The integration presented in Eq. (5.37) ( $PSM=1$ ) can be used.
- $u/d$  contribution: The mapping  $PSM = 2$  can be used twice, once for emitter  $d$ , as described in Eq. (5.43) (we will refer to it as  $PSM = 2d$ ), and once for emitter  $u$ , upon suitable modifications, i.e. interchanging the  $u$  and  $d$  legs ( $PSM = 2u$ ). The gluon can be emitted from either particles, therefore both mappings have to be used at the same time, similarly to the previous case.

Summarizing the real QCD contribution for the hadronic decay is given by

$$\begin{aligned} \int d\Phi_4 \overline{\sum} |\mathcal{M}(p_t; p_3, p_4, p_5, p_6)|^2 &= \int^{(1)} d\Phi_4 \overline{\sum} |\mathcal{M}_t + \mathcal{M}_b|^2 \\ &+ \int^{(2d)} d\Phi_4 \frac{s_{ug}}{s_{ug} + s_{dg}} \overline{\sum} |\mathcal{M}_u + \mathcal{M}_d|^2 + \int^{(2u)} d\Phi_4 \frac{s_{dg}}{s_{ug} + s_{dg}} \overline{\sum} |\mathcal{M}_u + \mathcal{M}_d|^2. \end{aligned} \quad (5.48)$$

- **EW corrections to the hadronic decay:**  $t(p_t) \rightarrow b(p_5) u(p_3) \bar{d}(p_4) \gamma(p_6)$ .

In this case the photon can be emitted by all the particles appearing in the process. The combination of integrals used for a better performance during the integration is

$$\begin{aligned} \int d\Phi_4 \overline{\sum} |\mathcal{M}(p_t; p_3, p_4, p_5, p_6)|^2 &= \int^{(2u)} d\Phi_4 \frac{s_{d\gamma}}{s_{u\gamma} + s_{d\gamma}} \frac{s_{t\gamma}s_{b\gamma}}{s_{t\gamma}s_{b\gamma} + s_{d\gamma}s_{u\gamma}} \overline{\sum} |\mathcal{M}|^2 \\ &+ \int^{(2d)} d\Phi_4 \frac{s_{u\gamma}}{s_{u\gamma} + s_{d\gamma}} \frac{s_{t\gamma}s_{b\gamma}}{s_{t\gamma}s_{b\gamma} + s_{d\gamma}s_{u\gamma}} \overline{\sum} |\mathcal{M}|^2 + \int^{(1)} d\Phi_4 \frac{s_{u\gamma}s_{d\gamma}}{s_{t\gamma}s_{b\gamma} + s_{d\gamma}s_{u\gamma}} \overline{\sum} |\mathcal{M}|^2. \end{aligned} \quad (5.49)$$

# Chapter 6

## Numerical results

In this chapter we present the numerical results for the NLO corrections to the top-quark partial decay widths, and we compare them to an independent calculation, whose settings are described in Sect. 6.1, and with the values obtained in the narrow-width approximation, calculated in App. A. In Sect. 6.2 the input parameters of the calculation are listed, while the details of the event selections are given in Sect. 6.3. The existence of a region where the corrections to the top width are independent from the technical cut parameter  $\Delta s$ , introduced when applying the OCSM (Chap. 4), is proven at the beginning of Sect. 6.4. Then, a well-defined value of  $\Delta s$  is chosen to get the final numbers. The calculation has been performed for the case of a semileptonic,  $t \rightarrow b \nu_\ell \ell^+$ , and a hadronic decay,  $t \rightarrow b u \bar{d}$ , and the integrated results are presented together with various differential distributions in Sects. 6.4.1 and 6.4.2, respectively. Finally, Sect. 6.5 shows a comparison of the theoretical total top-quark decay width with the existent experimental measurements.

### 6.1 Second independent calculation

A second independent calculation of the top-quark width has been implemented by L. Basso to cross check the results presented in this thesis. To produce the matrix elements and the counterterms needed in the calculation it uses the combined packages **FeynArts v3.6** [98] and **FormCalc v8.1** [99, 100]. The loop integrals, appearing in the virtual corrections, have been numerically integrated with the **COLLIER** library [86], after being regularized with mass regularization parameters within the complex-mass scheme. The infrared divergences have been treated using the dipole-subtraction formalism<sup>1</sup> [42, 44, 45] and the resulting amplitudes have been integrated by means of **VEGAS**. Furthermore, for the case of the EW corrections to the semileptonic decay, a third independent calculation, also employing the subtractions formalism, was performed by A. Huss. All results are in mutual agreement.

It is worth to mention that the application of the dipole-subtraction formalism for the second independent calculation required the extension of the formalism to treat decay kinematics which have not been considered in the literature in full detail so far. The respective subtraction terms for both massless and massive final-state particles, as well as for the case of non-collinear-safe observables, were developed in the context of the calculations presented in Refs. [46, 101, 102]

---

<sup>1</sup>For this reason, during the comparisons, the second calculation is labeled “subtr”.

and were employed here. The new results are collected and presented in Ref. [47], together with the technique based on the OCSM developed in this thesis for the  $1 \rightarrow n$  particle decay, and the numerical results for the top-quark width.

## 6.2 Input parameters

The input parameters used in this work are taken from Ref. [103]. The Higgs-boson mass is

$$M_H = 125.9 \text{ GeV}, \quad (6.1)$$

and the on-shell values of the masses and the widths of the  $W$  and  $Z$  bosons are

$$\begin{aligned} M_W^{OS} &= 80.385 \text{ GeV}, & \Gamma_W^{OS} &= 2.085 \text{ GeV}, \\ M_Z^{OS} &= 91.1876 \text{ GeV}, & \Gamma_Z^{OS} &= 2.4952 \text{ GeV}. \end{aligned} \quad (6.2)$$

The latter are converted to the corresponding pole masses and widths following

$$M_V = \frac{M_V^{OS}}{c_V}, \quad \Gamma_V = \frac{\Gamma_V^{OS}}{c_V}, \quad \text{where } c_V = \sqrt{1 + \left( \frac{\Gamma_V^{OS}}{M_V^{OS}} \right)^2} \quad \text{and } V = W, Z. \quad (6.3)$$

In this calculation we consider only the top and the bottom quarks as massive, while all the other fermions are considered massless. The massless fermions acquire nevertheless a fictitious mass via the mass regularization procedure, as described in Chap. 4. Even though the integrated result does not depend on the choice of those masses, we list for completeness the mass values for all fermions:

$$\begin{aligned} m_t &= 173.34 \text{ GeV}, & m_b &= 4.78 \text{ GeV}, \\ m_u &= 2.3 \text{ MeV}, & m_d &= 4.8 \text{ MeV}, \\ m_c &= 1.275 \text{ GeV}, & m_s &= 95 \text{ MeV}, \\ m_e &= 0.510998928 \text{ MeV}, & m_\mu &= 105.6583715 \text{ MeV}, \\ m_\tau &= 1.77682 \text{ MeV}, & & \end{aligned} \quad (6.4)$$

where  $m_b$  is the value for the pole mass, using the two-loop conversion formula presented in Ref. [103] and the value of  $m_t$  is taken from Ref. [104]. As stated in Sect. 2.2 the  $G_\mu$ -scheme, with

$$G_\mu = 1.1663787 \times 10^{-5} \text{ GeV}^{-2}, \quad (6.5)$$

has been used in this work. Consequently, inverting Eq. (2.45), we derive

$$\alpha = \frac{\sqrt{2} s_w^2 M_W^2}{\pi} G_\mu. \quad (6.6)$$

For the QCD corrections, we fix

$$\alpha_s(M_Z) = 0.119. \quad (6.7)$$

The CKM matrix is chosen equal to the unit matrix.

## 6.3 Event selection

The top quark can decay both hadronically and leptonically. Depending on the nature of the decay products, they are seen in different sectors of the detector. In particular, the positron and the photon can be detected by the electromagnetic calorimeter (ECAL), the muon is tracked in the dedicated muon chambers, and the coloured objects (quarks and gluons) evolve into jets and are finally detected into the hadronic calorimeter (HCAL). The  $b$ -jet can be efficiently identified using the  $b$ -tagging method<sup>2</sup>. The neutrino is a neutral and hardly interacting particle and escapes the detection. Nevertheless, its presence can be inferred due to the total momentum conservation. In a lepton collider, all components are deduced by requiring energy and momentum conservation. In a hadronic collider, instead, only the transverse components are directly measured. Because of this, the missing transverse momentum can be defined, where missing pertains to the sum of the invisible particles. For the case under investigation (only one invisible particle) it is possible to reconstruct the whole four-momentum of the neutrino by imposing suitable kinematical constraints.

It is not always possible to distinguish the particles of the process or to separate them when emitted collinearly. In this theoretical calculation, we try to be as close as possible to the experimental situation. We distinguish three scenarios:

- EW corrections to  $t \rightarrow b \nu_\mu \mu^+$

If the muon emits a photon, the two particles can be experimentally isolated, even if they are collinear, given that they are tracked in different parts of the detector. This means that we have to deal with non-collinear-safe observables. On the theoretical side, the case of a bare muon is thus treated following the procedure described in Sect. 4.2.

- EW corrections to  $t \rightarrow b \nu_e e^+$

If the photon is emitted almost collinearly to the positron or the  $b$  quark, they are experimentally indistinguishable and have therefore to be treated inclusively. This can be done applying a *photon-recombination procedure* [94]:

1. Exclude from the event selection the photons with a rapidity<sup>3</sup>  $y_\gamma > 3$ . They are considered part of the proton remnant.
2. If the photon passed step 1., define the quantities  $R_{f\gamma} = \sqrt{(y_f - y_\gamma)^2 + \phi_{f\gamma}^2}$ , where  $f = b, e^+$  and  $\phi_{f\gamma}$  is the angle between the fermion  $f$  and the photon.
3. If  $\min(R_{b\gamma}, R_{e^+\gamma})$  is smaller than the radius parameter  $R$ , fixed in this work at  $R = 0.1$ , recombine the two particles into a single object, identified with the fermion.

- QCD corrections to  $t \rightarrow b \nu_\ell \ell^+$  and NLO corrections to  $t \rightarrow b u \bar{d}$

In these cases (some of) the final-state particles are indistinguishable. To define IR-safe observables they need to be grouped into jets. The collection of rules in the following

---

<sup>2</sup>For our calculation we consider the  $b$ -jet as always identified (tagging probability equal to one).

<sup>3</sup>The rapidity is defined as  $y = \frac{1}{2} \ln \left( \frac{E - p_z}{E + p_z} \right)$ , where  $E$  is the energy of the particle and  $p_z$  is the component of the momentum along the beam axis.

allows us to define how close the colored states must be to be considered part of the same jet. It is the so-called jet-algorithm procedure [95]:

1. Calculate the distance  $d_{ij}$ , defined following the generalized anti- $k_t$  algorithm [105], for every pair of particles  $i, j$ , and the quantity  $d_{iB}$ , for every parton  $i$  [106]:

$$d_{ij} = \min \{E_i^{-2}, E_j^{-2}\} \frac{1 - \cos \theta_{ij}}{1 - \cos R}, \quad d_{iB} = E_i^{-2}, \quad (6.8)$$

using  $R = 0.6$ .

2. Find the smallest among the quantities defined in Eq. (6.8):
  - If  $d_{iB}$  is the smallest, declare  $i$  to be a jet candidate, remove it from the list of particles and return to step 1.
  - If  $d_{ij}$  is the smallest, recombine the particles  $i$  and  $j$  into a single object and return to step 1.
3. Stop when there are no particles left.

The jet containing the  $b$  quark is tagged as  $b$ -jet. In the following, we will refer as leading jet to the jet candidate with the highest transverse momentum.

## 6.4 Numerical results for the top-quark decay width

When evaluating the NLO corrections, the calculation separates into two parts (see Sect. 4.1): A hard region, where the amplitudes are numerically integrated over a  $1 \rightarrow 4$  particle phase space, and the remaining part, which is numerically integrated over the volume of a  $1 \rightarrow 3$  particle phase space. The latter region includes the virtual and the counterterms contributions, and the infrared region resulting from the real emission of a photon or a gluon. It is treated using the extension of the OCSM illustrated in detail in Chap. 4.

To perform the NLO corrections to the top-quark decay width, we check, first of all, the independence of the relative corrections, defined as  $\delta = \Gamma^{(1)}/\Gamma^{(0)}$ , from the technical cut parameter  $\Delta s$  introduced by the OCSM. This is shown in Figs. 6.1 and 6.2 for the semileptonic and hadronic decay, respectively. In the left panels, the soft contributions (in green) and the hard contributions (in black) are presented as functions of  $\Delta s$ . Their sum (in red) is almost constant. Zooming in the total relative corrections, the right panels illustrate indeed that the values are, for a certain range of  $\Delta s$ , constant within the errors and that they agree with the numbers calculated using the dipole-subtraction formalism (in blue). We stress that the OCSM is valid only under the assumption of  $\Delta s \rightarrow 0$ , which means that large values of  $\Delta s$  are not consistent, as apparent from the QCD corrections. Furthermore, there are also lower limits to the values of  $\Delta s$ , as shown clearly for the EW corrections to the hadronic decay, due to stability problems during the phase-space integration.

After finding the regions where the OCSM is valid, we fix the value of  $\Delta s$  taken from the plateau for the various types of corrections and final states. They are summarized in Table 6.1.

In the next sections, we present the numerical results for the top-quark width in the case of a semileptonic, Sect. 6.4.1, and a hadronic decay, Sect. 6.4.2. Several differential distributions

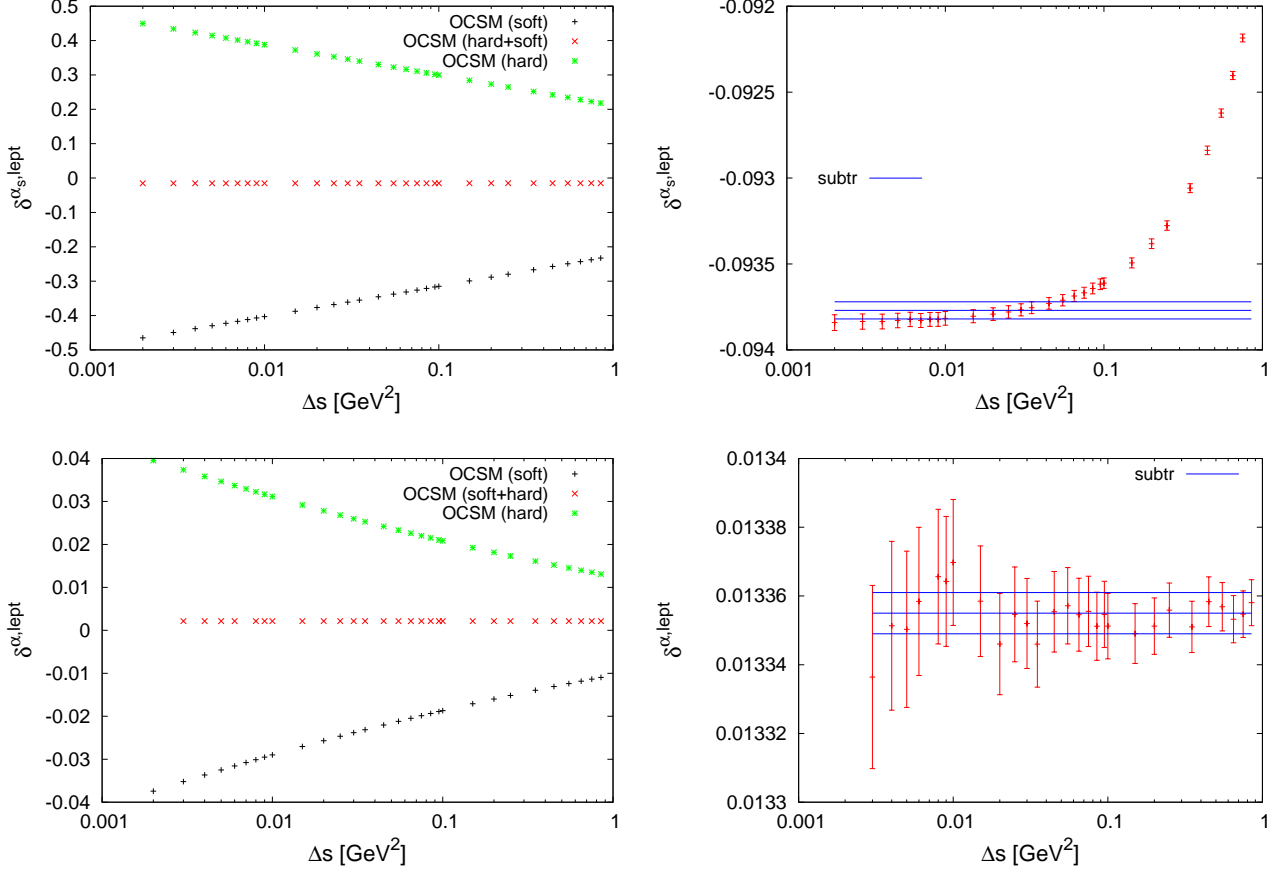


Figure 6.1: Relative QCD (top) and EW (bottom) corrections to the semileptonic top-quark decay width, calculated with the OCSM, as a function of the cut parameter  $\Delta s$ . On the left-hand side, the different contributions are shown: soft in green, hard in black, and the sum in red. On the right-hand side, the relative corrections are presented in comparison with the value calculated with the subtraction formalism (“subtr” in blue).

	QCD, lept	EW, lept	QCD, hadr	EW, hadr
$\Delta s$ (GeV <sup>2</sup> )	0.005	0.095	0.095	0.03

Table 6.1: Values of the cut parameter  $\Delta s$  chosen to perform the calculation for the different types of corrections and final states.

will be shown in a triple frame with the following conventions: The plot on top illustrates the absolute value of the corrections, in the middle one the relative corrections (in percent), calculated as  $\delta = \Gamma^{(1)}/\Gamma^{(0)}$ , are presented; the comparison (in percent) between the OCSM and the dipole-subtraction method is given in the bottom frame, with

$$\Delta_{\text{comp}} = \frac{\Gamma_{\text{OCSM}}^{\text{NLO}} - \Gamma_{\text{subtr}}^{\text{NLO}}}{\Gamma_{\text{OCSM}}^{\text{NLO}} + \Gamma_{\text{subtr}}^{\text{NLO}}} \quad \text{and} \quad \Gamma^{\text{NLO}} = \Gamma^{(0)} + \Gamma^{(1)}. \quad (6.9)$$

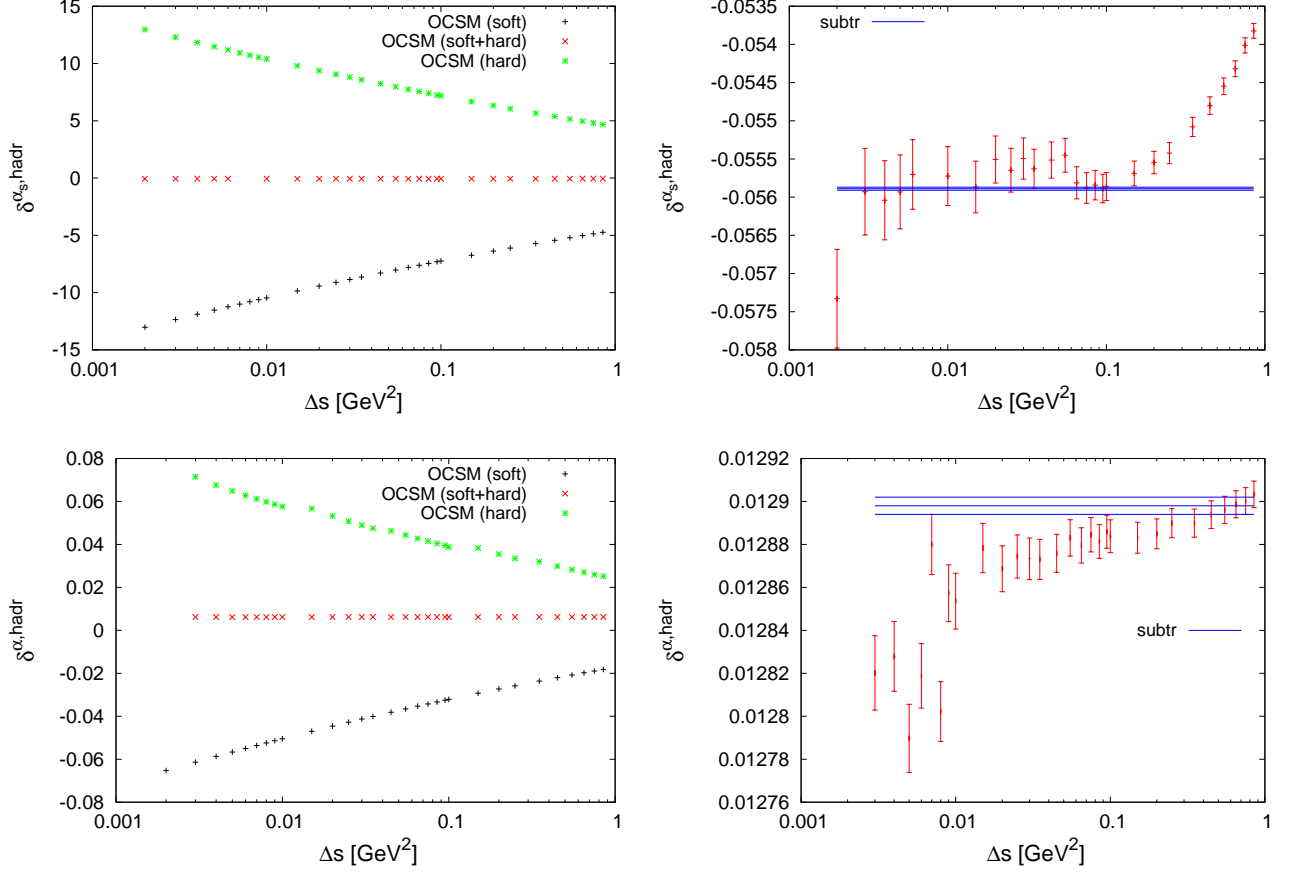


Figure 6.2: Relative QCD (top) and EW (bottom) corrections to the hadronic top-quark decay width, calculated with the OCSM, as a function of the cut parameter  $\Delta s$ . On the left-hand side, the different contributions are shown: soft in green, hard in black, and the sum in red. On the right-hand side, the relative corrections are presented in comparison with the value calculated with the subtraction formalism (“subtr” in blue).

The integrated values calculated in this thesis are collected in Tables 6.2 and 6.3, together with those obtained using the dipole-subtraction formalism and the NWA.

#### 6.4.1 Numerical results for the semileptonic decay

The integrated LO and NLO values of the semileptonic top-quark decay width are collected in Table 6.2. The LO decay width is  $\Gamma_{\text{lept}}^{(0)} = 0.1610645(3) \text{ GeV}$ , with an NLO QCD correction of  $\sim -9.4\%$  and an NLO EW correction of  $\sim +1.3\%$ . The results are presented in comparison with those obtained using the dipole-subtraction formalism. Moreover, Table 6.2 reports the results calculated in App. A using the NWA. The difference of the latter with respect to the full results obtained in this thesis is  $\sim 1.5\%$  already at LO and it increases to  $\sim 1.7\%$  at NLO. Furthermore, the QCD corrections to the semileptonic decay of the top quark have been already calculated by Jezabek and Kühn in Ref. [16]:

$$\Gamma_{\text{JK}}^{(0)} = 0.161064527(1) \text{ GeV} \quad \text{and} \quad \Gamma_{\text{JK}}^{\text{QCD}} = 0.1459589618(9) \text{ GeV} \quad (-9.3786\%). \quad (6.10)$$

	OCSM	subtr	NWA
$\Gamma_{\text{lept}}^{(0)} / \text{GeV}$	0.1610645(3)	0.161062(2)	0.1635547 (+1.55%)
$\delta_{\text{lept}}^{(1),\text{QCD}} / \%$	-9.379(3)	-9.377(5)	-9.377(1)
$\delta_{\text{lept}}^{(1),\text{EW}} / \%$	1.335(2)	1.3355(6)	1.4680(6)
$\Gamma_{\text{lept}}^{\text{NLO}} / \text{GeV}$	0.148108(6)	0.148109(2)	0.1506133(2) (+1.70%)

Table 6.2: Top decay widths and relative corrections calculated for the semileptonic decay with the input parameters listed in Sect. 6.2. The NWA values are calculated in Tab. A.1.

They are in perfect agreement with those presented in Table 6.2 <sup>4</sup>.

### QCD corrections to $t \rightarrow b \nu_\ell \ell^+$

In the following, the differential distributions for the QCD corrections are presented. The two methods of calculation (OCSM and subtraction formalism) are in very good agreement, as shown in the bottom frames. They reach a level of per mil in precision for all the observables considered in this work.

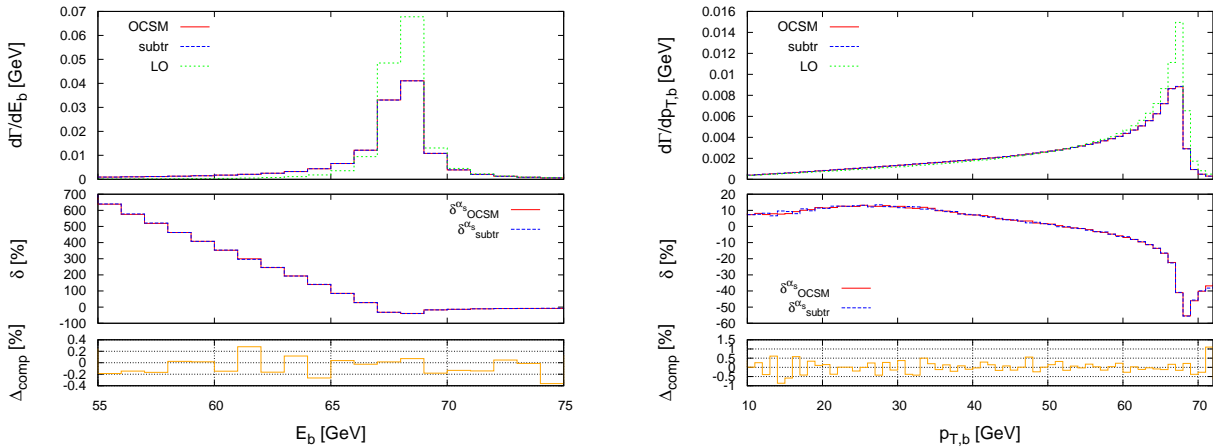


Figure 6.3: NLO QCD corrections to the semileptonic top-quark decay width as a function of the energy (left) and of the transverse momentum (right) of the  $b$ -jet.

The first observable, in the left panel of Fig. 6.3, is the energy of the  $b$ -jet. It is calculated, as every other observable presented in the following, in the top-quark rest frame. If we consider an on-shell  $W$  boson, we have a  $1 \rightarrow 2$  particle decay, and the energy of the  $b$ -jet can be analytically derived by

$$E_b = \frac{m_t^2 - M_W^2 + m_b^2}{2m_t}. \quad (6.11)$$

<sup>4</sup>A readjustment of the prefactor of the value in Ref. [16] is needed to be consistent with the CMS procedure introduced in Sect.2.3:  $G_F \rightarrow \frac{\text{Re}(s_w^2)}{s_w^2} G_F$ .

This explains the peak at  $\sim 70$  GeV of Fig. 6.3. The behavior of the corrections, negative after the peak value and positive in the low-energy tails, is due to the gluon radiation: When the gluon is emitted the energy of the other particles reduces. This effect fills the low-energy tail, i.e. NLO configurations with low-energy events are more frequent than LO ones. For this reason very high relative corrections at low  $E_b$  can be seen in the middle frame. They decrease, however, enlarging the radius  $R$  of the cone in the jet algorithm, as shown in more detail for the case of QCD corrections to the hadronic decay. The right-hand side of Fig. 6.3 illustrates the transverse momentum of the  $b$ -jet. Due to the fact that the top-quark decay is isotropic, we define  $p_{T,b}$  with respect to an arbitrary-chosen axis. Also in this case there is a peak at  $\sim 70$  GeV, with a correction of  $\sim -50\%$  in its proximity.

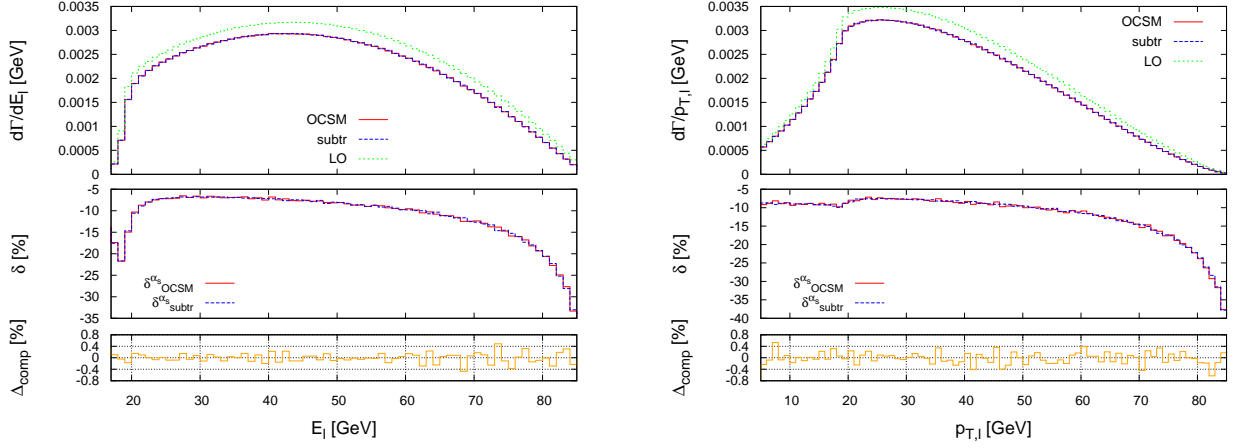


Figure 6.4: NLO QCD corrections to the semileptonic top-quark decay width as a function of the energy (left) and of the transverse momentum (right) of the lepton.

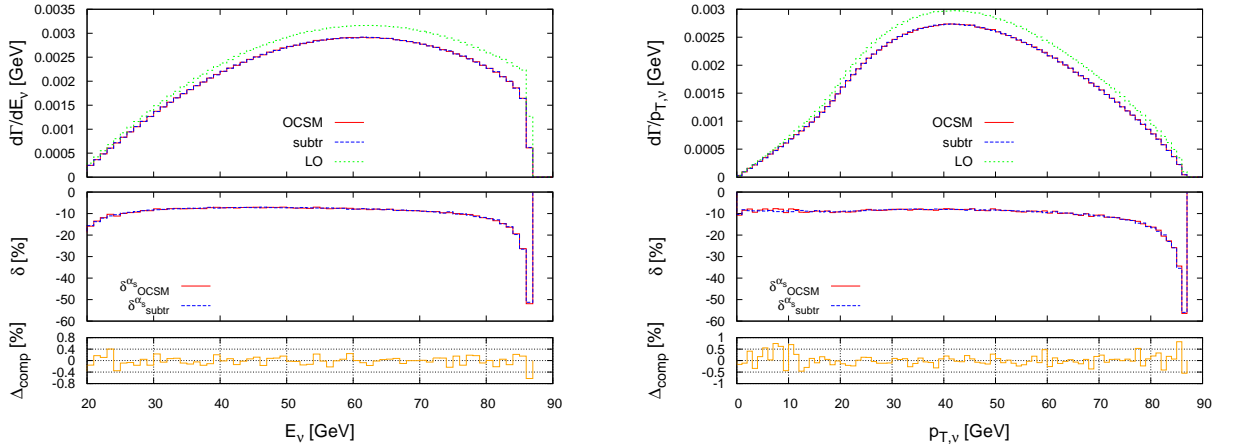


Figure 6.5: NLO QCD corrections to the semileptonic top-quark decay width as a function of the energy (left) and of the transverse momentum (right) of the neutrino.

In Figs. 6.4 and 6.5, the energy and the  $p_T$  of the lepton and of the corresponding neutrino are presented. In both cases, the relative corrections are almost flat at  $\sim -10\%$  in the regions

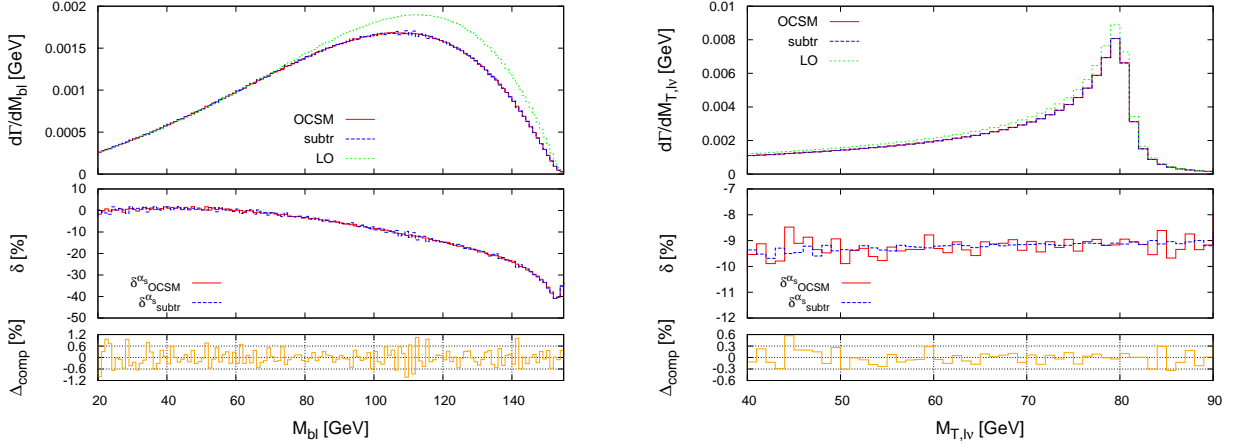


Figure 6.6: NLO QCD corrections to the semileptonic top-quark decay width as a function of the invariant mass of the  $b$ -jet and the lepton (left), and of the transverse mass of the lepton and the neutrino (right).

where the decay probability is high. In the tails, instead, the corrections can reach up to  $-35\%$  ( $-50\%$ ) for the charged lepton (neutrino), because of the negligible value of the LO.

For the invariant mass of the  $b$ -jet and the lepton, we see on the left-hand side of Fig. 6.6 a broad structure, with an increasing correction (in absolute value), reaching  $-40\%$  when approaching the kinematic limit. The transverse mass of the lepton and the neutrino<sup>5</sup> is displayed on the right panel. It peaks at the  $W$ -boson mass, with a width due to the inclusion of the full off-shellness of the boson in this calculation. The QCD corrections do not have an impact on the lepton's and neutrino's kinematic and have the constant value of  $-9\%$ .

In Fig. 6.7 we show the cosine of the angle between the  $b$ -jet and the lepton (left), and between the  $b$ -jet and the neutrino (right). The fact that the top quark is at rest implies a almost back-to-back emission of the  $b$ -jet and of the products of the decay of the boosted  $W$  boson, i.e. both  $\cos\theta_{b\ell}$  and  $\cos\theta_{b\nu}$  have a peak close to  $-1$ .

### EW corrections to $t \rightarrow b\nu_\ell\ell^+$

We consider now the EW corrections to the semileptonic top-quark decay width, for both the processes  $t \rightarrow b\nu_\mu\mu^+$  (“bare”) and  $t \rightarrow b\nu_e e^+$  (“rec”). The comparison of the two methods (OCSM and dipole-subtraction formalism) reaches a very good precision, as shown e.g. for the case of the positron in the bottom frames. We thus plot, in the top and middle frames, only the OCSM results. The discussion will focus on the comparison between the different final states. We expect that differences will appear only in observables related to the leptons.

Figure 6.8 displays the energy (left) and the transverse momentum (right) of the  $b$ -jet. The relative corrections reach in both observables only a few percents in the relevant kinematical regions. The EW corrections are, as expected, much smaller than the QCD ones.

The energy and the transverse momentum of the leptons are displayed in the left and right panels of Fig. 6.9, respectively. Here we can clearly distinguish between the two different final

<sup>5</sup>The transverse mass is defined as  $M_{T,\ell\nu} = \sqrt{2p_{T,\ell}p_{T,\nu}(1 - \cos\theta_{\ell\nu})}$ .

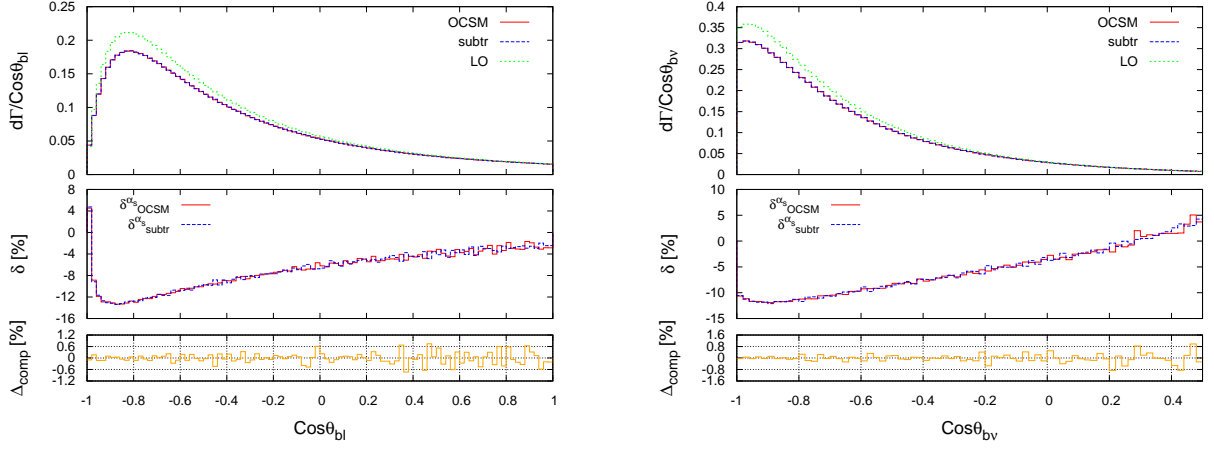


Figure 6.7: NLO QCD corrections to the semileptonic top-quark decay width as a function of the cosine of the angle between the  $b$ -jet and the lepton (left), and between the  $b$ -jet and the neutrino (right).

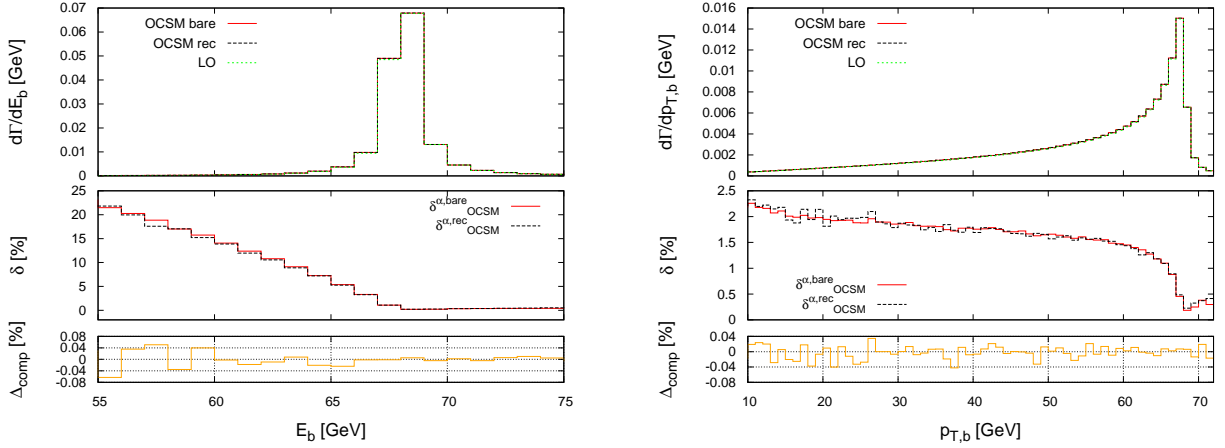


Figure 6.8: NLO EW corrections to the semileptonic top-quark decay width as a function of the energy (left) and of the transverse momentum (right) of the  $b$ -jet.

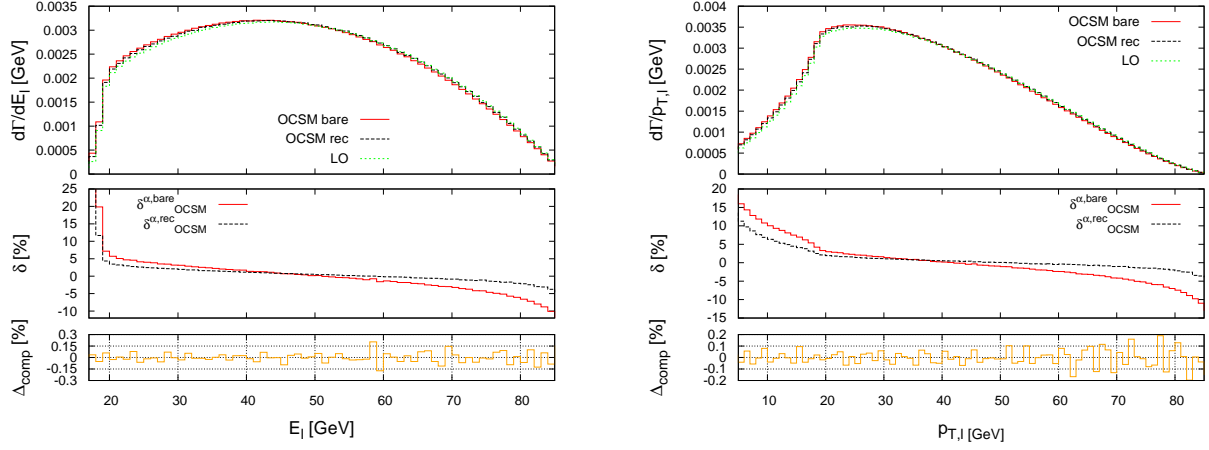


Figure 6.9: NLO EW corrections to the semileptonic top-quark decay width as a function of the energy (left) and of the transverse momentum (right) of the leptons.

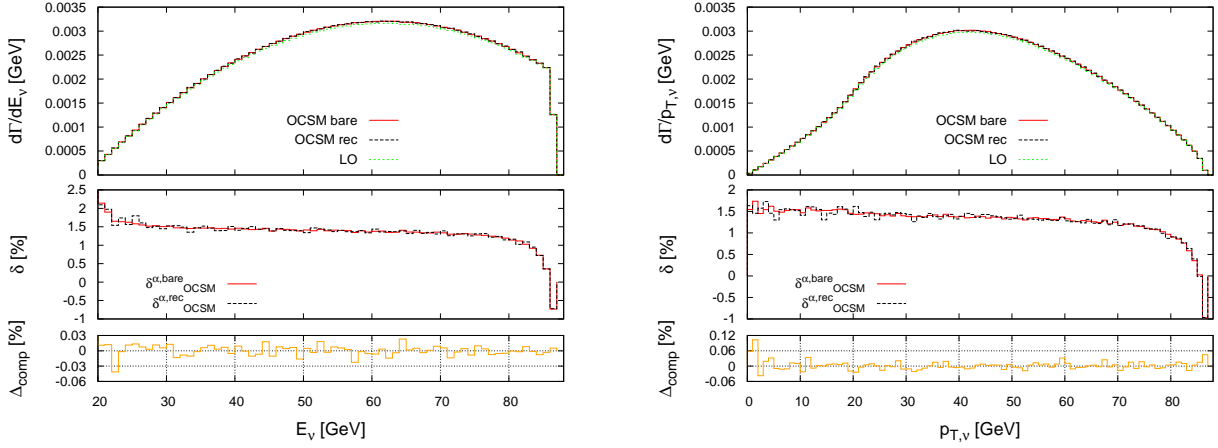


Figure 6.10: NLO EW corrections to the semileptonic top-quark decay width as a function of the energy (left) and of the transverse momentum (right) of the neutrinos.

states. The effect of the corrections is enhanced for the muonic final state: The fact that the observables are non-collinear safe implies mass-singular logarithmic terms contributing to the final result.

The EW corrections to the energy and to the transverse momentum of the neutrinos are presented in Fig. 6.10. Since the neutrino does not radiate photons, they have a constant value of +1.5%, excluding the regions with the lower decay probability.

The differential distributions of the invariant mass of the  $b$ -jet and the leptons, and of the transverse mass of the leptons and the neutrinos, are presented on the left and right panels of Fig. 6.11, respectively. As in the previous cases, the corrections to the final state with the muon are enhanced with respect to those calculated for the positron. The value of  $\delta$  decreases for  $M_{be}$  from +6% to -4%, while for  $M_{b\mu}$  it reduces from +8% to -10%. While for the QCD case the corrections to  $M_{T,\ell\nu}$  have a constant -9% value, in the EW case the emission of a photon makes the probability of a top-quark decay higher for lower values of the transverse mass. For this reason the positive relative corrections turn into negative in proximity of the peak. When

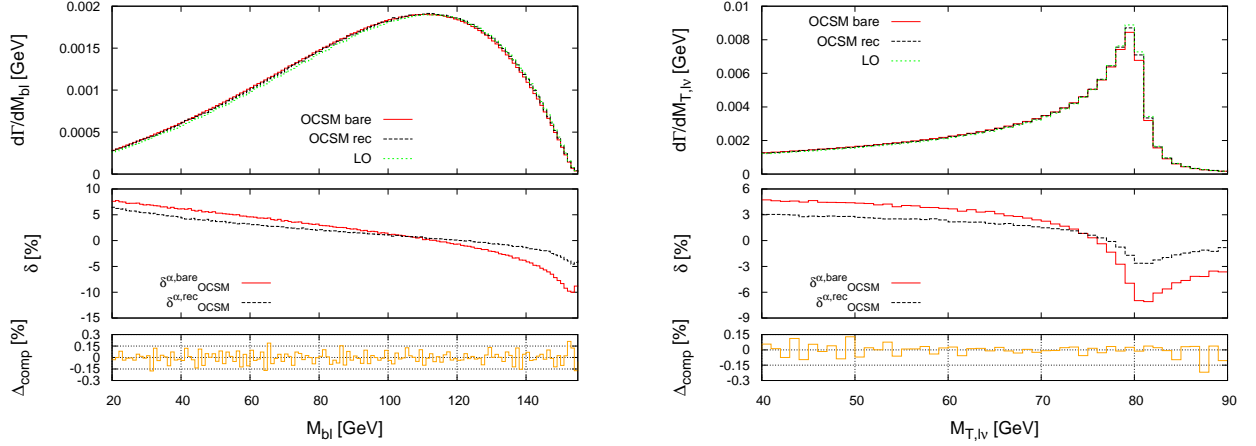


Figure 6.11: NLO EW corrections to the semileptonic top-quark decay width as a function of the invariant mass of the  $b$ -jet and the leptons (left) and of the transverse mass of the leptons and the neutrinos (right).

the photon recombination is applied, the collinear photon is absorbed in the redefinition of the final fermion. This makes the effect of the corrections milder for  $t \rightarrow b \nu_e e^+$  than for the case of a muonic decay.

In the left-hand (right-hand) side of Fig. 6.12 the cosine of the angle between the  $b$ -jet and the lepton (neutrino) is shown. There is no evident difference between the results obtained with the photon recombination ( $e^+$  emission) or applying Eq. (4.18) ( $\mu^+$  emission). The photon is indeed recombined only if collinear to the positron, i.e. it does not change the direction of the charged lepton. The corrections have a minimum in the proximity of the peak ( $\cos \theta_{bf} \sim -0.8$ ), are positive and are smaller than 2%. For comparison, the QCD corrections reach down to  $-12\%$ .

#### 6.4.2 Numerical results for the hadronic decay

We present in this section the results for the QCD and EW corrections to the hadronic top-quark decay width. The integrated values obtained in this work are collected in Table 6.3 together with those calculated using the subtraction formalism. For each of the processes,  $t \rightarrow b u \bar{d}$  and  $t \rightarrow b c \bar{s}$ , the LO width is  $\Gamma_{\text{hadr}}^{(0)} = 0.48319351(5) \text{ GeV}$ , with  $\delta_{\text{hadr}}^{(1),\text{QCD}} \sim -5.6\%$  and  $\delta_{\text{hadr}}^{(1),\text{EW}} \sim +1.3\%$ . Moreover, we compared the OCSM values with those obtained with the NWA, observing differences up to  $\sim 2\%$ .

As in the semileptonic case, also for the hadronic decay of the top quark we observe in the differential distributions a very good agreement between the two methods employed for the calculation (comparison shown in the bottom frames). In some observables we lost, however, one order of magnitude in precision with respect to the corresponding semileptonic variables. This is due to the complexity of the phase-space integration in case of a hadronic decay (the phase-space has to be split in multiple integrations, as explained in Chap. 5) and to the implementation of a jet-algorithm procedure.

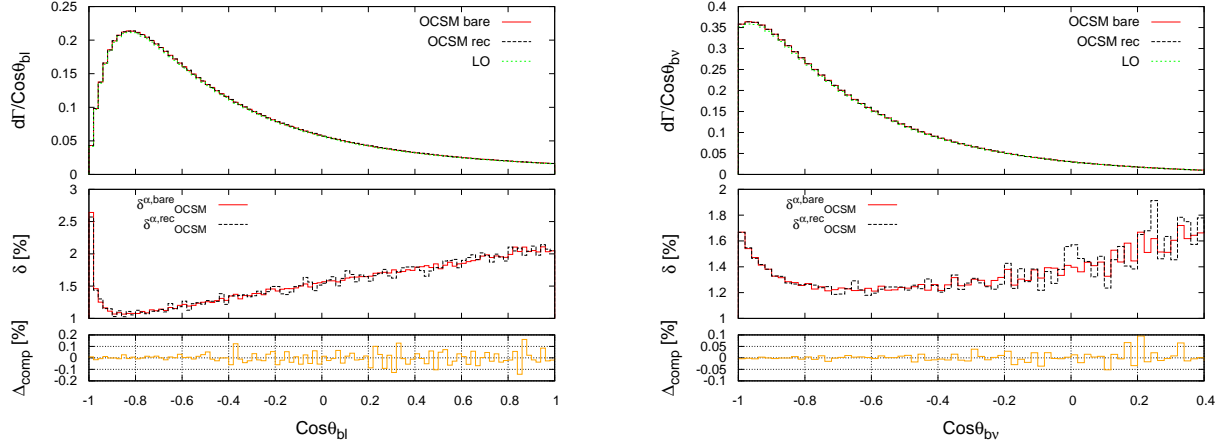


Figure 6.12: NLO EW corrections to the semileptonic top-quark decay width as a function of the cosine of the angle between the  $b$ -jet and the leptons (left) and between the  $b$ -jet and the neutrinos (right).

	OCSM	subtr	NWA
$\Gamma_{\text{hadr}}^{(0)} / \text{GeV}$	0.48319351(5)	0.483199(6)	0.4906645 (+1.55%)
$\delta_{\text{hadr}}^{(1),\text{QCD}} / \%$	-5.58(2)	-5.589(2)	-5.2779(1)
$\delta_{\text{hadr}}^{(1),\text{EW}} / \%$	1.2896(5)	1.2898(4)	1.4201(6)
$\Gamma_{\text{hadr}}^{\text{NLO}} / \text{GeV}$	0.46248(9)	0.462425(1)	0.471736(3) (+2.00%)

Table 6.3: Top decay widths and relative corrections calculated for the hadronic decay with the input parameters listed in Sect. 6.2. The NWA values are calculated in Tab. A.1.

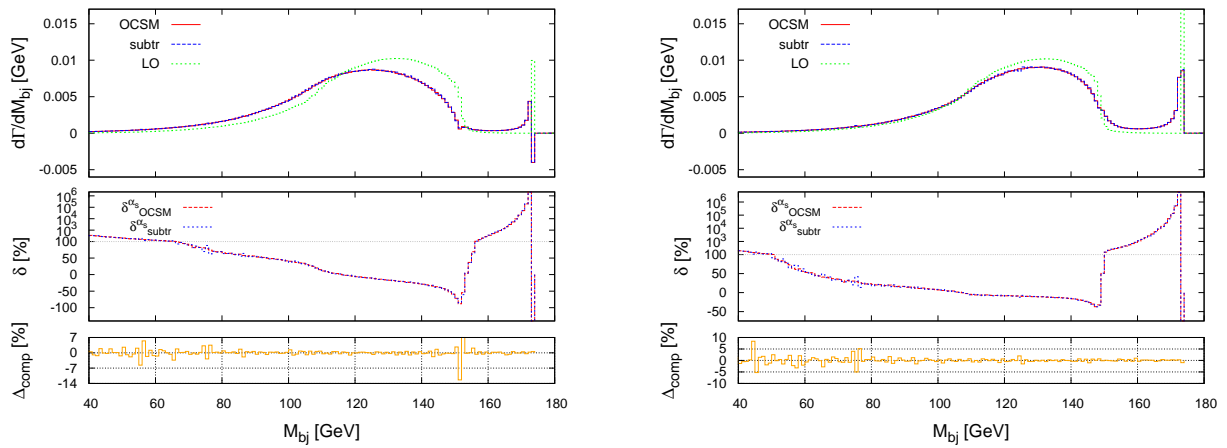


Figure 6.13: NLO QCD corrections to the hadronic top-quark decay width as a function of the invariant mass of the  $b$ -jet and the leading jet, calculated with  $R=0.6$  (left) and  $R=1$  (right).

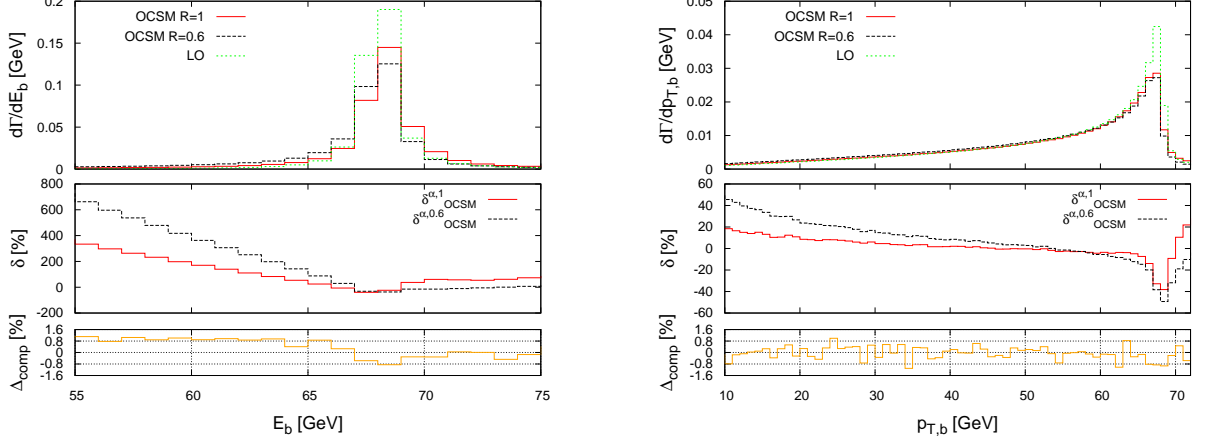


Figure 6.14: NLO QCD corrections to the hadronic top-quark decay width as a function of the energy (left) and of the transverse momentum (right) of the  $b$ -jet.

### QCD corrections to $t \rightarrow b u \bar{d}$

For the QCD corrections to the hadronic top-quark decay width we start analysing the distribution of the invariant mass of the  $b$ -jet and the leading jet, displayed in Fig. 6.13. In the upper frame on the left-hand side we notice that the absolute value of the distribution becomes negative at  $M_{bj} \sim 173$  GeV. This is of course an unphysical effect and can be interpreted as follows. During the jet-algorithm procedure a radius of the cone  $R = 0.6$  has been chosen (value taken from the ATLAS analysis, e.g. see Ref. [107]). For a too low value of  $R$ , however, recombination between the real and the virtual parts is not sufficiently inclusive and the IR divergence leaves a trace as  $\alpha_s \ln R$  corrections. This problem can be solved enlarging the cone, e.g.  $R = 1$ , as shown on the right-hand side of Fig. 6.13. With a wider cone, there is indeed a larger probability for the particles to be merged. In the case where all the final-state particles (excluding the  $b$  quark) are combined into a single jet, the invariant mass  $M_{bj}$  reproduces the top-quark mass value. This explains the appearance of a peak at  $M_{bj} = m_t$ . It is of course easier for the jet algorithm to cluster all jets (other than the  $b$  one) into a single merged object starting from a  $1 \rightarrow 3$  kinematics (as the LO) rather than at NLO. At NLO the presence of the extra gluon is such that  $M_{bj}$  can populate regions less probable at LO. This in turns explains the huge corrections in the middle frame of Fig. 6.13: The plotted  $\Gamma^{(1)}/\Gamma^{(0)}$  ratio explodes due to the almost null value of the LO in the normalization.

The distributions obtained choosing  $R = 1$  or  $R = 0.6$  are compared also for the other observables. The main difference is that the relative corrections induced by the larger radius are milder than those obtained with  $R = 0.6$ , as justified by the inclusiveness argument. This effect can be clearly seen in Fig. 6.14, where the QCD corrections to the energy and to the transverse momentum of the  $b$ -jet are presented. In the low-energy tail the relative corrections are very high, because of the normalization with the LO.

The energy of the leading jet, presented on the left-hand side of Fig. 6.15, receives positive QCD corrections due to gluon radiation, that turn negative after the energy peak at  $\sim 65$  GeV. As a consequence, the shape of the NLO energy distribution is shifted to the left, more evidently for  $R = 0.6$ . A similar effect can be seen for the transverse momentum of the leading jet.

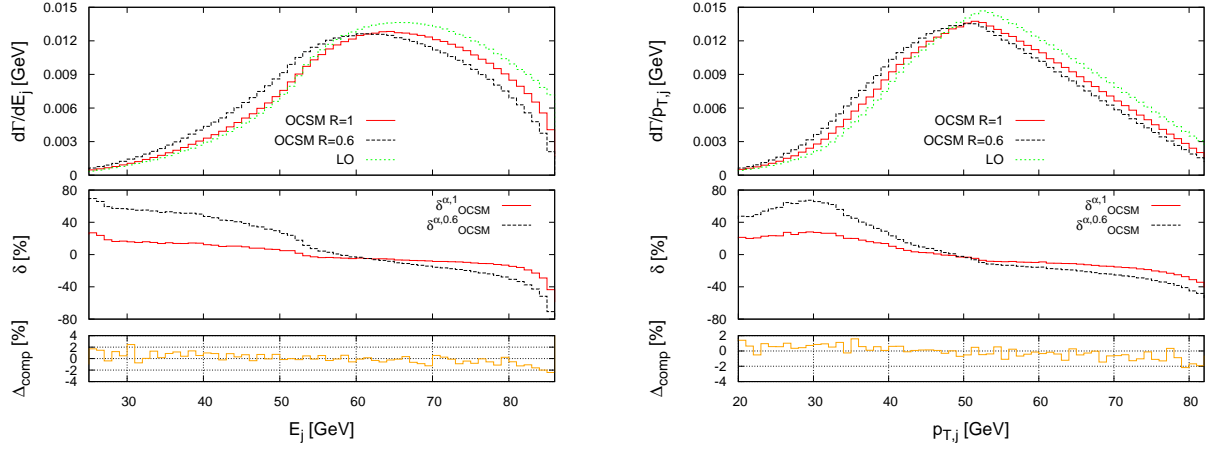


Figure 6.15: NLO QCD corrections to the hadronic top-quark decay width as a function of the energy (left) and of the transverse momentum (right) of the leading jet.

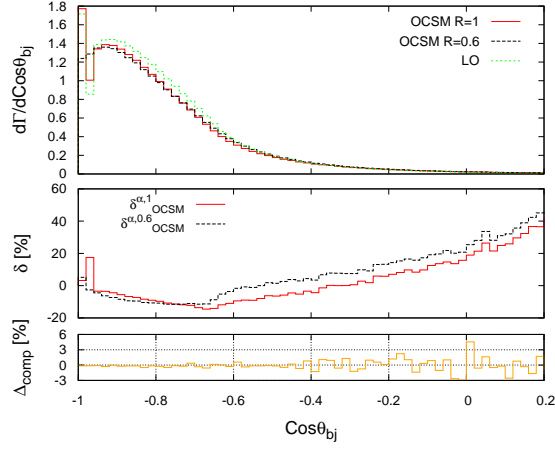


Figure 6.16: NLO QCD corrections to the hadronic top-quark decay width as a function of the cosine of the angle between the  $b$ -jet and the leading jet.

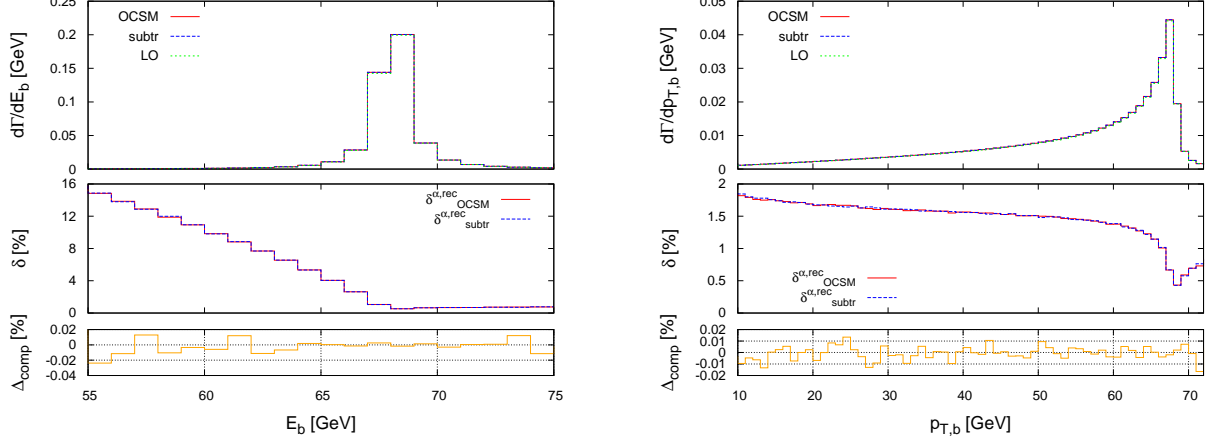


Figure 6.17: NLO EW corrections to the hadronic top-quark decay width as a function of the energy (left) and of the transverse momentum (right) of the  $b$ -jet.

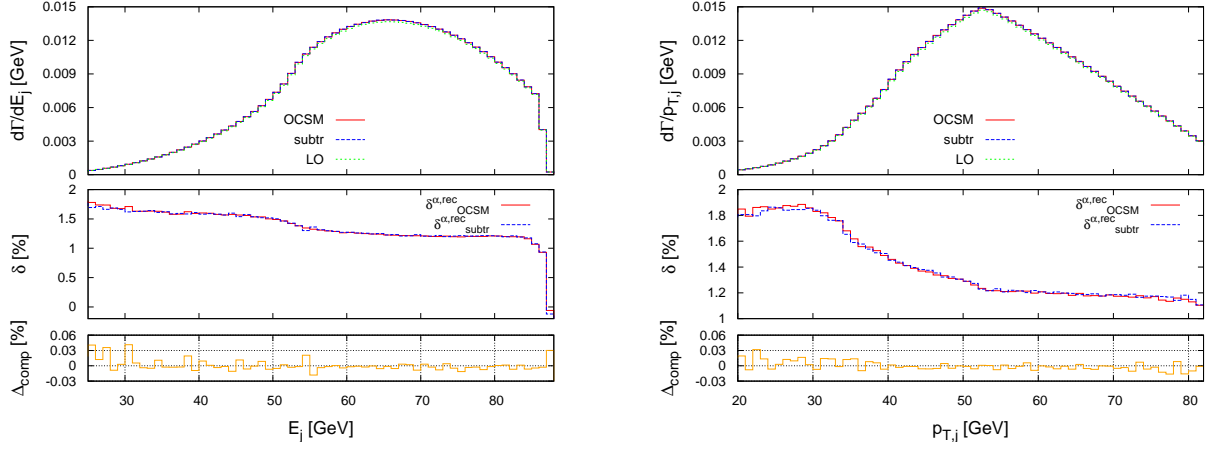


Figure 6.18: NLO EW corrections to the hadronic top-quark decay width as a function of the energy (left) and of the transverse momentum (right) of the leading jet.

Moreover, a difference between the two radiuses can be seen for the cosine of the angle between the  $b$ -jet and the leading jet, as displayed in Fig. 6.16. Only for  $R = 1$  a peak appears in the bin close to  $\cos\theta_{bj} = -1$ . It represents the case of all final-state particles ( $b$  quark excluded) merged into a single jet (more probable with a larger radius). In this calculation the top quark is considered at rest and the  $b$ -jet is indeed back-to-back to the remaining decay products.

### EW corrections to $t \rightarrow b u \bar{d}$

As in the semileptonic case, the EW corrections to the hadronic top-quark decay width are much smaller than the QCD ones and the differential distributions of the NLO corrections follow closely the LO value. Due to the low value of the EW corrections, the choice of  $R$ , the radius of the jet cone, does not substantially change the shape of the distributions. We use in the following  $R = 0.6$ .

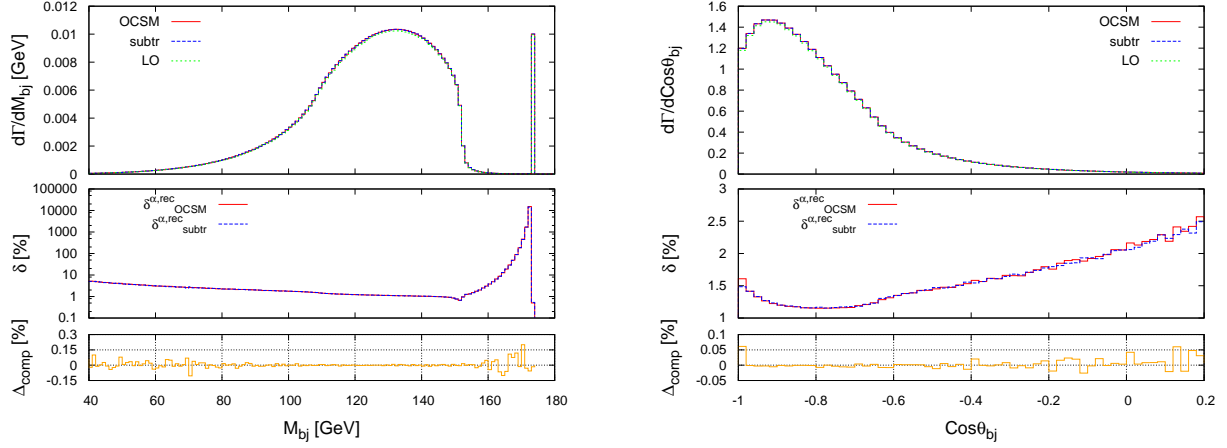


Figure 6.19: NLO EW corrections to the hadronic top-quark decay width as a function of the invariant mass (left) and of the cosine of the angle (right) of the  $b$ -jet and the leading jet.

Comparing the observables shown in Figs. 6.17 ( $E_b$  and  $p_{T,b}$ ), 6.18 ( $E_j$  and  $p_{T,j}$ ), and 6.19 ( $M_{bj}$  and  $\cos\theta_{bj}$ ) with those presented for the QCD case for  $R = 0.6$ , we see that the shapes of the EW corrections (middle frames) are very similar to the QCD ones. They are, however, about one order of magnitude lower and remain positive. Nevertheless, no fundamental differences need to be underlined.

## 6.5 Total top-quark decay width

Collecting the results presented in the previous section, we can write the NLO (QCD+EW) value of the partial decay width of the top quark. In the case of a semileptonic decay, for each lepton generation, we have

$$\Gamma_{\text{lept}}^{(0)} = 0.1610645(3) \text{ GeV}, \quad \Gamma_{\text{lept}}^{\text{NLO}} = 0.148108(6) \text{ GeV}, \quad (6.12)$$

while, for the hadronic decay, the partial width reads

$$\Gamma_{\text{hadr}}^{(0)} = 0.48319351(5) \text{ GeV}, \quad \Gamma_{\text{hadr}}^{\text{NLO}} = 0.46248(9) \text{ GeV}. \quad (6.13)$$

The total LO and NLO top-quark decay width can be finally calculated, summing the results in Eq. (6.12), for the three possible generations of leptons, to the values in Eq. (6.13), taking into account also the hadronic decay  $t \rightarrow b c \bar{s}$ . We obtain

$$\Gamma^{\text{LO}} = 1.4495805(9) \text{ GeV} \quad \text{and} \quad \Gamma^{\text{NLO}} = 1.3693(2) \text{ GeV}. \quad (6.14)$$

Comparing the full off-shell results of Eq. (6.14) with the values obtained using the NWA in App. A,

$$\Gamma_{\text{NWA}}^{\text{LO}} = 1.5021850 \text{ GeV} \quad (+3.63\%) \quad \text{and} \quad \Gamma_{\text{NWA}}^{\text{NLO}} = 1.38662(2) \text{ GeV} \quad (+1.26\%), \quad (6.15)$$

we see that the difference between the two predictions reaches up to  $\sim 3.6\%$  for the LO and is  $+1.3\%$  for the NLO corrections.

From the experimental side, the most recent achievements on the top-width measurement are the following:

- The direct top-quark width measurement in the lepton + jets channel of  $t\bar{t}$  events in  $p\bar{p}$  collisions at CDF II (Tevatron), with an integrated luminosity of  $8.7 \text{ fb}^{-1}$  [32]. They measured  $\Gamma_t = 2.21^{+1.84}_{-1.11} \text{ GeV}$  at 68% CL..
- The indirect measurement of D0 (Tevatron) [34]:  $\Gamma_t = 2.00^{+0.47}_{-0.43} \text{ GeV}$  for  $m_t = 170 \text{ GeV}$ , and at 95% CL.. They extracted the total width of the top quark, from the partial decay width  $\Gamma(t \rightarrow Wb)$  measured using the t-channel cross section for single-top-quark production and from the branching fraction  $B(t \rightarrow Wb)$  measured in  $t\bar{t}$  events using up to  $5.4 \text{ fb}^{-1}$ .
- The indirect measurement of CMS (LHC) [35]: They measured the ratio of the top-quark branching fractions  $R = BR(t \rightarrow Wb)/BR(t \rightarrow Wq)$ , with  $q = b, s, d$ , in the  $t\bar{t}$  dilepton final state with proton-proton collision data at  $\sqrt{s} = 8 \text{ TeV}$  from an integrated luminosity of  $19.7 \text{ fb}^{-1}$ . This result has been combined with a previous CMS measurement of the t-channel single-top-quark cross section [108] to determine the total top-quark decay width,  $\Gamma_t = 1.36 \pm 0.02(\text{stat})^{+0.14}_{-0.11}(\text{syst}) \text{ GeV}$ , assuming  $m_t = 172.5 \text{ GeV}$ .

A comparison between the theory results of Eq. (6.14) and the experimental values tells us that there is good agreement. The large errors of the direct measurement performed by CDF allows us only to confirm that the top-quark width is non-vanishing. For the D0 value only a rough comparison is possible: The value has been indeed calculated under the assumption of a top-quark mass  $m_t = 170 \text{ GeV}$ , different from the updated value chosen in this thesis. The top-quark width determined by CMS is more precise, but still not able to probe the level of precision reached in this work.

The LHC will certainly improve the value of  $\Gamma_t$ , but not necessarily this measurement will reach the theoretical precision. The main problem is that already now the error on the measurement is dominated by the systematic uncertainty, mainly via the jet energy scale, and it is yet not clear whether this important source of uncertainty can be significantly reduced. It is part of the physics program of the future lepton colliders to study the top-quark properties. The unique possibility to perform scans of the  $t\bar{t}$  production cross section around threshold allows to measure the top-quark decay width with unmatched precision: The ultimate ILC uncertainty is estimated to be around  $34 \text{ MeV}$ , while the FCC-ee (formerly TLEP) in the so-called ‘‘MegaTop’’ configuration, is confident to achieve an uncertainty of  $11 \text{ MeV}$  after 5 years of data taking [36]. The Compact Linear Collider (CLiC) will not improve this any further, since it is expected to reach a precision of  $220 \text{ MeV}$  by fitting the  $t\bar{t}$  cross section at  $\sqrt{s} = 500 \text{ GeV}$  [109].

# Chapter 7

## Conclusions

The top quark plays a special role in the Standard Model and in its most popular extensions. Due to its properties (the large mass, the short lifetime, the value of the Yukawa coupling, etc.), it is a good candidate to test the SM predictions, to look for new physics and to deepen our understanding of the mechanism of electroweak symmetry breaking. The top quark is predominantly produced at the LHC through the processes such as  $t\bar{t}$  production and single top production, which are therefore of large interest for the experimental measurements. In order to achieve the necessary theoretical precision, it is mandatory to take into account the decay of the top quarks and their radiative corrections. This entails a precise knowledge of the top-quark decay width  $\Gamma_t$ .

To this aim, we have calculated the NLO QCD and EW corrections to the semileptonic and to the hadronic top-quark decay widths, taking into account the off-shellness of the  $W$ -boson. For this purpose we implemented an in-house program. The matrix elements have been evaluated with the Weyl-van-der-Waerden spinorial formalism. The calculation of the virtual corrections has been automatized through another in-house code which makes use of the COLLIER library. We introduced counterterms following on-shell renormalization and included the off-shell effects of the  $W$  boson employing the complex-mass scheme.

The IR singularities, induced by soft and collinear photon/gluon radiation, are treated using mass regulators. In the context of this work, we have developed an extension of the one-cutoff phase-space slicing method for the case of a decay process with more than two particles in the final state. This technique allows to isolate the singularities from the real corrections, for the cases of both massive and massless final-state particles. It consists in identifying two different phase-space regions (a hard and a singular one) for the real emission of a photon or a gluon. The former region has been integrated numerically over a  $1 \rightarrow 4$  particle phase space, while the latter has been further subdivided. In one part of the singular region we considered the soft limit and we analytically integrated over the gluon/photon phase space. Later, we summed the obtained results to the virtual and counterterm contributions, and we integrated over the  $1 \rightarrow 3$  particle phase space. The remaining part of the singular region, the quasi-soft region, is a boundary region whose integration is done using the soft-photon/gluon approximation. Another possibility to deal with the IR singularities is the dipole-subtraction formalism, which has been used to implement a second independent calculation. The dipole approach has, however, the disadvantage to produce negative weights during the integration process, making a hypothetical generation of unweighted events with a Monte Carlo program more difficult.

The amplitudes have been numerically integrated by means of **VEGAS**, following the prescriptions of the one-cutoff slicing method and adapting the integrals, e.g. splitting them into different contributions.

The validity of the proposed method has been checked, in the case of the calculation of a top-quark decay width, finding a region where the integrated results do not depend on the introduced cut parameter  $\Delta s$ . Thereafter we have fixed a certain value of  $\Delta s$  to perform the calculation.

We have listed the integrated results for the partial top-quark decay widths. In particular, the QCD corrections to the semileptonic decay decrease the LO value by  $\sim -9.4\%$  and are in agreement with the values already existent in the literature. Concerning the new results obtained in this work, the EW corrections to the semileptonic decay are  $\sim 1.3\%$ . In the case of a hadronic decay the QCD and EW corrections are  $\sim -5.6\%$  and  $\sim 1.3\%$ , respectively. We have compared our values against the independent calculation performed using the dipole-subtraction formalism. The results are in mutual agreement. Moreover, a comparison with the values obtained using the narrow-width approximation has shown differences up to 2%.

Finally, after presenting differential distributions for the most interesting observables, we have collected our results to obtain the total top-quark decay width  $\Gamma_t$  at NLO precision. A comparison of  $\Gamma_t$  with the experimental measurements performed by D0, CDF, and CMS, shows a good agreement, even though the precision up to now reached by the experiments is not yet comparable with that of the new SM prediction. The experimental performance will certainly improve in the future: Higher precision will be reached by the LHC in the forthcoming years and by the future lepton colliders (ILC and FCC-ee) analyses, making the theoretical prediction described above more important.

A precise knowledge of  $\Gamma_t$  will become also essential to perform theoretical NLO EW predictions involving off-shell top-quarks, e.g. NLO EW corrections to the  $W^+W^-b\bar{b}$  production, which are not yet known. These kind of calculations need the top-quark width as an ingredient and demand, for consistency, the same NLO accuracy for the value of  $\Gamma_t$ .

Furthermore, the program developed in this work for the calculation of the NLO corrections to the top-quark decay width could be used as a basis for a Monte Carlo generator for top-quark decays with unweighted events at NLO precision. Direct applications could be, for example, an improvement to the calculation of the predictions for the  $t\bar{t}$ +jets and the  $t\bar{t}H$  channels via the addition of a top-quark decay.

# Appendix A

## Narrow-Width Approximation

The *narrow-width approximation* (NWA) is the simplest way to perform a calculation characterized by the presence of an unstable particle with a decay width small compared to its mass, even though it is limited in precision.

In the following, we will briefly describe the idea of the NWA, based on Refs. [81–83, 110], applied to the specific case of the top-quark decay, where the width of the  $W$  boson is  $\Gamma_W \ll M_W$ . Starting from the generic definition of an  $n$ -particles phase space, given in Eq. (3.2), and using the specific phase-space parameterization for the case  $n = 3$ , described in Sect. 5.3, the top-quark decay width at LO reads

$$\Gamma^{(0)}(t \rightarrow bf\bar{f}') = \frac{(2\pi)^{-5}}{2m_t} \int d\bar{s}_{34} \int d\phi_d(p_t^2, m_b^2, \bar{s}_{34}) \int d\phi_d(\bar{s}_{34}, m_f^2, m_{f'}^2) \overline{\sum} |\mathcal{M}(p_t; p_1, p_3, p_4)|^2, \quad (\text{A.1})$$

with the momenta of the particles involved in the process described in Fig. A.1. In Eq. (A.1) the virtuality of the  $W$  boson is represented by  $\sqrt{\bar{s}_{34}}$ . For small values of  $\Gamma_W/M_W$ , the dominating diagrams are the resonant ones, whose matrix elements factorize as

$$\mathcal{M}(p_t; p_b, p_f, p_{\bar{f}}')^{(\text{res})} = \mathcal{M}_{t \rightarrow bW \rightarrow bf\bar{f}'}^{(\text{res})} = \sum_{\lambda} \mathcal{M}_{t \rightarrow bW}^{(\lambda)} \frac{1}{\bar{s}_{34} - M_W^2 + iM_W\Gamma_W} \mathcal{M}_{W \rightarrow f\bar{f}'}^{(\lambda)}, \quad (\text{A.2})$$

where  $\lambda$  is the polarization vector of the  $W$  boson. After squaring the matrix element, a Breit-Wigner-shaped propagator appears

$$\left| \frac{1}{\bar{s}_{34} - M_W^2 + iM_W\Gamma_W} \right|^2 = \frac{1}{(\bar{s}_{34} - M_W^2)^2 + M_W^2\Gamma_W^2} \xrightarrow{\Gamma_W/M_W \rightarrow 0} \frac{\pi}{M_W\Gamma_W} \delta(\bar{s}_{34} - M_W^2). \quad (\text{A.3})$$

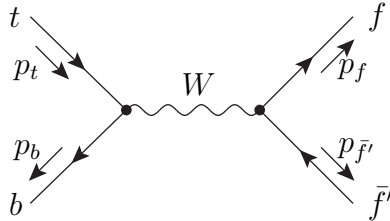


Figure A.1: LO diagram for the process  $t(p_t) \rightarrow b(p_b) f(p_f) \bar{f}'(p_{\bar{f}'})$ .

Equation (A.1) can be rewritten as

$$\begin{aligned}
\Gamma_{\text{NWA}}^{(0)}(t \rightarrow b f \bar{f}') & \underset{\Gamma_W/M_W \rightarrow 0}{\sim} \frac{(2\pi)^{-4}}{2m_t} \int \frac{d\bar{s}_{34}}{2M_W \Gamma_W} \delta(\bar{s}_{34} - M_W^2) \\
& \times \sum_{\lambda\lambda'} \int d\phi_d(p_t^2, m_b^2, \bar{s}_{34}) \mathcal{M}_{t \rightarrow bW}^{(\lambda)} \left( \mathcal{M}_{t \rightarrow bW}^{(\lambda')} \right)^* \int d\phi_d(\bar{s}_{34}, m_f^2, m_{f'}^2) \mathcal{M}_{W \rightarrow f \bar{f}'}^{(\lambda)} \left( \mathcal{M}_{W \rightarrow f \bar{f}'}^{(\lambda')} \right)^* \\
& = \frac{(2\pi)^{-2}}{2m_t} \int d\hat{\phi}_d(p_t^2, m_b^2, \bar{s}_{34}) \hat{\mathcal{M}}_{t \rightarrow bW}^{(\lambda)} \left( \hat{\mathcal{M}}_{t \rightarrow bW}^{(\lambda')} \right)^* \times \frac{1}{\Gamma_W} \\
& \times \frac{(2\pi)^{-2}}{2M_W} \int d\hat{\phi}_d(\bar{s}_{34}, m_f^2, m_{f'}^2) \hat{\mathcal{M}}_{W \rightarrow f \bar{f}'}^{(\lambda)} \left( \hat{\mathcal{M}}_{W \rightarrow f \bar{f}'}^{(\lambda')} \right)^*, \tag{A.4}
\end{aligned}$$

where the hat on  $\hat{\phi}$  and  $\hat{\mathcal{M}}$  fixes the on-shell condition  $\bar{s}_{34} = (\hat{p}_f + \hat{p}_{\bar{f}'})^2 = M_W^2$ . The rotational invariance in the  $W$ -boson rest frame implies

$$\int d\hat{\phi}_d(\bar{s}_{34}, m_f^2, m_{f'}^2) \hat{\mathcal{M}}_{W \rightarrow f \bar{f}'}^{(\lambda)} \left( \hat{\mathcal{M}}_{W \rightarrow f \bar{f}'}^{(\lambda')} \right)^* = \frac{2M_W}{(2\pi)^{-2}} \delta_{\lambda\lambda'} \Gamma^{(0)}(W \rightarrow f \bar{f}') \tag{A.5}$$

and therefore

$$\Gamma_{\text{NWA}}^{(0)}(t \rightarrow b f \bar{f}') \underset{\Gamma_W/M_W \rightarrow 0}{\sim} \Gamma^{(0)}(t \rightarrow Wb) \times \frac{\Gamma^{(0)}(W \rightarrow f \bar{f}')}{\Gamma_W}, \tag{A.6}$$

where  $\Gamma_W$  is the experimental value of the  $W$ -boson width. Thus, in the NWA, the top-quark partial width for the decay  $t \rightarrow b f \bar{f}'$  can be factorized into the partial decay width of  $t \rightarrow W^+ b$  times the branching ratio of the  $W$  boson decaying into a pair of fermions,  $BR^{(0)}(W \rightarrow f \bar{f}')$ :

$$\Gamma_{\text{NWA}}^{(0)}(t \rightarrow b f \bar{f}') \underset{\Gamma_W/M_W \rightarrow 0}{\sim} \Gamma^{(0)}(t \rightarrow Wb) \times BR^{(0)}(W \rightarrow f \bar{f}'). \tag{A.7}$$

For the NLO we consider the corrected version

$$\Gamma_{\text{NWA}}^{\text{NLO}}(t \rightarrow b f \bar{f}') \underset{\Gamma_W/M_W \rightarrow 0}{\sim} \Gamma^{(1)}(t \rightarrow Wb) \cdot BR^{(0)}(W \rightarrow f \bar{f}') + \Gamma^{(0)}(t \rightarrow Wb) \cdot BR^{(1)}(W \rightarrow f \bar{f}'), \tag{A.8}$$

with  $\Gamma^{\text{NLO}} = \Gamma^{(0)} + \Gamma^{(1)}$  and

$$BR^{(1)}(W \rightarrow f \bar{f}') = \frac{\Gamma^{\text{NLO}}(W \rightarrow f \bar{f}')}{\Gamma_W}. \tag{A.9}$$

The values calculated using Eq. (A.8) are compared with the full NLO calculation in Sect. 6.4.

Two-loops effects can be included in the following equation:

$$\Gamma_{\text{NWA}}^{(2)}(t \rightarrow b f \bar{f}') \underset{\Gamma_W/M_W \rightarrow 0}{\sim} \Gamma^{(1)}(t \rightarrow Wb) \times BR^{(1)}(W \rightarrow f \bar{f}'). \tag{A.10}$$

The results obtained using the input parameters of Sect. 6.2 are listed in Table A.1. They have been checked against an independent calculation implemented by L. Basso with the same settings presented in Sect. 6.1, and against the analytic results presented in Ref. [20, 22]. The difference  $|\Gamma_{\text{NWA}}^{(2)} - \Gamma_{\text{NWA}}^{(1)}|$  can be used as a conservative measure of uncertainty from higher orders beyond NLO.

	$\Gamma_{\text{NWA}}^{(0)} / \text{GeV}$	$\delta_{\text{NWA}}^{(1),\text{QCD}} / \%$	$\delta_{\text{NWA}}^{(1),\text{EW}} / \%$	$\Gamma_{\text{NWA}}^{\text{NLO}} / \text{GeV}$	$\Gamma_{\text{NWA}}^{\text{NNLO}} / \text{GeV}$
$t \rightarrow W^+ b$	1.5021850	$-9.377(1)$	$1.6843(1)$	$1.38662(2)$	
$W \rightarrow u \bar{d}$	0.6810316	$4.100(1)$	$-0.26425(5)$	$0.70715(1)$	
$BR(W^+ \rightarrow u \bar{d})$	0.3266339			$0.339161(6)$	
$W^+ \rightarrow \nu_\ell \ell$	0.2270105		$-0.2163(2)$	$0.2265195(5)$	
$BR(W^+ \rightarrow \nu_\ell \ell)$	0.1088779			$0.1086424(3)$	
$t \rightarrow b u \bar{d}$	0.4906645	$-5.2779(1)$	$1.4201(6)$	$0.471736(3)$	$0.469828(3)$
$t \rightarrow b \nu_\ell \ell$	0.1635547	$-9.377(1)$	$1.4680(6)$	$0.1506131(2)$	$0.1506133(2)$

Table A.1: Top-quark decay widths calculated in the NWA with the input parameters listed in Sect. 6.2, and with  $\delta_{\text{NWA}}^{(1)} = \frac{\Gamma_{\text{NWA}}^{(1)}}{\Gamma_{\text{NWA}}^{(0)}}$  and  $\Gamma_{\text{NWA}}^{\text{NNLO}} = \Gamma_{\text{NWA}}^{(0)} + \Gamma_{\text{NWA}}^{(2)}$ .



# Appendix B

## Soft-photon approximation

We consider the generic process, represented in Fig. B.1 (a), of an incoming fermion with momentum  $p_f$ , mass  $m_f$  and charge  $Q_f$ . The LO matrix element reads

$$\mathcal{M}_0 = A(p_f)u(p_f), \quad (\text{B.1})$$

where  $u(p_f)$  is the spinor of the incoming fermion and  $A(p_f)$  is the remaining part. If the fermion emits a photon with momentum  $q$  and polarization vector  $\varepsilon$  (Fig. B.1 (b)) the matrix element is

$$\mathcal{M}_{1,s}^{(\text{in})} = A(p_f - q) \frac{i(\not{p}_f - \not{q} + m_f)}{(p_f - q)^2 - m_f^2} (ieQ_f) \not{\varepsilon} u(p_f). \quad (\text{B.2})$$

The soft-photon approximation is obtained neglecting all the terms proportional to  $q$  in the numerator. After some algebra, one obtains

$$\mathcal{M}_1 = eQ_f \frac{p_f \varepsilon}{p_f q} \mathcal{M}_0, \quad (\text{B.3})$$

where the Born matrix element  $\mathcal{M}_0$  factorizes. The same result is obtained in the case of an incoming vector line.

In case of an outgoing fermion or vector (generally labeled with  $i$ ) the matrix element differs from the incoming one by a sign:

$$\mathcal{M}_{1,s}^{(\text{out})} = -eQ_i \frac{p_i \varepsilon}{p_i q} \mathcal{M}_0. \quad (\text{B.4})$$

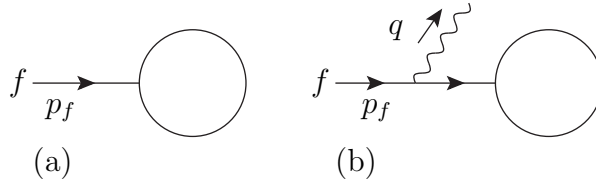


Figure B.1: Generic diagram with an incoming fermion  $f$  without (a) and with (b) a photon emission.

The radiation from an internal line does not lead to a singular contribution and thus can be omitted in the soft-photon approximation, as proved in Ref. [111].

In general, the matrix element for the real emission of a soft photon is proportional to the Born matrix element  $\mathcal{M}_0$  as

$$\mathcal{M}_1 = -e\mathcal{M}_0 \sum_i (\pm Q_i) e_i(q), \quad (\text{B.5})$$

where the quantity

$$e_i(q) = \frac{p_i \varepsilon}{p_i q} \quad (\text{B.6})$$

is called *eikonal factor*. More details can be found in Ref. [22].

In QCD the scattering amplitudes can be decomposed as a product of a colour factor and colour-ordered amplitudes. In case of a soft-gluon emission, the latter can themselves factorize into an eikonal factor, similarly to the case of a soft-photon emission.

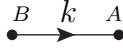
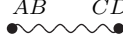
# Appendix C


## Feynman rules

We list the Feynman rules needed in this thesis in the WvdW formalism, following Refs. [22,85].

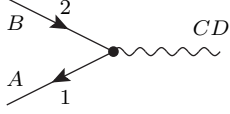
The labels  $S$ ,  $F$ , and  $V$  denote scalar, fermion and vector fields, respectively, while  $s = s_w$  and  $c = c_w$ . All the momenta are considered as incoming. We use the 't Hooft Feynman gauge.

- Feynman rules for propagators and counterterms

Propagators:	
	$\frac{i}{k^2 - m_f^2} \begin{pmatrix} m_f \delta_A^B & K_{A\dot{B}} \\ K^{\dot{A}B} & m_f \delta_{\dot{B}}^{\dot{A}} \end{pmatrix}$
	$\frac{-2i\epsilon_{\dot{A}\dot{C}}\epsilon_{BD}}{k^2 - M_V^2}$

VV-counterterm:	
	$-2i\epsilon_{\dot{A}\dot{C}}\epsilon_{BD} [\delta Z_W(k^2 - M_W^2) - \delta M_W^2]$

• Feynman rules for vertices

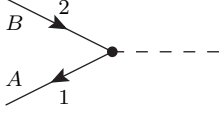
VFF-vertex:	
	$ie \begin{pmatrix} 0 & C_{V\bar{f}_1 f_2}^- \delta_B^{\dot{C}} \delta_A^D \\ C_{V\bar{f}_1 f_2}^+ \epsilon^{\dot{A} \dot{C}} \epsilon^{BD} & 0 \end{pmatrix}$

$$\begin{aligned}
C_{\gamma \bar{f}_i f_j}^+ &= -Q_f \left[ \delta_{ij} \left( 1 + \delta Z_e + \frac{1}{2} \delta Z_{AA} \right) + \frac{1}{2} (\delta Z_{ij}^{f,R} + \delta Z_{ij}^{f,R\dagger}) \right] + \delta_{ij} g_f^+ \frac{1}{2} \delta Z_{ZA}, \\
C_{\gamma \bar{f}_i f_j}^- &= -Q_f \left[ \delta_{ij} \left( 1 + \delta Z_e + \frac{1}{2} \delta Z_{AA} \right) + \frac{1}{2} (\delta Z_{ij}^{f,L} + \delta Z_{ij}^{f,L\dagger}) \right] + \delta_{ij} g_f^- \frac{1}{2} \delta Z_{ZA}, \\
C_{Z \bar{f}_i f_j}^+ &= g_f^+ \left[ \delta_{ij} \left( 1 + \frac{1}{2} \delta Z_{ZZ} \right) + \frac{1}{2} (\delta Z_{ij}^{f,R} + \delta Z_{ij}^{f,R\dagger}) \right] - \delta_{ij} Q_f \frac{1}{2} \delta Z_{AZ}, \\
C_{Z \bar{f}_i f_j}^- &= g_f^- \left[ \delta_{ij} \left( 1 + \frac{1}{2} \delta Z_{ZZ} \right) + \frac{1}{2} (\delta Z_{ij}^{f,L} + \delta Z_{ij}^{f,L\dagger}) \right] - \delta_{ij} Q_f \frac{1}{2} \delta Z_{AZ}, \\
C_{W^- \bar{d}_j u_i}^+ &= 0, \\
C_{W^- \bar{d}_j u_i}^- &= \frac{1}{\sqrt{2} s_w} \left[ \left( 1 + \delta Z_e - \frac{\delta s_w}{s_w} + \frac{1}{2} \delta Z_W \right) + \frac{1}{2} \sum_k (\delta Z_{jk}^{d,L\dagger} + \delta Z_{ki}^{u,L}) \right], \\
C_{W^+ \bar{u}_i d_j}^+ &= 0, \\
C_{W^+ \bar{u}_i d_j}^- &= \frac{1}{\sqrt{2} s} \left[ V_{ij} \left( 1 + \delta Z_e - \frac{\delta s}{s} + \frac{1}{2} \delta Z_W \right) + \delta V_{ij} \right. \\
&\quad \left. + \frac{1}{2} \sum_k (\delta Z_{ik}^{u,L\dagger} V_{kj} + V_{ik} \delta Z_{kj}^{d,L}) \right], \\
C_{W^- \bar{l}_j \nu_i}^+ &= 0, \\
C_{W^- \bar{l}_j \nu_i}^- &= \frac{1}{\sqrt{2} s_w} \delta_{ij} \left[ 1 + \delta Z_e - \frac{\delta s_w}{s_w} + \frac{1}{2} \delta Z_W + \frac{1}{2} (\delta Z_{ii}^{l,L\dagger} + \delta Z_{ii}^{\nu,L}) \right], \\
C_{W^+ \bar{\nu}_i l_j}^+ &= 0, \\
C_{W^+ \bar{\nu}_i l_j}^- &= \frac{1}{\sqrt{2} s} \delta_{ij} \left[ 1 + \delta Z_e - \frac{\delta s}{s} + \frac{1}{2} \delta Z_W + \frac{1}{2} (\delta Z_{ii}^{\nu,L\dagger} + \delta Z_{ii}^{l,L}) \right], \tag{C.1}
\end{aligned}$$

where

$$g_f^+ = -\frac{s_w}{c_w} Q_f \quad \text{and} \quad g_f^- = \frac{I_f^3 - s_w^2 Q_f}{s_w c_w}. \tag{C.2}$$

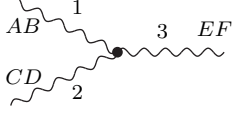
SFF-vertex:



$$ie \begin{pmatrix} C_{S\bar{f}_1 f_2}^+ \delta_A^B & 0 \\ 0 & C_{S\bar{f}_1 f_2}^- \delta_B^A \end{pmatrix}$$

$$\begin{aligned}
C_{H\bar{f}_i f_j}^+ &= -\frac{1}{2s} \frac{1}{M_W} \left[ \delta_{ij} m_{f,i} \left( 1 + \delta Z_e - \frac{\delta s}{s} + \frac{\delta m_{f,i}}{m_{f,i}} - \frac{\delta M_W}{M_W} + \frac{1}{2} \delta Z_H \right) \right. \\
&\quad \left. + \frac{1}{2} (m_{f,i} \delta Z_{ij}^{f,R} + \delta Z_{ij}^{f,L\dagger} m_{f,j}) \right], \\
C_{H\bar{f}_i f_j}^- &= -\frac{1}{2s} \frac{1}{M_W} \left[ \delta_{ij} m_{f,i} \left( 1 + \delta Z_e - \frac{\delta s}{s} + \frac{\delta m_{f,i}}{m_{f,i}} - \frac{\delta M_W}{M_W} + \frac{1}{2} \delta Z_H \right) \right. \\
&\quad \left. + \frac{1}{2} (m_{f,i} \delta Z_{ij}^{f,L} + \delta Z_{ij}^{f,R\dagger} m_{f,j}) \right], \\
C_{\chi\bar{f}_i f_j}^+ &= i \frac{1}{2s} 2I_{W,f}^3 \frac{1}{M_W} \left[ \delta_{ij} m_{f,i} \left( 1 + \delta Z_e - \frac{\delta s}{s} + \frac{\delta m_{f,i}}{m_{f,i}} - \frac{\delta M_W}{M_W} \right) \right. \\
&\quad \left. + \frac{1}{2} (m_{f,i} \delta Z_{ij}^{f,R} + \delta Z_{ij}^{f,L\dagger} m_{f,j}) \right], \\
C_{\chi\bar{f}_i f_j}^- &= -i \frac{1}{2s} 2I_{W,f}^3 \frac{1}{M_W} \left[ \delta_{ij} m_{f,i} \left( 1 + \delta Z_e - \frac{\delta s}{s} + \frac{\delta m_{f,i}}{m_{f,i}} - \frac{\delta M_W}{M_W} \right) \right. \\
&\quad \left. + \frac{1}{2} (m_{f,i} \delta Z_{ij}^{f,L} + \delta Z_{ij}^{f,R\dagger} m_{f,j}) \right], \\
C_{\phi^+ \bar{u}_i d_j}^+ &= -\frac{1}{\sqrt{2}s} \frac{1}{M_W} \left[ V_{ij} m_{d,j} \left( 1 + \delta Z_e - \frac{\delta s}{s} + \frac{\delta m_{d,j}}{m_{d,j}} - \frac{\delta M_W}{M_W} \right) + \delta V_{ij} m_{d,j} \right. \\
&\quad \left. + \frac{1}{2} \sum_k (\delta Z_{ik}^{u,L\dagger} V_{kj} m_{d,j} + V_{ik} m_{d,k} \delta Z_{kj}^{d,R}) \right], \\
C_{\phi^+ \bar{u}_i d_j}^- &= \frac{1}{\sqrt{2}s} \frac{1}{M_W} \left[ m_{u,i} V_{ij} \left( 1 + \delta Z_e - \frac{\delta s}{s} + \frac{\delta m_{u,i}}{m_{u,i}} - \frac{\delta M_W}{M_W} \right) + m_{u,i} \delta V_{ij} \right. \\
&\quad \left. + \frac{1}{2} \sum_k (\delta Z_{ik}^{u,R\dagger} m_{u,k} V_{kj} + m_{u,i} V_{ik} \delta Z_{kj}^{d,L}) \right], \\
C_{\phi^- \bar{d}_j u_i}^+ &= -\frac{1}{\sqrt{2}s_w} \frac{m_{u,i}}{M_W} \delta_{ij} \left[ 1 + \delta Z_e - \frac{\delta s_w}{s_w} - \frac{\delta M_W}{M_W} + \frac{1}{2} (\delta Z_{ii}^{d,L\dagger} + \delta Z_{ii}^{u,R}) \right], \\
C_{\phi^- \bar{d}_j u_i}^- &= -\frac{1}{\sqrt{2}s_w} \frac{m_{d,j}}{M_W} \delta_{ij} \left[ 1 + \delta Z_e - \frac{\delta s_w}{s_w} - \frac{\delta M_W}{M_W} + \frac{1}{2} (\delta Z_{jj}^{d,R\dagger} + \delta Z_{jj}^{u,L}) \right], \\
C_{\phi^+ \bar{\nu}_i l_j}^+ &= -\frac{1}{\sqrt{2}s} \frac{m_{l,i}}{M_W} \delta_{ij} \left[ 1 + \delta Z_e - \frac{\delta s}{s} + \frac{\delta m_{l,i}}{m_{l,i}} - \frac{\delta M_W}{M_W} + \frac{1}{2} (\delta Z_{ii}^{\nu,L\dagger} + \delta Z_{ii}^{l,R}) \right], \\
C_{\phi^+ \bar{\nu}_i l_j}^- &= 0, \\
C_{\phi^- \bar{l}_j \nu_i}^+ &= 0, \\
C_{\phi^- \bar{l}_j \nu_i}^- &= -\frac{1}{\sqrt{2}s} \frac{m_{l,i}}{M_W} \delta_{ij} \left[ 1 + \delta Z_e - \frac{\delta s}{s} + \frac{\delta m_{l,i}}{m_{l,i}} - \frac{\delta M_W}{M_W} + \frac{1}{2} (\delta Z_{ii}^{l,R\dagger} + \delta Z_{ii}^{\nu,L}) \right]. \quad (C.3)
\end{aligned}$$

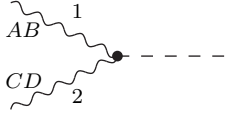
VVV-vertex:



$$\frac{i}{4}eC_{V_1V_2V_3} \left[ \epsilon^{\dot{A}\dot{C}}\epsilon^{BD}(K_1 - K_2)\dot{E}F + \epsilon^{\dot{C}\dot{E}}\epsilon^{DF}(K_2 - K_3)\dot{A}B \right. \\ \left. + \epsilon^{\dot{A}\dot{E}}\epsilon^{BF}(K_3 - K_1)\dot{C}D \right]$$

$$C_{AW+W^-} = 1 + \delta Z_e + \delta Z_W + \frac{1}{2}\delta Z_{AA} - \frac{1}{2}\frac{c}{s}\delta Z_{ZA}, \\ C_{ZW+W^-} = -\frac{c}{s}(1 + \delta Z_e - \frac{1}{c^2}\frac{\delta s}{s} + \delta Z_W + \frac{1}{2}\delta Z_{ZZ}) + \frac{1}{2}\delta Z_{AZ}. \quad (C.4)$$

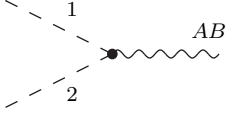
SVV-vertex:



$$\frac{i}{2}eC_{SV_1V_2}\epsilon^{\dot{A}\dot{C}}\epsilon^{BD}$$

$$C_{HW+W^-} = M_W \frac{1}{s} \left[ 1 + \delta Z_e - \frac{\delta s}{s} + \frac{1}{2} \frac{\delta M_W^2}{M_W^2} + \frac{1}{2} \delta Z_H + \delta Z_W \right], \\ C_{HZZ} = M_W \frac{1}{s c^2} \left[ 1 + \delta Z_e + \frac{2s^2 - c^2}{c^2} \frac{\delta s}{s} + \frac{1}{2} \frac{\delta M_W^2}{M_W^2} + \frac{1}{2} \delta Z_H + \delta Z_{ZZ} \right], \\ C_{HZA} = M_W \frac{1}{s c^2} \frac{1}{2} \delta Z_{ZA}, \\ C_{\phi^\pm W^\mp Z} = -M_W \frac{s}{c} \left[ 1 + \delta Z_e + \frac{1}{c^2} \frac{\delta s}{s} + \frac{1}{2} \frac{\delta M_W^2}{M_W^2} + \frac{1}{2} \delta Z_W + \frac{1}{2} \delta Z_{ZZ} \right] - M_W \frac{1}{2} \delta Z_{AZ}, \\ C_{\phi^\pm W^\mp A} = -M_W \left[ 1 + \delta Z_e + \frac{1}{2} \frac{\delta M_W^2}{M_W^2} + \frac{1}{2} \delta Z_W + \frac{1}{2} \delta Z_{AA} \right] - M_W \frac{s}{c} \frac{1}{2} \delta Z_{ZA}. \quad (C.5)$$

VSS-vertex:



$$\frac{i}{2}eC_{VS_1S_2}(K_1 - K_2)^{AB}$$

$$\begin{aligned}
C_{A\chi H} &= -\frac{i}{2cs}\frac{1}{2}\delta Z_{ZA}, \\
C_{Z\chi H} &= -\frac{i}{2cs}\left[1 + \delta Z_e + \frac{s^2 - c^2}{c^2}\frac{\delta s}{s} + \frac{1}{2}\delta Z_H + \frac{1}{2}\delta Z_{ZZ}\right], \\
C_{A\phi^+\phi^-} &= -\left[1 + \delta Z_e + \frac{1}{2}\delta Z_{AA} + \frac{s^2 - c^2}{2sc}\frac{1}{2}\delta Z_{ZA}\right], \\
C_{Z\phi^+\phi^-} &= -\frac{s^2 - c^2}{2sc}\left[1 + \delta Z_e + \frac{1}{(s^2 - c^2)c^2}\frac{\delta s}{s} + \frac{1}{2}\delta Z_{ZZ}\right] - \frac{1}{2}\delta Z_{AZ}, \\
C_{W^\pm\phi^\mp H} &= \mp\frac{1}{2s}\left[1 + \delta Z_e - \frac{\delta s}{s} + \frac{1}{2}\delta Z_W + \frac{1}{2}\delta Z_H\right], \\
C_{W^\pm\phi^\mp\chi} &= -\frac{i}{2s}\left[1 + \delta Z_e - \frac{\delta s}{s} + \frac{1}{2}\delta Z_W\right].
\end{aligned} \tag{C.6}$$



# Bibliography

- [1] F. Abe *et al.*, “Observation of top quark production in  $\bar{p}p$  collisions,” *Phys.Rev.Lett.* **74**, pp. 2626–2631, 1995. arXiv:hep-ex/9503002 [hep-ex] .
- [2] S. Abachi *et al.*, “Observation of the top quark,” *Phys.Rev.Lett.* **74**, pp. 2632–2637, 1995. arXiv:hep-ex/9503003 [hep-ex] .
- [3] I. I. Bigi, “The QCD perspective on lifetimes of heavy flavor hadrons,” 1995. arXiv:hep-ph/9508408 [hep-ph] .
- [4] M. Czakon, P. Fiedler, A. Mitov, and J. Rojo, “Further exploration of top pair hadroproduction at NNLO,” 2013. arXiv:1305.3892 [hep-ph] .
- [5] A. Denner, S. Dittmaier, S. Kallweit, and S. Pozzorini, “NLO QCD corrections to  $W^+W^-b\bar{b}$  production at hadron colliders,” *Phys.Rev.Lett.* **106**, p. 052001, 2011. arXiv:1012.3975 [hep-ph] .
- [6] G. Bevilacqua, M. Czakon, A. van Hameren, C. G. Papadopoulos, and M. Worek, “Complete off-shell effects in top quark pair hadroproduction with leptonic decay at next-to-leading order,” *JHEP* **1102**, p. 083, 2011. arXiv:1012.4230 [hep-ph] .
- [7] A. Denner, S. Dittmaier, S. Kallweit, and S. Pozzorini, “NLO QCD corrections to off-shell  $t\bar{t}$  production at hadron colliders,” *PoS* **LL2012**, p. 015, 2012. arXiv:1208.4053 [hep-ph] .
- [8] F. Cascioli, S. Kallweit, P. Maierhöfer, and S. Pozzorini, “A unified NLO description of top-pair and associated  $Wt$  production,” *Eur.Phys.J.* **C74**, p. 2783, 2014. arXiv:1312.0546 [hep-ph] .
- [9] A. Denner, S. Dittmaier, M. Roth, and D. Wackeroth, “Predictions for all processes  $e^+e^- \rightarrow 4$  fermions +  $\gamma$ ,” *Nucl.Phys.* **B560**, pp. 33–65, 1999. arXiv:hep-ph/9904472 [hep-ph] .
- [10] A. Denner, S. Dittmaier, M. Roth, and L. Wieders, “Electroweak corrections to charged-current  $e^+e^- \rightarrow 4$  fermions processes: Technical details and further results,” *Nucl.Phys.* **B724**, pp. 247–294, 2005. arXiv:hep-ph/0505042 [hep-ph] .
- [11] A. Denner and S. Dittmaier, “The Complex-mass scheme for perturbative calculations with unstable particles,” *Nucl.Phys.Proc.Suppl.* **160**, pp. 22–26, 2006. arXiv:hep-ph/0605312 [hep-ph] .

- [12] D. Bardin, S. Bondarenko, P. Christova, L. Kalinovskaya, V. Kolesnikov, *et al.*, “Standard SANC modules for NLO QCD Radiative Corrections to Single-top Production,” 2011. arXiv:1110.3622 [hep-ph] .
- [13] K. Fujikawa, “Heavy Fermions in the Standard Sequential Scheme,” *Prog.Theor.Phys.* **61**, p. 1186, 1979.
- [14] J. H. Kuhn and K. Streng, “Measurement of Weak Couplings Through Toponium Decays,” *Nucl.Phys.* **B198**, p. 71, 1982.
- [15] M. Jezabek and J. H. Kuhn, “Semileptonic Decays of Top Quarks,” *Phys.Lett.* **B207**, p. 91, 1988.
- [16] M. Jezabek and J. H. Kühn, “QCD Corrections to Semileptonic Decays of Heavy Quarks,” *Nucl.Phys.* **B314**, p. 1, 1989.
- [17] A. Czarnecki, “QCD corrections to the decay  $t \rightarrow Wb$  in dimensional regularization,” *Phys.Lett.* **B252**, pp. 467–470, 1990.
- [18] C. S. Li, R. J. Oakes, and T. C. Yuan, “QCD corrections to  $t \rightarrow W^+b$ ,” *Phys.Rev.* **D43**, pp. 3759–3762, 1991.
- [19] J.-a. Liu and Y.-P. Yao, “One loop radiative corrections to a heavy top decay in the standard model,” *Int.J.Mod.Phys.* **A6**, pp. 4925–4948, 1991.
- [20] A. Denner and T. Sack, “The Top width,” *Nucl.Phys.* **B358**, pp. 46–58, 1991.
- [21] G. Eilam, R. Mendel, R. Migneron, and A. Soni, “Radiative corrections to top quark decay,” *Phys.Rev.Lett.* **66**, pp. 3105–3108, 1991.
- [22] A. Denner, “Techniques for calculation of electroweak radiative corrections at the one loop level and results for W physics at LEP-200,” *Fortsch.Phys.* **41**, pp. 307–420, 1993. arXiv:0709.1075 [hep-ph] .
- [23] M. Jezabek and J. H. Kühn, “The Top width: Theoretical update,” *Phys.Rev.* **D48**, pp. 1910–1913, 1993. arXiv:hep-ph/9302295 [hep-ph] .
- [24] M. Jezabek and J. H. Kühn, “The top width: Theoretical update,” 1993.
- [25] S. Oliveira, L. Brucher, R. Santos, and A. Barroso, “Electroweak corrections to the top quark decay,” *Phys.Rev.* **D64**, p. 017301, 2001. arXiv:hep-ph/0011324 [hep-ph] .
- [26] A. Czarnecki, “Two loop light quark corrections to the top width,” *Acta Phys.Polon.* **B26**, pp. 845–849, 1995. arXiv:hep-ph/9503444 [hep-ph] .
- [27] A. Czarnecki and K. Melnikov, “Two loop QCD corrections to top quark width,” *Nucl.Phys.* **B544**, pp. 520–531, 1999. arXiv:hep-ph/9806244 [hep-ph] .
- [28] K. Chetyrkin, R. Harlander, T. Seidensticker, and M. Steinhauser, “Second order QCD corrections to  $\Gamma(t \rightarrow Wb)$ ,” *Phys.Rev.* **D60**, p. 114015, 1999. arXiv:hep-ph/9906273 [hep-ph] .

- [29] J. Gao, C. S. Li, and H. X. Zhu, “Top Quark Decay at Next-to-Next-to Leading Order in QCD,” *Phys.Rev.Lett.* **110**, p. 042001, 2013. arXiv:1210.2808 [hep-ph] .
- [30] T. Aaltonen *et al.*, “First Direct Bound on the Total Width of the Top Quark in  $p\bar{p}$  Collisions at  $\sqrt{s} = 1.96$  TeV,” *Phys.Rev.Lett.* **102**, p. 042001, 2009. arXiv:0808.2167 [hep-ex] .
- [31] T. Aaltonen *et al.*, “Direct Top-Quark Width Measurement CDF,” *Phys.Rev.Lett.* **105**, p. 232003, 2010. arXiv:1008.3891 [hep-ex] .
- [32] T. A. Aaltonen *et al.*, “Direct Measurement of the Total Decay Width of the Top Quark,” *Phys.Rev.Lett.* **111**(20), p. 202001, 2013. arXiv:1308.4050 [hep-ex] .
- [33] V. M. Abazov *et al.*, “Determination of the width of the top quark,” *Phys.Rev.Lett.* **106**, p. 022001, 2011. arXiv:1009.5686 [hep-ex] .
- [34] V. M. Abazov *et al.*, “An Improved determination of the width of the top quark,” *Phys.Rev.* **D85**, p. 091104, 2012. arXiv:1201.4156 [hep-ex] .
- [35] V. Khachatryan *et al.*, “Measurement of the ratio  $B(t \rightarrow Wb)/B(t \rightarrow Wq)$  in pp collisions at  $\sqrt{s} = 8$  TeV,” *Phys.Lett.* **B736**, p. 33, 2014. arXiv:1404.2292 [hep-ex] .
- [36] M. Bicer, H. D. Yildiz, I. Yildiz, G. Coignet, M. Delmastro, *et al.*, “First look at the physics case of tlep,” *JHEP* **1401**, p. 164, 2014. arXiv:1308.6176 [hep-ex] .
- [37] W. Giele and E. N. Glover, “Higher order corrections to jet cross-sections in  $e^+e^-$  annihilation,” *Phys.Rev.* **D46**, pp. 1980–2010, 1992.
- [38] W. Giele, E. N. Glover, and D. A. Kosower, “Higher order corrections to jet cross-sections in hadron colliders,” *Nucl.Phys.* **B403**, pp. 633–670, 1993. arXiv:hep-ph/9302225 [hep-ph] .
- [39] B. Harris, E. Laenen, L. Phaf, Z. Sullivan, and S. Weinzierl, “The Fully differential single top quark cross-section in next to leading order QCD,” *Phys.Rev.* **D66**, p. 054024, 2002. arXiv:hep-ph/0207055 [hep-ph] .
- [40] S. Keller and E. Laenen, “Next-to-leading order cross-sections for tagged reactions,” *Phys.Rev.* **D59**, p. 114004, 1999. arXiv:hep-ph/9812415 [hep-ph] .
- [41] Q.-H. Cao, “Demonstration of One Cutoff Phase Space Slicing Method: Next-to-Leading Order QCD Corrections to the  $tW$  Associated Production in Hadron Collision,” 2008. arXiv:0801.1539 [hep-ph] .
- [42] S. Catani and M. Seymour, “The Dipole formalism for the calculation of QCD jet cross-sections at next-to-leading order,” *Phys.Lett.* **B378**, pp. 287–301, 1996. arXiv:hep-ph/9602277 [hep-ph] .
- [43] S. Catani and M. Seymour, “A General algorithm for calculating jet cross-sections in NLO QCD,” *Nucl.Phys.* **B485**, pp. 291–419, 1997. arXiv:hep-ph/9605323 [hep-ph] .

- [44] S. Dittmaier, “A General approach to photon radiation off fermions,” *Nucl.Phys.* **B565**, pp. 69–122, 2000. arXiv:hep-ph/9904440 [hep-ph] .
- [45] S. Dittmaier, A. Kabelschacht, and T. Kasprzik, “Polarized QED splittings of massive fermions and dipole subtraction for non-collinear-safe observables,” *Nucl.Phys.* **B800**, pp. 146–189, 2008. arXiv:0802.1405 [hep-ph] .
- [46] A. Huss, “Mixed QCD-electroweak  $\mathcal{O}(\alpha_s\alpha)$  corrections to Drell-Yan processes in the resonance region,” Albert-Ludwigs-Universität Freiburg, 2014.
- [47] L. Basso, S. Dittmaier, A. Huss, and L. Oggero , in preparation.
- [48] S. Glashow, J. Iliopoulos, and L. Maiani, “Weak Interactions with Lepton-Hadron Symmetry,” *Phys.Rev.* **D2**, pp. 1285–1292, 1970.
- [49] S. Weinberg, “A Model of Leptons,” *Phys.Rev.Lett.* **19**, pp. 1264–1266, 1967.
- [50] A. Salam, “Weak and Electromagnetic Interactions,” *Conf.Proc.* **C680519**, pp. 367–377, 1968.
- [51] M. Böhm, A. Denner, and H. Joos, “Gauge theories of the strong and electroweak interaction,” 2001.
- [52] M. E. Peskin and D. V. Schroeder, “An Introduction to quantum field theory,” 1995.
- [53] S. Weinberg, “The Quantum theory of fields. Vol. 1: Foundations,” 1995.
- [54] S. Weinberg, “The quantum theory of fields. Vol. 2: Modern applications,” 1996.
- [55] R. K. Ellis, W. J. Stirling, and B. Webber, “QCD and collider physics,” *Camb.Monogr.Part.Phys.Nucl.Phys.Cosmol.* **8**, pp. 1–435, 1996.
- [56] F. Englert and R. Brout, “Broken Symmetry and the Mass of Gauge Vector Mesons,” *Phys.Rev.Lett.* **13**, pp. 321–323, 1964.
- [57] P. W. Higgs, “Broken symmetries, massless particles and gauge fields,” *Phys. Lett.* **12**, pp. 132–133, 1964.
- [58] P. W. Higgs, “Broken Symmetries and the Masses of Gauge Bosons,” *Phys.Rev.Lett.* **13**, pp. 508–509, 1964.
- [59] G. Guralnik, C. Hagen, and T. Kibble, “Global Conservation Laws and Massless Particles,” *Phys.Rev.Lett.* **13**, pp. 585–587, 1964.
- [60] T. W. B. Kibble, “Symmetry breaking in non-abelian gauge theories,” *Phys. Rev.* **155**, pp. 1554–1561, 1967.
- [61] G. Aad *et al.*, “Observation of a new particle in the search for the standard model higgs boson with the atlas detector at the lh,” *Phys.Lett.* **B716**, pp. 1–29, 2012. arXiv:1207.7214 [hep-ex] .

- [62] S. Chatrchyan *et al.*, “Observation of a new boson at a mass of 125 gev with the cms experiment at the lhc,” *Phys.Lett.* **B716**, pp. 30–61, 2012. arXiv:1207.7235 [hep-ex] .
- [63] Y. Nambu, “Quasiparticles and Gauge Invariance in the Theory of Superconductivity,” *Phys.Rev.* **117**, pp. 648–663, 1960.
- [64] J. Goldstone, “Field Theories with Superconductor Solutions,” *Nuovo Cim.* **19**, pp. 154–164, 1961.
- [65] N. Cabibbo, “Unitary Symmetry and Leptonic Decays,” *Phys.Rev.Lett.* **10**, pp. 531–533, 1963.
- [66] M. Kobayashi and T. Maskawa, “CP Violation in the Renormalizable Theory of Weak Interaction,” *Prog.Theor.Phys.* **49**, pp. 652–657, 1973.
- [67] S. M. Bilenky and S. Petcov, “Massive Neutrinos and Neutrino Oscillations,” *Rev.Mod.Phys.* **59**, p. 671, 1987.
- [68] L. Faddeev and V. Popov, “Feynman Diagrams for the Yang-Mills Field,” *Phys.Lett.* **B25**, pp. 29–30, 1967.
- [69] G. ’t Hooft, “Renormalization of Massless Yang-Mills Fields,” *Nucl.Phys.* **B33**, pp. 173–199, 1971.
- [70] G. ’t Hooft, “Renormalizable Lagrangians for Massive Yang-Mills Fields,” *Nucl.Phys.* **B35**, pp. 167–188, 1971.
- [71] G. ’t Hooft and M. Veltman, “Regularization and Renormalization of Gauge Fields,” *Nucl.Phys.* **B44**, pp. 189–213, 1972.
- [72] C. Bollini and J. Giambiagi, “Dimensional Renormalization: The Number of Dimensions as a Regularizing Parameter,” *Nuovo Cim.* **B12**, pp. 20–25, 1972.
- [73] D. Ross and J. Taylor, “Renormalization of a unified theory of weak and electromagnetic interactions,” *Nucl.Phys.* **B51**, pp. 125–144, 1973.
- [74] A. Sirlin, “Radiative Corrections in the  $SU(2)_L \times U(1)$  theory: A Simple Renormalization Framework,” *Phys.Rev.* **D22**, pp. 971–981, 1980.
- [75] W. Marciano and A. Sirlin, “Radiative Corrections to Neutrino Induced Neutral Current Phenomena in the  $SU(2)_L \times U(1)$  Theory,” *Phys.Rev.* **D22**, p. 2695, 1980.
- [76] A. Sirlin and W. Marciano, “Radiative Corrections to Muon-neutrino  $\nu_\mu + N \rightarrow \mu^- + X$  and their Effect on the Determination of  $\rho^2$  and  $\sin^2_{\Theta_W}$ ,” *Nucl.Phys.* **B189**, p. 442, 1981.
- [77] R. Behrends, R. Finkelstein, and A. Sirlin, “Radiative corrections to decay processes,” *Phys.Rev.* **101**, pp. 866–873, 1956.
- [78] T. Kinoshita and A. Sirlin, “Radiative corrections to Fermi interactions,” *Phys.Rev.* **113**, pp. 1652–1660, 1959.

- [79] Y. Kurihara, D. Perret-Gallix, and Y. Shimizu, “ $e^+e^- \rightarrow e^-\bar{\nu}_e u\bar{d}$  from LEP to linear collider energies,” *Phys.Lett.* **B349**, pp. 367–374, 1995. arXiv:hep-ph/9412215 [hep-ph] .
- [80] E. N. Argyres, W. Beenakker, G. J. van Oldenborgh, A. Denner, S. Dittmaier, *et al.*, “Stable calculations for unstable particles: Restoring gauge invariance,” *Phys.Lett.* **B358**, pp. 339–346, 1995. arXiv:hep-ph/9507216 [hep-ph] .
- [81] J. Butterworth, G. Dissertori, S. Dittmaier, D. de Florian, N. Glover, *et al.*, “Les Houches 2013: Physics at TeV Colliders: Standard Model Working Group Report,” 2014. arXiv:1405.1067 [hep-ph] .
- [82] C. Uhlemann and N. Kauer, “Narrow-width approximation accuracy,” *Nucl.Phys.* **B814**, pp. 195–211, 2009. arXiv:0807.4112 [hep-ph] .
- [83] N. Kauer, “Narrow-width approximation limitations,” *Phys.Lett.* **B649**, pp. 413–416, 2007. arXiv:hep-ph/0703077 [hep-ph] .
- [84] A. Denner and J.-N. Lang, “The Complex-Mass Scheme and Unitarity in perturbative Quantum Field Theory,” 2014. arXiv:1406.6280 [hep-ph] .
- [85] S. Dittmaier, “Weyl-van der Waerden formalism for helicity amplitudes of massive particles,” *Phys.Rev.* **D59**, p. 016007, 1998. arXiv:hep-ph/9805445 [hep-ph] .
- [86] A. Denner, S. Dittmaier, and L. Hofer, “COLLIER – A fortran-library for one-loop integrals,” 2014. arXiv:1407.0087 [hep-ph] .
- [87] T. Kinoshita, “Mass singularities of Feynman amplitudes,” *J.Math.Phys.* **3**, pp. 650–677, 1962.
- [88] T. Lee and M. Nauenberg, “Degenerate Systems and Mass Singularities,” *Phys.Rev.* **133**, pp. B1549–B1562, 1964.
- [89] S. Dittmaier, “Separation of soft and collinear singularities from one loop N point integrals,” *Nucl.Phys.* **B675**, pp. 447–466, 2003. arXiv:hep-ph/0308246 [hep-ph] .
- [90] B. Humpert and W. van Neerven, “Infrared and Mass Regularization in Af Field Theories. 1.  $\phi^3$  in Six-dimensions,” *Nucl.Phys.* **B178**, p. 498, 1981.
- [91] B. Humpert and W. van Neerven, “Infrared and Mass Regularization in Af Field Theories 2. QCD,” *Nucl.Phys.* **B184**, p. 225, 1981.
- [92] H. van Dam and M. Veltman, “Massive and massless Yang-Mills and gravitational fields,” *Nucl.Phys.* **B22**, pp. 397–411, 1970.
- [93] B. Harris and J. Owens, “The Two cutoff phase space slicing method,” *Phys.Rev.* **D65**, p. 094032, 2002. arXiv:hep-ph/0102128 [hep-ph] .
- [94] S. Dittmaier and M. Huber, “Radiative corrections to the neutral-current Drell-Yan process in the Standard Model and its minimal supersymmetric extension,” *JHEP* **1001**, p. 060, 2010. arXiv:0911.2329 [hep-ph] .

- [95] G. P. Salam, “Towards Jetography,” *Eur.Phys.J.* **C67**, pp. 637–686, 2010. arXiv:0906.1833 [hep-ph] .
- [96] G. P. Lepage, “VEGAS: An adaptive multidimensional integration program,” 1980.
- [97] M. Roth, “Precise predictions for four fermion production in electron positron annihilation,” 1999. arXiv:hep-ph/0008033 [hep-ph] .
- [98] T. Hahn, “Generating Feynman diagrams and amplitudes with FeynArts 3,” *Comput.Phys.Commun.* **140**, pp. 418–431, 2001. arXiv:hep-ph/0012260 [hep-ph] .
- [99] T. Hahn and M. Perez-Victoria, “Automatized one loop calculations in four-dimensions and D-dimensions,” *Comput.Phys.Commun.* **118**, pp. 153–165, 1999. arXiv:hep-ph/9807565 [hep-ph] .
- [100] B. Chokoufe Nejad, T. Hahn, J.-N. Lang, and E. Mirabella, “FormCalc 8: Better Algebra and Vectorization,” *J.Phys.Conf.Ser.* **523**, p. 012050, 2014. arXiv:1310.0274 [hep-ph] .
- [101] S. Dittmaier, A. Huss, and C. Schwinn, “Mixed QCD-electroweak  $O(\alpha_s\alpha)$  corrections to Drell-Yan processes in the resonance region: pole approximation and non-factorizable corrections,” 2014. arXiv:1403.3216 [hep-ph] .
- [102] S. Dittmaier, A. Huss, and C. Schwinn in preparation.
- [103] J. Beringer *et al.*, “Review of Particle Physics (RPP),” *Phys.Rev.* **D86**, p. 010001, 2012.
- [104] “First combination of Tevatron and LHC measurements of the top-quark mass,” 2014. arXiv:1403.4427 [hep-ex] .
- [105] M. Cacciari, G. P. Salam, and G. Soyez, “The Anti-k(t) jet clustering algorithm,” *JHEP* **0804**, p. 063, 2008. arXiv:0802.1189 [hep-ph] .
- [106] E. Gerwick, S. Schumann, B. Gripaios, and B. Webber, “QCD Jet Rates with the Inclusive Generalized kt Algorithms,” *JHEP* **1304**, p. 089, 2013. arXiv:1212.5235 .
- [107] G. Aad *et al.*, “Jet energy measurement with the ATLAS detector in proton-proton collisions at  $\sqrt{s} = 7$  TeV,” *Eur.Phys.J.* **C73**, p. 2304, 2013. arXiv:1112.6426 [hep-ex] .
- [108] S. Chatrchyan *et al.*, “Measurement of the single-top-quark  $t$ -channel cross section in  $pp$  collisions at  $\sqrt{s} = 7$  TeV,” *JHEP* **1212**, p. 035, 2012. arXiv:1209.4533 [hep-ex] .
- [109] K. Seidel, F. Simon, M. Tesar, and S. Poss, “Top quark mass measurements at and above threshold at CLIC,” *Eur.Phys.J.* **C73**, p. 2530, 2013. arXiv:1303.3758 [hep-ex] .
- [110] S. Dittmaier, S. Kallweit, and P. Uwer, “NLO QCD corrections to  $pp/p\bar{p} \rightarrow WW + jet + X$  including leptonic W-boson decays,” *Nucl.Phys.* **B826**, pp. 18–70, 2010. arXiv:0908.4124 [hep-ph] .
- [111] D. Yennie, S. C. Frautschi, and H. Suura, “The infrared divergence phenomena and high-energy processes,” *Annals Phys.* **13**, pp. 379–452, 1961.



# Acknowledgements

First of all I would like to thank Prof. Dr. Stefan Dittmaier, for suggesting me this interesting topic, for his support, for having always time to answer my questions and for the opportunity to work in this amazing group.

I would also like to thank Lorenzo. He is first of all a friend, a person that listens to me, gives me advices and with whom I shared many nice moments. And he is the colleague that had the patience to help me, correct my scripts, and follow me during this project. Many many thanks.

My gratitude goes also to Alex, the person that can solve every kind of problem in less than five days. Thanks for supporting me and helping me in every kind of situation.

Thanks to Michael and Lukas, and to all the 8th floor for these four years: for the helpful discussions, for the kicker, for the Käsespätzle recipe, the evenings at the ElPi and much more. A special thanks goes to Markus: for sharing the office, for his help with the German language, with the bureaucracy and with my work, and overall for his friendship. He has been there from the beginning, without even the need to ask.

I would also like to thank Alessandro Ballestrero, for giving me the opportunity to start this experience and for all the good advices that helped me during the PhD. Moreover, I would like to thank Prof. Dr. M. Mühlleitner for being my mentor and for helping me to understand myself and to find my own way.

Thanks to Michael and Monika: I have been really lucky to have met such kind and caring landlords, that allowed me to feel home in Freiburg.

Furthermore, I want to thank all the friends I met in Freiburg: Romain for the music moments and for being present every time I needed, Manuela for our limitless chat about “the meaning of life”, Edoardo for always listening to me and sharing special moments, Francesca, Lucie, Tara, Manfredi, Claudia, Emily, Michele, JP, Vlad, Valerio, Alberto and all the others, with whom I shared this extraordinary experience of living abroad.

A special thanks goes to Riccardo, for being, together with all Sulzburgerstrasse 26, my second family. One world is enough to understand each other, or maybe we simply need a glass of wine to share the beauty of our lives.

E sempre per “colpa” di Riccardo, posso avere la fortuna di ringraziare Antonio. Grazie per essermi stata vicina e avermi regalato momenti di pura felicità in questi ultimi stressanti mesi di tesi. Grazie a te, come direbbe qualcuno, finalmente “sento il diritto di sentirmi leggera”.

Un grazie di cuore anche a coloro che mi hanno sostenuta “a distanza” dall’Italia (e non solo) in tutti questi anni. Siete tanti, e anche senza scrivere il vostro nome sapete che il mio ringraziamento va a voi. Un grazie speciale a Max, Antonella, Chappy, Francesco e Andrea. La distanza non può far nulla di fronte ad una vera e sincera amicizia, e senza la vostra fiducia sarebbe stato tutto più difficile. Grazie a Matteo, perchè, nonostante la vita ci abbia fatto

prendere strade diverse, abbiamo condiviso in questa esperienza tanti bei momenti. Grazie a zii, zie, cugini e cugine, che con i loro messaggi, le loro chiamate e i loro barattolini di cibo, mi hanno fatto sentire la loro vicinanza.

La parola grazie non sarà mai abbastanza per esprimere ciò che provo nei confronti della mia famiglia e di Fredina. Solo voi sapete cosa hanno davvero significato per me questi quattro anni, quanto questa esperienza mi abbia fatto crescere e quale grande opportunità sia stata per me. Grazie per avermi permesso di essere qui, per avermi sostenuta in tutte le mie decisioni e per esserci stati in qualunque momento.